

Time-Domain Distortion Analysis of Wideband Electromagnetic Field Sensors Using Orthogonal Polynomial Subspaces

by

Shekoofeh Saboktakinrizi

A Thesis submitted to the Faculty of Graduate Studies of

The University of Manitoba

in partial fulfillment of the requirements for the degree of

Master of Science

Department of Electrical and Computer Engineering

The University of Manitoba

Winnipeg, MB, Canada

© 2011 by Shekoofeh Saboktakinrizi

To my wonderful parents.

To Bahar,

and,

Bibi.

Abstract

In this thesis, a method of distortion analysis of electromagnetic field sensors using orthogonal polynomial subspaces is presented. The effective height of the sensor is viewed as the impulse response of a linear system. The impulse response corresponds to a linear transformation which maps every electromagnetic incident field waveform to a received voltage waveform. Hermite and Laguerre orthogonal polynomials are used as the basis sets for the subspace of incident electromagnetic field waveforms. Using the selected basis set, a transformation matrix is calculated for the sensors. The transformation matrices are compared to a reference transformation matrix as a measure of distortion.

The transformation matrices can describe the sensor behavior up to a certain frequency range. The limits on this frequency range are investigated for both Hermite-Gauss and Laguerre functions. The unique property of Laguerre functions is used to prove that the transformation matrix has a particular pattern. This method is applied on case studied sensors both in computer simulation and measurements.

Acknowledgments

I would like to thank my adviser, Dr. Behzad Kordi, for his guidance, patience and motivation throughout this research. I am also grateful to the examining committee, Dr. Joe LoVetri and Dr. Shaun Lui, for their time and consideration to review this work. My sincere thanks also goes to Dr. Joe LoVetri for giving me the opportunity to perform my measurements in the Microwave Imaging lab. I am also grateful to Majid Ostadrahimi for helping me to do the experiments. Financial support provided by NSERC, Manitoba Hydro, and MITACS Accelerate Manitoba is greatly acknowledged. Last but certainly not least, I would like to thank my wonderful family and friends for their priceless help and support.

Contents

Abstract	i
Contents	iii
List of Figures	v
List of Tables	xi
1 Introduction	1
1.1 Problem Definition	2
1.2 Motivation	3
1.3 Thesis Outline	4
2 Background	5
2.1 Frequency-Domain Antenna Characteristics	5
2.2 Time-Domain Antenna Characteristics	13
2.2.1 Time-domain definitions complying to frequency-domain definitions	14
2.2.2 Time-domain definitions specifically defined in time domain	17
2.2.3 Antenna Time-Domain Distortion Analysis	24
3 Distortion Analysis Using Signal Subspaces	29
3.1 General Remarks	30
3.2 Finite Dimensional Analysis	32
3.2.1 Finite Dimensional Terminology	33
3.2.2 Linear-Operator Representation of Sensors	34
3.2.3 Calculation of the Transformation Matrix	36
3.2.4 Distortion Analysis	36
3.2.5 Hermite-Gauss Functions as the Basis Vectors	39
3.3 Infinite Dimensional Analysis	39
3.3.1 Distortion Analysis Using Laguerre Functions	40

4	Interpretation of the Transformation Matrix	42
4.1	Finite-Dimensional Analysis	43
4.1.1	Hermite-Gauss Functions	43
4.1.2	Selection of a Proper Scaling Factor	48
4.1.3	Distortion Analysis in a Certain Frequency Range	51
4.1.4	Examples	52
4.2	Infinite-dimensional Analysis	57
4.2.1	Laguerre Functions	59
4.2.2	Transformation Matrix Calculated in Laguerre Subspace	61
4.2.3	Distortion Analysis in Laguerre Subspace	65
4.2.4	Selection of a Proper Scaling Factor	67
4.2.5	Distortion Analysis in a Certain Frequency Range	68
4.2.6	Example	68
5	Simulation and Measurement Results	70
5.1	Simulation Method	72
5.2	Finite-Dimensional Analysis	74
5.2.1	Interpretation of the Results	74
5.2.2	Sensitivity Analysis	88
5.2.3	Calculating the Transformation Matrix Using Measurement Data	90
5.3	Infinite-Dimensional Analysis	96
5.3.1	Calculating the Effective Height Using one Set of Measurement	103
6	Concluding Remarks and Future Work	106
6.1	Concluding Remarks	106
6.2	Future Work	108
	Bibliography	109
A	Appendix A	113
B	Appendix B	115
C	Appendix C	120
D	Appendix D	122
D.1	Hermite Polynomials	122
D.2	Hermite Polynomials Properties	123
D.3	Hermite-Gauss Functions and Their Properties	124
E	Appendix E	126
E.1	Laguerre Polynomials	126
E.2	Laguerre Polynomials Properties	127
E.3	Associated Laguerre Polynomials and Properties	128
E.4	Laguerre Functions	129

List of Figures

2.1	Antenna circuit model without considering a transmission line a) antenna in the transmit mode, and b) antenna in the receive mode.	9
2.2	Antenna circuit model considering a transmission line a) antenna in the transmit mode, and b) antenna in the receive mode.	11
4.1	Hermite-Gauss functions for different orders and $\sigma = 1$ in a) the time domain and, b) the frequency domain.	44
4.2	Variation of a) the time duration where time-domain Hermite-Gauss functions fall to 1% of their maximum and, b) the frequency range where the magnitude of the Fourier transform of Hermite-Gauss functions fall to 1% of their maximum , when $\sigma = 1$ is selected.	47
4.3	Transformation matrices calculated for an ideal differentiator with $\sigma = 2ns$ for a) normalized outputs, b) unnormalized outputs.	54
4.4	Transformation matrix calculated for a lowpass filter with a cut off frequency of 500 MHz using $\sigma = 2$ ns.	55

4.5 Transformation matrix calculated for a highpass filter with a cut off frequency of 500 MHz using $\sigma = 2$ ns. 56

4.6 Transformation matrix calculated for a bandpass filter with a passband frequencies larger than 400 MHz and smaller than 600 MHz using $\sigma = 2ns$. 56

4.7 Variation of the calculated η_N for three different values of N using $\sigma = 2$ ns, for lowpass filters with respect to the lowpass filter cut-off frequency . . 58

4.8 Different orders of Laguerre functions for $p=1$ 60

4.9 Variation of a) time duration where Laguerre functions fall to 1% of the maximum with respect to the order and, b) magnitude of the Fourier transform of Laguerre functions with respect to the frequency. 62

4.10 Transformation matrix for a sensor associated with the impulse response $h(t)$ expanded as $h(t) = \sum_{k=0}^{\infty} h_k l_k^p(t)$, using Laguerre functions. 65

4.11 Different values obtained for η_{∞} for lowpass filters with different cut-off frequencies when different values of p is used. 69

5.1 Photo of the 3×3 cm parallel plate sensor with 2 mm air dielectric, used in the experiments and modeled in the simulation. 71

5.2 Photo of the 5 cm heigh AD-S30 ACD manufactured by Prodyn, uses in the experiments and modeled in the simulations. 71

5.3 Photo of the wire monopole used in the experiments and modeled in the simulations. 72

5.4	ACD wire model used in the time-domain simulations and the electromagnetic field. The sensor is terminated at a 50Ω load. An EFEI is solved using MOM to determine the voltage at the terminal of the sensor.	73
5.5	Transformation matrices calculated for the ACD using $\sigma = 2$ ns for a) the received voltage and, b) the integral of received voltage.	75
5.6	Transformation matrices calculated for the 15 cm monopole using $\sigma = 2$ ns for a) the received voltage and, b) the integral of received voltage. . . .	76
5.7	Transformation matrices calculated for the 10 cm monopole using $\sigma = 2$ ns for a) the received voltage and, b) the integral of received voltage. . . .	77
5.8	Transformation matrices calculated for the 5 cm monopole using $\sigma = 2$ ns for a) the received voltage and, b) the integral of received voltage.	78
5.9	Transformation matrices calculated for the 3×3 cm parallel plate with 2 mm air dielectric, using $\sigma = 2$ ns for a) the received voltage and, b) the integral of received voltage.	79
5.10	Transformation matrices calculated for the ACD using $\sigma = 4$ ns for a) the received voltage and, b) the integral of received voltage.	80
5.11	Transformation matrices calculated for the 15 cm monopole using $\sigma = 4$ ns for a) the received voltage and, b) the integral of received voltage. . . .	81
5.12	Transformation matrices calculated for the 10 cm monopole using $\sigma = 4$ ns for a) the received voltage and, b) the integral of received voltage. . . .	82

5.13	Transformation matrices calculated for the 5 cm monopole using $\sigma = 4$ ns for a) the received voltage and, b) the integral of received voltage.	83
5.14	Transformation matrices calculated for the 3×3 cm parallel plate with 2 mm air filling, using $\sigma = 4$ ns for a) the received voltage and, b) the integral of received voltage.	84
5.15	Received voltages when the incident electric field has a Gaussian waveform with 1 GHz bandwidth.	89
5.16	The measurement setup, including a GTEM cell as the test environment, the impulse generator and the DSO.	93
5.17	The voltage generator time-domain pulse directly measured by the DSO.	93
5.18	Time-domain measured voltages at the terminals of the sensors when located inside the GTEM cell.	94
5.19	The circuit model for the parallel plate sensor with capacitance of C and height h	95
5.20	Measured time-domain electric field in the GTEM cell at the location of the sensors, using the parallel plate sensor.	96
5.21	Calculated transformation matrix for the ACD using the time-domain measured voltage for $\sigma = 2$ ns, when the incident electric field varies as Fig. 5.20.	97

5.22	Calculated transformation matrix for the 15 cm monopole antenna using the time-domain measured voltage for $\sigma = 2$ ns, when the incident electric field varies as Fig. 5.20.	97
5.23	Calculated transformation matrix for the 10 cm monopole antenna using the time-domain measured voltage for $\sigma = 2$ ns, when the incident electric field varies as Fig. 5.20.	98
5.24	Calculated transformation matrix for the 5 cm monopole antenna using the time-domain measured voltage for $\sigma = 2$ ns, when the incident electric field varies as Fig. 5.20.	98
5.25	Calculated transformation matrix using Laguerre functions with $p = 10^{10}$ for a 5 cm monopole antenna.	100
5.26	Calculated transformation matrix using Laguerre functions with $p = 10^{10}$ for a 10 cm monopole antenna.	100
5.27	Calculated transformation matrix using Laguerre functions with $p = 10^{10}$ for a 15 cm monopole antenna.	101
5.28	Calculated transformation matrix using Laguerre functions with $p = 10^{10}$ for a 5 cm ACD.	101
5.29	Effective heights calculated for the electric field sensors, when the sensors received voltages are simulated when illuminated by an incident electric field which has a Gaussian waveform with a 10 GHz bandwidth.	102

5.30 Calculated η_∞ for the sensors effective heights. 102

5.31 Calculated η_∞ for the integral of sensors effective heights. 103

List of Tables

5.1	Calculated η_N for simulated voltages ($\sigma = 2ns$), for $N = 60$ which corresponds to a maximum frequency rang of 1 GHz. The ACD has the least distortion as an identity system.	87
5.2	Calculated η_N for the integral of simulated voltages ($\sigma = 2ns$), for $N = 61$ which is corresponding to a maximum frequency of 1 GHz. The parallel plate and 5 cm monopole have the least distortion introduced as a differentiator.	87
5.3	Calculated η_N for the integral of simulated voltages ($\sigma = 4ns$).	88
5.4	Calculated η_N for the integral of simulated voltages ($\sigma = 2 ns$).	89
5.5	Calculated η_N for the the simulated voltages ($\sigma = 2ns$)	89
5.6	Calculated η_N for the the simulated and measured voltages ($\sigma = 2ns$) . . .	96

Chapter 1

Introduction

IEEE standard for “Calibration of Electromagnetic Field Sensors and Probes, Excluding Antennas, from 9 kHz to 40 GHz” defines an electromagnetic field sensor as “An electrically small device without electronics (*i.e.*, passive) that is used for measuring electric or magnetic fields, with a minimum of perturbation to the field being measured [1].” The ratio of the electric voltage or current at the terminals of the sensor to the electromagnetic field is called the sensor transfer function. Physical and electrical properties of the sensor determine the transfer function [1], [2]. Electromagnetic field sensors are used to measure the electromagnetic field variations with time. Applications include measurement of electrical field in medical imaging, Partial Discharge (PD) measurements, Electromagnetic Compatibility (EMC) tests, Electromagnetic Pulse (EMP) experiments [3], etc. In a general sense, electromagnetic field sensors are divided into two groups of “free field” and “ground plane” sensors. Dipole and loop antennas are prototypes for the free field electric

and magnetic field sensors, respectively. Electric and magnetic field sensors over a ground plane have monopole and half-loop structures [1]. In addition to this, the sensors which deliver the derivative of the incident field flux density at their output are considered as an important class and are denoted as \dot{D} and \dot{B} for the electric and magnetic field sensors, respectively.

1.1 Problem Definition

In this thesis, a general distortion analysis for electromagnetic field sensors is presented. The proposed distortion characteristic should be able to describe the sensor performance over a specific range of frequency. The way the term “distortion” is defined, determines the characteristic we are seeking. For now, we refer to distortion as any unsimilarity introduced to the output waveform of an electromagnetic field sensor, compared to the expected signal when both signals are normalized. As it is denoted in [1], the expected ideal signal waveform is a linear transformation of the incident field. For instance, \dot{D} sensors deliver a voltage at their terminals which is proportional to the first derivative of the incident electric field waveform with respect to time.

In order to establish characteristics for electromagnetic field sensors, one should refer to the well defined antenna characteristics standardized in [4] as the sensors are modeled as antennas in the receiving mode. Most of the conventional antenna characteristics are frequency-domain parameters, such as gain, directivity, radiation pattern, beam-width,

etc. For sensor characterization, however, there is a need to evaluate the frequency-domain definitions for a range of frequencies. In addition, there is no frequency-domain distortion characterization which is applicable for sensor application. Precisely speaking, frequency-domain return loss can be viewed as a distortion measure, but there are cases which return loss is not sufficient to decide how well an antenna receives a signal that covers a wide frequency spectrum.¹

Further to pursuing a general methodology to analyze the distortion characteristic, one has to establish a relationship between this characteristic and other important characteristics such as sensitivity. As it is shown in the upcoming chapters, it is not realistic to compare the distortion characteristics of different sensors without considering their sensitivities. There is always a trade-off between the sensitivity of the sensor to the incident electric field and the distortion behavior. In other words, a combined parameter should be introduced which includes both the distortion character and sensitivity of a sensor.

1.2 Motivation

In applications using electromagnetic field sensors, distortion analysis is necessary to have a measure of sensor accuracy. Distortion characteristic has only been defined in the time domain. The classical time-domain distortion characteristic known as “fidelity” is a wave-form dependent parameter [6]. A more general approach based on system linearity and

¹The example is the Vivaldi antenna, which has a very good return loss, but the phase center is varying with respect to frequency, not having a good distortion characteristic [5].

Hermite orthogonal polynomials can give a more general understanding of the distortion introduced by the sensor has been introduced by Carro and De Mingo [7]. In addition to a distortion measure, this approach gives a general system identification. Frequency-domain system characterization is sometimes a tedious task for systems performing under the transient regime. Both the characterization and measurement has to be performed repeatedly in the whole frequency range to obtain a sufficient resolution. On the contrary, time-domain measurement and characterization can be more efficient. More importantly, time-domain approach gives a more comprehensible vision of the transient behavior of the system.

1.3 Thesis Outline

A background on the characterization of antennas in the time domain is presented in Chapter 2. The subspaces methodology is described in Chapter 3. Chapter 4 discusses the interpretation of the results obtained from employing different polynomials using the subspaces method. Finally, the distortion characteristic obtained from simulation data is compared to the one obtained from measurement data for some prototype sensors in Chapter 5. The concluding remarks and the future work are summarized in Chapter 6.

Chapter 2

Background

In this chapter a review on the existing literature on antenna characterization is presented. Electromagnetic field sensor characterization is an especial case of antenna characterization. This is why antenna characterization is applicable to electromagnetic field sensors. To begin with, some of the classical antenna frequency-domain characteristics are presented. Then the time-domain generalization of antenna characteristics are reviewed. Finally, considering all of these characterization methods, distortion characterization is investigated. It should be noted that not all of the characteristics summarized in this chapter are used in this thesis. However, time-domain characteristics are described briefly in order to document the performed literature review.

2.1 Frequency-Domain Antenna Characteristics

The parameters originally defined in IEEE standard for “Definitions of terms for antennas” [4], are frequency-domain definitions. The following has been selected from many

frequency-domain characteristics defined in [4]. The terms in quotation marks are adopted from [4]. These characteristics are outlined in this thesis for the sake of the completeness of this document.

- Far-field region

“That region of the field of an antenna where the angular field distribution is essentially independent of the distance from the antenna. If the antenna has a maximum overall dimension D , the far-field region is commonly taken to exist at distances greater than $2D^2/\lambda$ from the antenna, λ being the wavelength [4].” In the far-field region, the electromagnetic fields are in the TEM mode¹ and electromagnetic fields vary inversely proportional to the distance from the source [8].

- Radiation pattern $RP(\theta, \phi)$

“A mathematical function or a graphical representation of the radiation properties of the antenna as a function of space coordinates. In most cases, the radiation pattern is determined in the far-field region and is represented as a function of the directional coordinates. Radiation properties include power flux density, radiation intensity, field strength, directivity, phase or polarization[8] and [4].” For example

¹TEM mode is the Transverse Electro-Magnetic mode where the electric and magnetic field vectors are perpendicular to each other and to the direction of propagation and, in free space, hold a ratio of $\eta_0 = 377\Omega$ between their magnitudes.

if the transmitted energy is considered, the radiation pattern can be defined as [6]

$$RP(\theta, \phi) = \frac{1}{2\pi\eta_0} \int_{-\infty}^{\infty} |\mathbf{E}_t(r, \theta, \phi, \omega)|^2 r^2 d\omega \quad (2.1)$$

where η_0 is the free space impedance equal to $377 \Omega^2$ and $\mathbf{E}_t(r, \theta, \phi, \omega)$ is the transmitted electric field the location (r, θ, ϕ) and frequency $\omega/2\pi$.

- Radiated power

“The average power radiated by the antenna [8].” If the power density term is assigned to the time average Poynting vector that is

$$\mathbf{W}_{rad} = \frac{1}{2} \text{Real} \{ \mathbf{E} \times \mathbf{H}^* \}, \quad (2.2)$$

then the radiated power is defined as,

$$P_{rad} = \int \int \mathbf{W}_{rad} \cdot d\mathbf{s}. \quad (2.3)$$

- Radiation intensity $\mathbf{U}(\theta, \phi, \omega)$

“The power radiated from an antenna per unit solid angle [4], ” in a certain direction is called the radiation intensity. As Radiation intensity is a far-field parameter, it can be obtained by multiplying the radiation power density in the square of distance

²In [6] the r^2 coefficient in the integrand is not considered which has been corrected in [9].

[8] as,

$$\mathbf{U}(\theta, \phi, \omega) = r^2 \mathbf{W}_{ave}(\theta, \phi, \omega). \quad (2.4)$$

- Directivity $D(\theta, \phi, \omega)$

“The ratio of the of radiation intensity in a given direction from the antenna to the radiation intensity averaged over all directions [4]” is called directivity and is given by,

$$D(\theta, \phi, \omega) = \frac{4\pi U(\theta, \phi, \omega)}{P_{rad}}, \quad (2.5)$$

where, U is the magnitude of the vector \mathbf{U} in the desired direction.

- Gain $G(\theta, \phi, \omega)$

“The ratio of the radiation intensity in a given direction to the radiation intensity that would be obtained if the power accepted by the antenna were radiated isotropically. The radiation intensity corresponding to the isotropically radiated power is equal to the power accepted (input) by the antenna divided by 4π [4].” The radiated power is a fraction of the input power to the antenna as³ [8],

$$P_{rad} = e_{cd} P_{in}, \quad (2.6)$$

where, e_{cd} is a positive number smaller than one. Directivity and gain are related

³Also called antenna radiation efficiency.

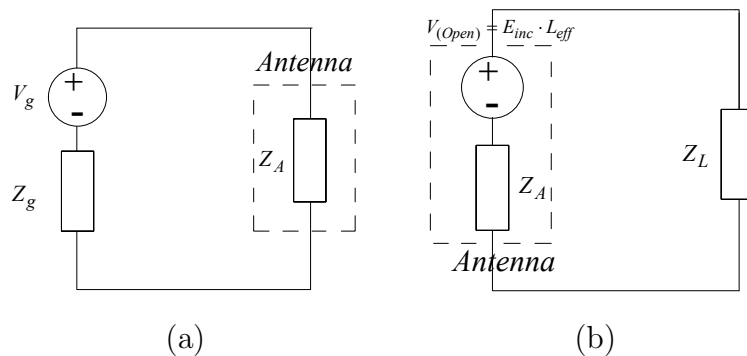


Figure 2.1: Antenna circuit model without considering a transmission line a) antenna in the transmit mode, and b) antenna in the receive mode.

by the same factor as,

$$G(\theta, \phi, \omega) = e_{cd} D(\theta, \phi, \omega). \quad (2.7)$$

- Antenna field factor $\mathbf{F}(\omega, \mathbf{r})$

“The antenna is the transitional structure between free-space and a guiding device [8]. ”Antenna field factor is a function which when multiplied by the antenna voltage/current will give the propagating electric field at a given distance. Antenna field factor can be defined in different ways with respect to the generator voltage or current. The definition also differs when different circuit models are assumed for an antenna in the transmit mode. In [6], for the circuit model of Fig. 2.1a, the transmitted electric field, \mathbf{E}_t , is related to the generator voltage V_g by,

$$\mathbf{E}_t(\mathbf{r}, \omega) = \frac{jV_g(\omega)\eta_0}{Z_g + Z_A} \mathbf{F}(\mathbf{r}, \omega) \frac{e^{-jkr}}{4\pi r}, \quad (2.8)$$

where, Z_g and Z_A are the generator and the antenna impedances, respectively. In (2.8), \mathbf{F} is the antenna field factor, $\mathbf{E}_t(\mathbf{r}, \omega)$ is the transmitted electric field at the location \mathbf{r} and frequency $\omega/2\pi$. A similar idea appears in [10] with consideration of a transmission line in the antenna circuit model as seen in Fig. 2.2a. If the generator impedance is assumed to be purely resistive, equal to the transmission line characteristic impedance, then the radiated electric field is related to the generator voltage using,

$$\mathbf{E}_t(\mathbf{r}, \omega) = \frac{e^{-jkr}}{r} \mathbf{F}_{Baum}(\mathbf{r}, \omega) V_g(\omega). \quad (2.9)$$

Antenna field factor can be defined with respect to the current or voltage. These definitions are presented in [11]. In addition, Shlivinski *et al.* [12], have used a definition for field factor⁴ which is related to reflection-free current traveling along the transmission line. In [12], the field factor, $\mathbf{F}_{Shlivinski}$, is defined so that the transmitted electric field is found using,

$$\mathbf{E}_t(\mathbf{r}, \omega) = -\frac{\mu}{4\pi r} I^+(\mathbf{r}, \omega) \cdot \mathbf{F}_{Shlivinski}(\mathbf{r}, \omega), \quad (2.10)$$

where, in Fig. 2.2a, the generator impedance is assumed to be matched to the transmission line and I^+ is the reflection-less line current. Eqs. (2.8)-(2.10) show that the field factor is proportional to the current distribution of an infinitesimal

⁴The field factor is alternatively denoted as antenna effective height in the transmit mode in [12].

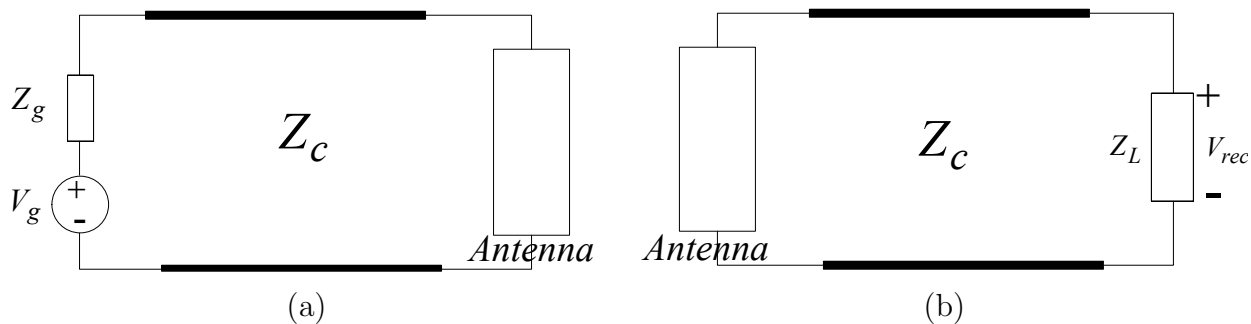


Figure 2.2: Antenna circuit model considering a transmission line a) antenna in the transmit mode, and b) antenna in the receive mode.

dipole⁵ which radiates the same field as the antenna under study. Antenna field factor is the antenna transfer function in the transmit mode.

- Antenna effective length $L_{eff}(\theta, \phi, \omega)$

In [4], the antenna effective length is defined as “for a linearly polarized antenna receiving a plane wave from a given direction, the ratio of the magnitude of the open circuit voltage developed at the terminals of the antenna to the magnitude of the electric field strength in the direction of the antenna polarization.” This means,

$$L_{eff}(\theta, \phi, \omega) = \frac{V_{rec}^{open}(\omega)}{E_{rec}(\theta, \phi, \omega)}. \quad (2.11)$$

- Effective height $\mathbf{H}_{eff}(\theta, \phi, \omega)$

⁵A current element which has a spatial current distribution proportional to $\delta(\mathbf{r})$.

In [11], “other vectors” are defined with respect to Fig. 2.1b as,

$$\mathbf{h}_I(\omega, \mathbf{r}) = -\frac{1}{Z_A} L_{eff}(\omega, \mathbf{r}) \mathbf{l}_e, \quad (2.12)$$

$$\mathbf{h}_W(\omega, \mathbf{r}) = \frac{Z_L}{Z_A + Z_L} L_{eff}(\omega, \mathbf{r}) \mathbf{l}_e, \quad (2.13)$$

where, \mathbf{l}_e is the antenna polarization vector and $\mathbf{h}_I(\omega, \mathbf{r})$ and $\mathbf{h}_W(\omega, \mathbf{r})$ represent effective heights defined with respect to the input current or voltage, respectively.

This leads to the vector definition of effective height. As defined in [10], the received voltage in Fig. 2.2b is given by,

$$V_{rec} = \mathbf{H}_{eff}(\theta, \phi, \omega) \cdot \mathbf{E}_{inc}(\theta, \phi, \omega), \quad (2.14)$$

where, \cdot represents the inner product of vectors. The load impedance, Z_L , is assumed to match the characteristic impedance of the transmission line. The effective height is antenna transfer function in the receive mode.

- Reciprocity theorem in the frequency domain

Antenna field factor and the effective height as defined in (2.9) and (2.14) are related to each other as [11],

$$\mathbf{F}_{Baum}(\theta, \phi, \omega) = -\frac{j\omega\mu_0}{4\pi Z_c} \mathbf{H}_{eff}(\theta, \phi, \omega), \quad (2.15)$$

where Z_c is the transmission line characteristic impedance. This means that an

antenna transmits the same electric field waveform as the one it has received when illuminated by a specific incident electric field if the generator voltage has the form of the integral of the incident electric field.

2.2 Time-Domain Antenna Characteristics

Frequency-domain characterization is appropriate for narrow-band systems. Transient analysis techniques for systems which deal with pulses⁶, are inherently required to possess certain characteristics for a wide range of frequencies, therefore one has to sweep a frequency range to acquire the desired frequency-domain characteristics. Further, it is both easier and more efficient to measure and characterize wideband systems in the time domain [13]. For example in time-domain measurements, unwanted reflections can be removed by applying an appropriate time window [14]. This could be of great value in comparison to the cost and complexity imposed by frequency-domain reflection cancellation methods. A time-domain measurement process essentially consists of transmitting and/or receiving a transient pulse which is more straightforward than repeating the same measurement for the whole frequency spectrum. Instead of preventing the reflections using expensive anechoic chambers, the reflections can be eliminated using proper time-windowing techniques in the time-domain measurement.

Furthermore, there are some characteristics which are intrinsically time-domain concepts

⁶Precisely speaking, these pulses have risetimes of less than 1 ns [6].

such as distortion characteristic. In the frequency domain, distortion characterization has to be related to the input impedance of an antenna or similarly to the return loss. Although these parameters compare the antenna performance with an ideal case which is a matched impedance situation, this is not always sufficient for a complete distortion analysis [5]. In addition to return loss the phase center of an antenna should be inspected to be stable otherwise it gives rise to distortion in the time domain [5]. In the time-domain on the contrary, there is a parameter defined as “fidelity” which considers solely the distortion behavior of the antenna.

The main approach for defining most of the time-domain characteristics is to adapt the same frequency-domain definitions in the time domain using an appropriate mathematical norm. In this section, time-domain definitions for antenna gain and radiation pattern are presented in correspondence to their frequency-domain counterparts.

2.2.1 Time-domain definitions complying to frequency-domain definitions

These are the definitions which are based on the same ideas as those the frequency-domain definitions rely on. The only change is to use an appropriate norm to convert time-domain functions into scalars/vectors which are not functions of time. Parseval theorem⁷ makes the connection between the time and frequency domains whenever an energy parameter

⁷Parseval theorem states if $F(\omega)$ is the Fourier transform of the time-domain function $f(t)$ then $\int_{-\infty}^{\infty} |f(t)|^2 dt = \frac{1}{2\pi} \int_{-\infty}^{\infty} |F(\omega)|^2 d\omega$.

is used.

- Time-domain far-field zone

The criteria for the far-field zone can be translated into the time-domain terms [12].

A given point in spherical coordinates as (r, θ, ϕ) is located in the far-field zone of an antenna with dimension l when [12],

$$r \gg \frac{l^2}{c\tau}, \quad (2.16)$$

where, τ is the time-domain pulse risetime and c is the speed of light in free space.

If $\omega = 1/\tau$ is considered, (2.16) will result in the frequency-domain far-field zone criteria.

- Time-domain radiation pattern RP_{TD}

A similar idea as (2.1) can be applied to define the time-domain radiation pattern.

Using the Parseval theorem one can find the same definition for the radiated energy pattern as [6],

$$RP_{TD}(\theta, \phi) = \frac{1}{\eta_0} \int_{-\infty}^{\infty} |\mathbf{e}_t(r, \theta, \phi, t)|^2 r^2 dt. {}^8 In(2.17),$$

$\mathbf{e}_t(r, \theta, \phi, t)$ is the time-domain transmitted electric field. (2.17)

⁸The r^2 factor has not been included in [6] which has been corrected in [9].

- Time-domain antenna field factor $F_{time}(\theta, \phi)$

Equation (2.8) suggests that antenna field factor is proportional to the ratio of the transmitted electric field to the applied voltage at a specified frequency. Similarly, one can apply an appropriate norm on the time-domain electric field and voltage and define the ratio as the time-domain field factor. This is the idea presented in [15], although named as “transmitting antenna factor”, the defined parameter is the time-domain counterpart for the antenna field factor as defined in (2.8). The so-defined time-domain antenna field factor is given by [15],

$$F_{time}(\theta, \phi) = \frac{\max_t |e_{t(r=1m)}(r, \theta, \phi, t)|}{\max_t |v_g(t)|}. \quad (2.18)$$

- Time-domain transmitting antenna energy factor $F_{time}^{energy}(\theta, \phi)$

Energy factor is defined in the same way as the field factor. The 2-norm is used to convert the time-domain transmitted electric field and generator voltage to scalar values. In [15], energy factor is defined as,

$$F_{time}^{energy}(\theta, \phi) = \sqrt{\frac{\int_{-\infty}^{\infty} |\mathbf{e}_t(\theta, \phi, t)|^2 dt}{\int_{-\infty}^{\infty} |v_g(t)|^2 dt}}. \quad (2.19)$$

- Time-domain effective length (Allen *et al.* definition) L_{time}^{eff}

Known as “antenna effective height”, a definition is given in [15] which matches effective length definition as given by (2.11). The ∞ -norm is applied on the time-

domain functions that yields,

$$L_{time}^{eff} = \frac{\max_t |v_{open}(\theta, \phi, t)|}{\max_t |\mathbf{e}_{inc}(\theta, \phi, t)|}. \quad (2.20)$$

In (2.20), $\mathbf{e}_{inc}(\theta, \phi, t)$ is the incident electric field and v_{open} is the open circuit voltage.

- Time-domain antenna gain $G_{time}(\theta, \phi)$

Antenna gain is defined in the transmit mode of an antenna as [15],

$$G_{time}(\theta, \phi) = \frac{4\pi r^2 \int_{t=-\infty}^{\infty} |e_t(\theta, \phi, t)|^2 dt}{\eta_0 \int_{t=-\infty}^{\infty} v_g(t) i_g(t) dt}. \quad (2.21)$$

In (2.21), $v_g(t) i_g(t)$ gives the input power.

- Time-domain directivity $D_{time}(\theta, \phi)$

Following the same definition as given in (2.5) will result in [15],

$$\mathbf{D}_{time}(\theta, \phi) = \frac{\int_{-\infty}^{\infty} |\mathbf{e}_t(\theta, \phi, t)|^2 dt}{\frac{1}{4\pi} \int_0^{2\pi} \int_0^\pi \int_{-\infty}^{\infty} |\mathbf{e}_t(\theta, \phi, t)|^2 dt d\theta d\phi}. \quad (2.22)$$

2.2.2 Time-domain definitions specifically defined in time domain

- Time-domain antenna field factor (Baum and Farr's definition [10]) $\mathbf{F}_{time}^{Baum}(\theta, \phi, t)$

Taking the inverse Fourier transform of (2.9), Baum and Farr give the time-domain

radiated electric field as,

$$\mathbf{e}_t(\tau) = \frac{1}{r} [\mathbf{F}_{time}^{Baum}(\theta, \phi) * v_g](\tau) \quad (2.23)$$

where $\tau = t - \frac{r}{c}$ is the propagation delay. In (2.23), $*$ represents the convolution operator and the vector \mathbf{e}_t is obtained by convolving the scalar v_g with every component of the vector \mathbf{F}_{time}^{Baum} .

- Time-domain antenna field factor (Shlivinski's definition [12]) $\mathbf{F}_{time}^{Shliv.}(\theta, \phi)$

Using (2.10), the time-domain radiated electric field is given by,

$$\mathbf{e}_t = -\frac{\mu}{8\pi r Z_c} [v_g(\cdot) * \mathbf{F}_{time}^{Shliv.}(\theta, \phi, \cdot)](\tau) \quad (2.24)$$

where, as noted before, τ is the delayed time.

- Time-domain effective length (Baum and Farr definition) $\mathbf{L}_{time}^{eff}(\theta, \phi, t)$

This definition relies on the exact inverse transform of the frequency-domain effective length used in [10]. The time-domain open circuit voltage received by an antenna is the convolution of the time-domain effective length⁹ and the time-domain incident electric field as [10],

$$v_{rec}^{open}(t) = [\mathbf{L}_{time}^{eff}(\cdot) \odot \mathbf{e}_{inc}(\theta, \phi, \cdot)](t). \quad (2.25)$$

⁹Also called the effective height in Baum's note [11].

In (2.25), the effective length has been defined as a vector which is in the direction of the antenna polarization. The symbol \odot stands for temporal convolution of two vectors¹⁰. This is the time-domain equivalent of frequency-domain definition given in the IEEE standard for antenna definitions [4].

- Time-domain antenna effective height(Defined by Baum and Farr [10]) $\mathbf{h}_{eff}^{Baum}(\theta, \phi, t)$

For the circuit model shown in Fig. 2.2b, with the condition of matched load ($Z_L = Z_c$), the effective height is defined with respect to the voltage received in a matched load as,

$$v_{rec}(t) = \mathbf{h}_{eff}^{Baum}(\theta, \phi, t) \odot \mathbf{e}_t(\theta, \phi, t). \quad (2.26)$$

- Time-domain antenna effective height (Defined by Shlivinski *et al.* [12]) $\mathbf{h}_{eff}^{Shliv.}(\theta, \phi, t)$

Using a circuit model as shown in Fig. 2.2b, Shlivinski *et al.* define the effective height of an antenna when the generator is matched to the transmission line. They define the time-domain effective height so that the reflection-less received voltage shown as $v_{rec}^-(t)$ is given by

$$v_{rec}^-(t) = [\mathbf{h}_{eff}^{Shliv.}(\theta, \phi, \cdot) \odot \mathbf{e}_t(\theta, \phi, \cdot)](t). \quad (2.27)$$

- Antenna as a linear system

For the circuit model shown in Fig. 2.2 (which assumes the transmission line is

¹⁰If $\mathbf{A}(t) = (A_x(t), A_y(t), A_z(t))$ and $\mathbf{B}(t) = (B_x(t), B_y(t), B_z(t))$ then $\mathbf{A}(t) \odot \mathbf{B}(t) \equiv (A_x(t) * B_x(t), A_y(t) * B_y(t), A_z(t) * B_z(t))$.

matched to both the load impedance in the receive mode and to the generator impedance in the transmit mode), antenna field factor and effective height as described in equations (2.23), (2.26), (2.24), and (2.27) are the impulse responses in either transmit or receive mode according to different definitions.

- Antenna reciprocity in the time domain

Eq. (2.15) states that the frequency-domain field factor is proportional to the frequency-domain effective height with a coefficient which is a linear function of $j\omega$. In the time domain, this means that time-domain field factor is proportional to the time derivative of the effective height. For the definitions given by Baum and Farr we have [10], [11],

$$\mathbf{F}_{time}^{Baum}(\theta, \phi, t) = -\frac{\partial}{\partial t} \left(\frac{\mu_0}{4\pi Z_c} \mathbf{h}_{eff}^{Baum}(\theta, \phi, t) \right). \quad (2.28)$$

- Time-domain antenna gain (Baum and Farr's modified definition [10]) $G_{time}^{Baum}(\theta, \phi)$

Baum and Farr's definition for gain follows the frequency domain concept of gain which is the ratio of the output signal to the input signal. However, there exist important contributions in their time-domain definitions.

1- As the input and output in the antenna case will be time-dependent waveforms, there should be appropriate norms to convert the time-domain functions into scalar values. Baum and Farr use a general concept of norms for signals. Unlike (2.22)

and (2.21) which use the energy norm, they define the time-domain definition independent from the norm used. The mathematical norm could be selected from the family of p-norms.¹¹

2- In addition to introducing proper norms, they have used operator norms. An operator norm is a norm which determines the possible values of an operator can yield when a specific norm is taken [16]. In antenna time-domain analysis this is of great value because convolution with the effective height and the field factor appears frequently as an operator. Using the properties of p-norms, operator norms and impulse responses of antennas, maximum achievable values for specific types of antennas has been derived in [10].

3- Gain as defined (2.21) considers only the transmit mode of an antenna. In [10] definitions for both the transmit and receive mode gains are given. Receive mode gain is defined as,

$$G_{RX}^{Baum}(\theta, \phi) = \frac{\sqrt{Z_c} \|v_{rec}(t)\|}{\sqrt{\eta_0} \|\mathbf{e}_{inc}(\theta, \phi, t)\|}, \quad (2.29)$$

where $\|\cdot\|$ is the selected norm. For the transmit mode, the gain is defined with a slight modification to 2.21. As stated in (2.28) time-domain field factor is proportional to the derivative of the time-domain effective height. In order to have similar gains for both the receive and transmit modes, one has to define gains with

¹¹If $f(t) : \mathfrak{R} \mapsto \mathfrak{R}$ is a function in \mathfrak{R} , the p -norm of $f(t)$ is defined as a function which maps $f(t)$ to $[\int_{t=-\infty}^{\infty} |f(t)|^p dt]^{\frac{1}{p}}$

respect to similar outputs. The output in the transmit mode is proportional to the derivative of the output of the antenna in the receive mode when the inputs are set the same. Considering this, Baum and Farr have used the integral of the transmitted electric field instead of the electric field itself to define the transmit mode gain $G_{TX}(\theta, \phi)$ [10] as,

$$G_{TX}^{Baum}(\theta, \phi) = \lim_{r \rightarrow \infty} \frac{2\pi c \sqrt{Z_c} \left\| \int r \mathbf{e}_t(\theta, \phi, t) \cdot \mathbf{l}_e dt \right\|}{\sqrt{\eta_0} \|v_g(t)\|}. \quad (2.30)$$

In (2.30), the infinity limit of $r \mathbf{e}_t(\theta, \phi, t)$ with respect to r is taken to cancel the dependency on distance, r , in the far-field zone. \mathbf{l}_e is the desired polarization vector.

- Time-domain antenna gain (Defined by Shlivinski *et al.* $G^{Shliv.}(\theta, \phi, \zeta)$ [12])

In contrary to the definitions for antenna gain given in (2.21), (2.29), and (2.29) which are all time-independent values, Shlivinski *et al.* define antenna gain as a function of time. There are two remarks to this definition:

- 1- Time-independent gain defined in (2.21) is a especial case of this time-dependent gain. If the 2-norm is used in (2.29), the new formulation gives result to it as an especial case too.
- 2- Using a time-dependent gain, a transmit-receive system can be described in the time domain as a counterpart for the radar equation in the frequency domain [12].
- 3- Definition of gain in either receive or transmit modes is proportional to the an-

tenna impulse response in that mode.

As (2.24) suggests, antenna transmitted electric field is proportional to the convolution of the antenna field factor and the generator voltage. The time-domain gain is defined such that it relates autocorrelation functions, corresponding to the transmitted electric field, $\mathbf{R}_{\mathbf{e}}(\theta, \phi, \zeta)$ ¹², and the generator voltage, $\bar{\mathbf{R}}_{v_g}(\zeta)$ as

$$\mathbf{R}_{\mathbf{e}}(\theta, \phi, \zeta) = \frac{\eta e_g}{4\pi r^2} (G_{TX}^{Shliv.}(\theta, \phi, \cdot) * \bar{\mathbf{R}}_{v_g}(\cdot))(t).^{13} \quad (2.31)$$

In (2.31), e_g is defined as,

$$e_g = \frac{1}{4} \frac{\|v_g\|^2}{Z_c}, \quad (2.32)$$

where, $\|\cdot\|$ stands for the 2-norm and Z_c is the matched generator impedance as shown in Fig. 2.2a. It can be proved¹⁴ that the auto-correlation of convolution of two functions is equal to the convolution of autocorrelation of the two. Considering equations (2.24) and (2.31) yields in an structural description for the gain as

$$G_{TX}^{Shliv.}(\theta, \phi, t) = \frac{1}{4\pi c^2} \mathbf{R}_{\mathbf{F}}^{Shliv.}(\theta, \phi, t). \quad (2.33)$$

¹²If $x(t)$ represents a function of t then its autocorrelation function, \mathbf{R}_x is defined as, $\mathbf{R}_x(\zeta)a = \int_{-\infty}^{\infty} x(t)x(t-\zeta)dt$.

¹³ $\mathbf{R}_{\mathbf{e}} = \mathbf{R}_{\mathbf{e}_x} \mathbf{a}_x + \mathbf{R}_{\mathbf{e}_y} \mathbf{a}_y + \mathbf{R}_{\mathbf{e}_z} \mathbf{a}_z$ and $\mathbf{R}_{v_g}(t) = \frac{\bar{\mathbf{R}}_{v_g}(t)}{\bar{\mathbf{R}}_{v_g}(0)}$.

¹⁴The proof is presented in appendix A.

The energy gain defined as (2.21) is now given as an especial case by

$$G(\theta, \phi) = |G_{TX}^{Shliv.}(\theta, \phi, t) * \bar{\mathbf{R}}_{v_g}(t)|_{t=0}. \quad (2.34)$$

A similar definition to (2.33) can be derived for the antenna gain in the receive mode with respect to the antenna effective height autocorrelation function.

2.2.3 Antenna Time-Domain Distortion Analysis

In the time-domain, distortion analysis is analogous to the recognition of any dissimilarity between the antenna response and the excitation waveform. In the receive mode, which describes electromagnetic field sensors for instance, the antenna's received voltage and the expected voltage are compared. Below is a summary of some distortion measures.

- Fidelity

The classical distortion analysis introduces a parameter known as “fidelity” which measures the similarity between the two waveforms [6]. For a receiving antenna, the distortion introduced by the antenna is measured by calculating the mean square error of the actual and expected waveform.¹⁵ For two signals $f(t)$ and $r(t)$, considering the time shift τ , the mean square error, d , is

$$d = \min_{\tau} \int_{-\infty}^{\infty} |\hat{r}(t + \tau) - \hat{f}(t)|^2 dt. \quad (2.35)$$

¹⁵The mean square error(MSE) is statistical difference between an estimated value and the actual value. $MSE = E[(X - X_0)^2]$ [17].

$\hat{f}(t)$ and $\hat{r}(t)$ are normalized signals defined as,

$$\hat{f}(t) = \frac{f(t)}{\sqrt{\int_{-\infty}^{\infty} |f(t)|^2 dt}} \quad (2.36)$$

$$\hat{r}(t) = \frac{r(t)}{\sqrt{\int_{-\infty}^{\infty} |r(t)|^2 dt}}. \quad (2.37)$$

Equation (2.35) can be written as,

$$d = \min_{\tau} \left[\int_{-\infty}^{\infty} |\hat{r}(t + \tau)|^2 dt + \int_{-\infty}^{\infty} |\hat{f}(t)|^2 dt - 2 \int_{-\infty}^{\infty} \hat{r}(t + \tau) \hat{f}(t) dt \right] \quad (2.38)$$

$$= \min_{\tau} [2 - 2 \int_{-\infty}^{\infty} \hat{r}(t + \tau) \hat{f}(t) dt]. \quad (2.39)$$

In (2.38), the term $\int_{-\infty}^{\infty} \hat{r}(t + \tau) \hat{f}(t) dt$ is the the cross-correlation between the two normalized signals which varies between zero and one. The more the similarity between the signals, the closer this number to unity. The fidelity is defined as the cross-correlation of the antenna output, $y(t)$, and the expected one. For an antenna as a linear system, the expected waveform is a linear transformation of the input signal provided to the antenna. If $L[x(t)]$ represents this linear transformation, then the fidelity, F is defined as [6],

$$F = \max_{\tau} \left[\int_{-\infty}^{\infty} \hat{y}(t + \tau) \hat{L}[x(t)] dt \right].^{16} \quad (2.40)$$

Instead of using a fixed definition for the reference signal, a linear transformation

¹⁶Both $y(t)$ and $L[x(t)]$ are normalized similar to equation (2.36).

of the electric/magnetic field is considered because many sensors such as \dot{D} and \dot{B} sensors deliver a time derivative version of the incident field in their output. For a single antenna, fidelity should be calculated for every single incident field waveform separately.

- Correlation pattern

A spatial distortion characteristic is introduced in [9] as the correlation pattern. The correlation pattern measures the similarity of the transmitted or received signal to a certain template signal $\mathbf{T}(\theta, \phi, t)$. It is assumed that the time and spacial coordinates are separable in the template function as,

$$\mathbf{T}(\theta, \phi, t) = T(t)\mathbf{a}(\theta, \phi, t). \quad (2.41)$$

The radiation pattern is then defined as [9],

$$RP^{corr.} = \frac{\left[\int_{-\infty}^{\infty} \mathbf{e}(\theta, \phi, t) \cdot \mathbf{a}(\theta, \phi, t) T(t) r dt \right]^2}{\eta_0 \int_{-\infty}^{\infty} |\mathbf{T}(t)|^2 r dt}. \quad (2.42)$$

Cauchy-Schwartz inequality for integrals implies the radiation pattern defined in 2.41 is always less than or equal to the radiation pattern defined in (2.17). The equality happens only if

$$\mathbf{e}(\theta, \phi, t) = T(t)\mathbf{f}(\theta, \phi) \quad (2.43)$$

where, $\mathbf{e}(\theta, \phi, t)$ is separated into product of a time-dependent function $T(t)$ and a

location-dependent function, $\mathbf{f}(\theta, \phi)$ is a spatial vector.

- Pulse width stretch ratio SR

For transmitting a pulse $s(t)$, the temporal width is defined as the time interval which contains 90% of the total pulse energy. If the normalized cumulative energy function is defined as

$$E_s(t) = \frac{\int_{-\infty}^t |s(t)|^2 dt}{\int_{-\infty}^{\infty} |s(t)|^2 dt} \quad (2.44)$$

then the signal pulse width for 90% energy $W(s)$, is obtained using,

$$W(s) = E_s^{-1}(0.95) - E_s^{-1}(0.05). \quad (2.45)$$

The stretch ratio is then defined as the transmitted electric field pulse, E_t , width to the generator voltage pulse, v_g , width as [18],

$$SR = \frac{W(e_t)}{W(v_g)}. \quad (2.46)$$

The stretch factor is calculated using the far-field transmitted electric field. It measures the distortion introduced by the antenna in the transmitted waveform which usually results in a larger temporal width.

- Subspaces Method

Eq. (2.40) shows a clear dependence upon the incident field waveform. In other

words, to compare the distortion characteristics of different antennas one has to calculate fidelity for every single time-domain waveform. This is the main motivation for the new approach given in [7]. The operation of an antenna is assumed to be a linear transformation. For every linear transformation there is a matrix representation which relates the input signal n-tuple representation to the output n-tuple representation [19]. The analysis perused in this thesis can be categorized in this class of time-domain distortion analysis. In addition to Hermite-Gauss functions used in [7], application of Laguerre functions are also studied in this thesis.

Chapter 3

Distortion Analysis Using Signal Subspaces

Distortion analysis using signal subspaces is based on the fact that an electromagnetic field sensor is a linear time-invariant system and can be viewed as a linear operator. In the linear system representation of electromagnetic field sensors, the incident electric/magnetic field waveform is the input signal and the received voltage/current is considered as the output signal. In order to find the corresponding operator for the sensor under study, one has to first define a vector space which contains the input and output signals. The other thing to be determined is whether the analysis is being done in an infinite-dimensional vector space or a finite-dimensional subspace of it. Although the methodology and problem statement are the same in both approaches, interpretation of results will be different. In this chapter, the methodology used in the rest of this thesis is described in two scenarios. The first one includes the method used in [7] using Hermite-Gauss signal subspaces.

The other method presented in this thesis relies on an infinite dimensional vector space and uses unique properties of Laguerre polynomials. Before proceeding to describe any of those approaches, a few general remarks are presented in the next section.

3.1 General Remarks

Electromagnetic field sensors are basically antennas in the receiving mode. Depending on the definition of input and output signal set, terminal impedance, and sensor polarization, different transfer functions can be defined for them in the frequency domain. The so-defined transfer function corresponds to a time-domain impulse response. As it will be shown in the following sections, the definition used for the transfer function is the focal point in the methodology used in this thesis. The following is a list of remarks and conventions used in the rest of this thesis:

- 1- The sensors are assumed to be located in the far-field zone of the electromagnetic field radiating source.
- 2- It is assumed that the sensors are terminated at 50Ω loads.
- 3- For the electric field sensors, the input signal is assumed to be the electric field waveform while the output signal is the voltage waveform received at the sensor terminals.
- 4- For the magnetic field sensors, the input signal is assumed to be the magnetic field waveform and the output is the current waveform received at the sensor terminals.
- 5- Considering the above conditions, the definitions given in Chapter 2 in (2.14) and (2.26)

are equivalent to the electric field sensor transfer function. For magnetic field sensors, a similar definition can be made replacing the electric field with the magnetic field.

6- For simplicity, the electric field sensor terminology is used in the rest of this thesis for the sake of formulation. The same arguments will be applicable to magnetic field sensors replacing the electric field with the magnetic field.

7- Sensor effective height is a vector. The spatial inner product in the frequency domain (or similarly spatial convolution in the time domain) of this vector and the incident field results in the scalar received voltage. In this thesis, sensor transfer function (sensor effective height) is considered for only one direction and that is the direction which the electric/magnetic field is polarized. This convention adds simplicity to the analysis without the loss of generality, as the frequency-domain transfer function or correspondingly the time-domain impulse response will be a scalar. Equivalently (2.14) and (2.26), vector inner product of the effective height and the electric field vector will be simplified to multiplication of magnitudes of the electric field and the effective height. It is also reasonable to study sensors only in one direction, as most of the electric field sensors are omni-directional.

8- Mathematical definition of terms which are denoted in italic letters is given in more details in Appendix B.

3.2 Finite Dimensional Analysis

The sensor as a linear system is associated with a *linear transformation*, T , which maps the electric field (input signal) to the received voltage (output signal) as,

$$T \{e_{inc}(t)\} = v_{rec}(t), \quad (3.1)$$

where, $e_{inc}(t)$ is the incident electric field and $v_{rec}(t)$ is the received voltage. As both input and output signals are finite energy signals they belong to the the set of *quadratically integrable functions* $L^2(\mathfrak{R})^1$,

$$e_{inc}(t), v_{rec}(t) \in L^2(\mathfrak{R}). \quad (3.2)$$

In linear algebra, the set of quadratically integrable functions, $L^2(\mathfrak{R})$, forms a *vector space* over the complex numbers *field*. The inner product operation for two arbitrary real functions $x(t)$ and $y(t)$ in $L^2(\mathfrak{R})$ is defined as,

$$\langle x(t), y(t) \rangle \triangleq \int_{-\infty}^{\infty} x(t)y(t)dt. \quad (3.3)$$

For an arbitrary function in $L^2(\mathfrak{R})$, $x(t)$, the *norm* is defined as,

$$\|x(t)\| \equiv \sqrt{\langle x(t), x(t) \rangle}. \quad (3.4)$$

¹ $L^2(\mathfrak{R})$ is also known as the *Lebesgue space* for $p = 2$.

3.2.1 Finite Dimensional Terminology

For every vector space, there is a set of *linearly independent* vectors, which *span* the whole space. This set is called the *basis set*. Every element in the vector space can be decomposed into a linear summation of basis vectors. For example, if the basis set is $B = \{b_1, b_2, b_3, \dots, b_i, \dots\}$, the element x in vector space V can be expressed as,

$$x = x_1 b_1 + x_2 b_2 + x_3 b_3 + \dots + x_i b_i + \dots \quad (3.5)$$

The decomposition in (3.5) is unique, meaning that $x_i|_{i=1,2,\dots}$ coefficients are unique. Therefore for every element x in the vector space V there is a vector representation as,

$$\mathbf{x} = [x_1, x_2, \dots, x_i, \dots]^t, \quad (3.6)$$

which describes the element x . In (3.6), bold letters refer to column vector and super-script t means matrix transposition. The number of basis vectors in the basis set is equivalent to the number of dimension of the space. Although $L^2(\mathfrak{R})$ is an infinite dimensional vector space, in a finite dimensional analysis, a sufficiently big *subspace* of $L^2(\mathfrak{R})$ is chosen which essentially has finite number of basis vectors. Assume that the desired N-dimensional subspace of $L^2(\mathfrak{R})$ is named V_N and it includes an approximation of $e_{inc}(t)$ and $v_{rec}(t)$

such that,

$$e_{inc}(t) = \sum_{i=1}^N e_i b_i(t), \quad (3.7)$$

$$v_{rec}(t) = \sum_{i=1}^N v_i b_i(t). \quad (3.8)$$

In (3.7), it is assumed that $B = \{b_1, b_2, b_3, \dots, b_N\}$ spans V_N . It is also notable that vector representation for $e_{inc}(t)$ and $v_{rec}(t)$ are actually n -tuple representations,

$$\mathbf{e}_{inc} = [e_1, e_2, \dots, e_N]^t, \quad (3.9)$$

$$\mathbf{v}_{rec} = [v_1, v_2, \dots, v_N]^t. \quad (3.10)$$

3.2.2 Linear-Operator Representation of Sensors

A *Linear operator* is basically the matrix representation for a linear transformation. Eq. (3.1) is expressed in an N -dimensional subspace of $L^2(\mathfrak{R})$ as,

$$T : \mathbf{e}_{inc} \mapsto \mathbf{v}_{rec}. \quad (3.11)$$

For every linear transformation, there is a matrix which relates the *domain subspace* to the *range subspace* [19], [20]. For the case of a sensor, the domain and the range subspaces are both an N -dimensional subspace of $L^2(\mathfrak{R})$. Therefore, there exists an $N \times N$ matrix, known as the transformation matrix \mathbf{L} , which gives the N -tuple representation of the received voltage \mathbf{v}_{rec} , when it is multiplied by the vector representation of the incident

electric field \mathbf{e}_{inc} as,

$$\mathbf{v}_{rec} = \mathbf{L} \cdot \mathbf{e}_{inc}. \quad (3.12)$$

Calculation of transformation matrix is dependent on the choice of the basis sets for the domain and range subspaces. For the electric field sensor with linear transformation T , both subspaces are assumed to be the same with one similar set of basis set $B = \{b_1, b_2, \dots, b_N\}$. The ij element of matrix $\mathbf{L} = [l_{ij}]_{i,j=1,2,\dots,N}$, l_{ij} is calculated as [20],

$$l_{ij} = \langle T(b_j(t)), b_i(t) \rangle. \quad (3.13)$$

The sensor linear transformation can be stated as a convolution with the sensor impulse response in the direction of the electric field polarization or,

$$v_{rec}(t) = h(t) * e_{inc}(t), \quad (3.14)$$

and, (3.13) can be written as,

$$l_{ij} = \langle h(t) * b_j(t), b_i(t) \rangle, \quad (3.15)$$

where, h is the component of the sensor effective height which is parallel to the electric field.

3.2.3 Calculation of the Transformation Matrix

Eqs. (3.13) and (3.15) can be summarized in the following steps:

- 1- A set of basis functions should be selected.
- 2- N-tuple representation of sensor response to the i^{th} basis vector forms the i^{th} column in the transformation matrix.

3.2.4 Distortion Analysis

In this thesis, distortion is defined as any unsimilarity between the received voltage and the expected voltage for a particular incident electric field. To carry out a finite dimensional distortion analysis using signal subspaces one has to choose a subspace with sufficiently large number of dimensions. The number of dimensions is selected so that signals with a minimum risetime can be approximated by the basis functions expansion. When the basis functions are set the following steps can be followed:

- 1- A reference sensor which ideally delivers the expected signal is selected. The reference transformation matrix, \mathbf{R} , is calculated. In many cases, it is desired to have the similar waveforms in the received voltage and the incident field. This is the case for identity linear transformation which corresponds to an $N \times N$ identity matrix, \mathbf{I}_N . There are also cases where it is possible to find an inverse transformation for the reference system. Applying the inverse transformation on the sensor linear transformation, one can compare the results to the identity system. A common example is the \dot{D} sensor. Rather than

comparing the transformation matrix for a \dot{D} sensor and an ideal differentiator, one can calculate the transformation matrix for the integrated voltages and compare the obtained matrix to the identity matrix.

2- In calculating the transformation matrix, the response of the sensor (or alternatively the desired transformation of response of the sensor) to each basis vector should be normalized to its norm as defined in (3.4). This is also the case for calculating the transformation matrix for the ideal sensor. This is the approach in [7] to focus on the shape of the signals only and not on the sensitivity of the sensors.

3- The actual and reference transformation matrices are being compared. A more detailed comparison scheme is presented in the next chapter. The main comparison tool would be the norm of difference of the matrices. *Frobenius norm* or the *HilbertSchmidt* norm is selected among other possible matrix norms [7], [20]. In [7], the distortion measure is defined as,

$$\eta_N = \frac{\|\mathbf{L} - \mathbf{R}\|_F}{\sqrt{N}}, \quad (3.16)$$

where, sub-script F stands for Frobenius norm and \mathbf{R} is the reference transformation matrix. Frobenius norm of an $M \times N$ matrix such as $\mathbf{A} = [a_{ij}]_{1 \leq i \leq M, 1 \leq j \leq N}$ is calculated as,

$$\|\mathbf{A}\|_F = \sqrt{\sum_{j=1}^N \sum_{i=1}^M a_{ij}^2}. \quad (3.17)$$

If the reference matrix \mathbf{R} is the identity matrix \mathbf{I}_N then the above equation is simplified to,

$$\eta_N = \sqrt{1 + \frac{\text{tr}(\mathbf{L}\mathbf{L}^H) - 2\text{tr}(\mathbf{L})}{N}}. \quad (3.18)$$

In (3.18), $\text{tr}(\cdot)$ stands for trace of the matrix or the summation of diagonal elements. The superscript H stands for transpose-conjugate operator. The proof of (3.18) is presented in Appendix C. Because of normalization used in calculating the transformation matrices, η_N varies between 0 to $\sqrt{2}$. The maximum value corresponds to the maximum difference between the matrices and hence the maximum distortion. One can use the distortion measure given in (3.16) to obtain the distortion characteristics for a subspace of incident electric fields. This approach has the following advantages over the classical fidelity analysis:

- 1- The value of fidelity is dependent on the incident field waveform. When two or more sensors are being compared one has to calculate the value of fidelity for all of the possible incident field waveforms for all of the sensors [7].
- 2- Using proper basis sets, different rows and columns on the transformation matrix can be interpreted differently in terms of bandwidth/risetime.

3.2.5 Hermite-Gauss Functions as the Basis Vectors

Hermite-Gauss functions form a complete basis set for $L^2(\mathfrak{R})$. Hermite-Gauss functions are the result of a Gram-Schmidt² procedure on Gaussian functions [21], [22]. They have many interesting properties which are discussed in Appendix D in more details. The following properties make Hermite-Gauss functions attractive for being used as the basis set in finite-dimensional analysis:

1- Hermite-Gauss functions of orders zero to N-1 form an N dimensional basis set for a subspace of $L^2(\mathfrak{R})$ which has a specific bandwidth. The relation of the order of Hermite-Gauss functions to the bandwidth will be given in the next chapter.

2- Hermite-Gauss functions are the eigenfunctions of the Fourier transform [23]. This means that their Fourier transform has the same form as the time-domain signal [24]. This makes it possible to calculate the transformation matrix from data collected in one set of measurement as it will be shown in Chapter 5.

Interpretation of the transformation matrix when Hermite-Gauss functions are used is described in Chapter 4.

3.3 Infinite Dimensional Analysis

In this approach, the sensor is assumed to be a linear operator which maps an *infinite-dimensional* domain vector space space to an infinite dimensional range vector space [25].

²Is employed to obtain orthogonal functions from a set of non-orthogonal functions.

A infinite dimensional vector space is defined similar to a finite dimensional vector space.

In addition, the following properties hold [25]:

- 1- The basis set has infinite number of vectors. In other words, it is denumerable.³
- 2- The linear decomposition for every arbitrary signal has the form of (3.5) and is an infinite series expansion.
- 3- The vector representation for the functions in an infinite-dimensional vector space would be a column matrix with infinite number of rows. The entries are decomposition coefficient just as in (3.6).
- 4- The transformation matrix would have the same definition as the it has in an N-dimensional vector space. The matrix is not bounded.

$L^2(\mathfrak{R})$ is an infinite-dimensional vector space, however vector norms are all bounded due to the definition for norm of a vector in (3.4) and the definition of $L^2(\mathfrak{R})$ which is the set of quadratically integrable functions.

3.3.1 Distortion Analysis Using Laguerre Functions

Unlike finite-dimensional analysis, a norm of distance measure as in (3.16) is not practical to calculate for a transformation matrix with infinite numbers of rows and columns, in the general case. However, it is possible to choose a set of basis functions which their associated transformation matrix has a predictable pattern. Interestingly, this is the case when Laguerre polynomials are used. In the next chapter, it is shown how a distortion

³A denumerable set is a set which has infinite number of members but is countable.

measure is extracted from a transformation matrix calculated using Laguerre functions.

Laguerre functions and their properties are discussed in Appendix E.

Chapter 4

Interpretation of the Transformation Matrix

As given in (3.16), the norm of the distance matrix is a measure of the distortion introduced by the sensor when the analysis is performed in a finite-dimensional vector space. In infinite-dimensional analysis the matrix norm should be calculated too. One should be able to relate this distortion measures to different risetimes/bandwidths of the incident field waveform. This spectral interpretation is completely dependent on the choice of the basis set. In addition, the choice of basis set is crucially important in infinite-dimensional analysis. A proper basis set should be selected in order to be able to calculate the norm of an unbounded distance matrix.

In the first section of this chapter, interpretation of the transformation matrix is described when Hermite-Gauss functions are used as the basis set. In the second section, distortion

analysis in an infinite-dimensional vector space is described based on Laguerre functions.

Along with each analysis, simulated examples are provided.

4.1 Finite-Dimensional Analysis

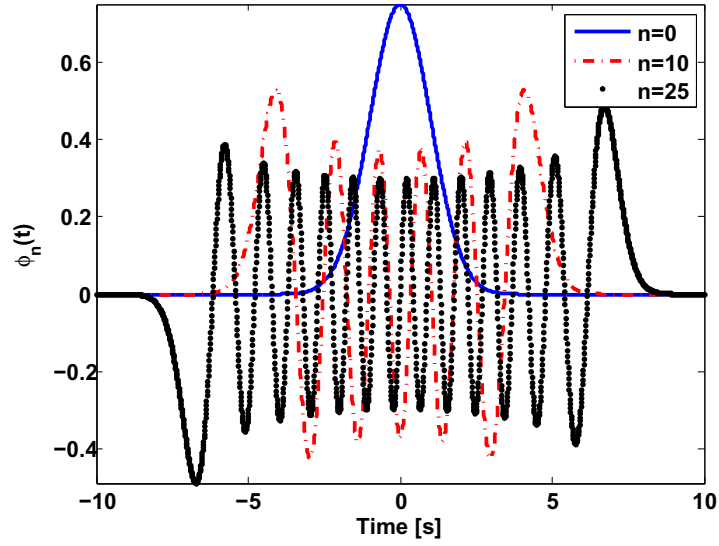
In the finite-dimensional distortion analysis as described in section 3.2, a basis set with finite number of basis vectors is chosen. The distortion analysis is performed for the subspace of incident field waveforms which is spanned by the basis set. If the basis vectors are Hermite-Gauss functions of orders 0 to $N - 1$ then the spanned subspace contains waveform with risetimes bigger than a certain value. This is a consequence of Hermite-Gauss functions properties in the time and frequency domain. Hermite-Gauss functions and their properties are reviewed in Appendix D in detail. A summary is given in the following section.

4.1.1 Hermite-Gauss Functions

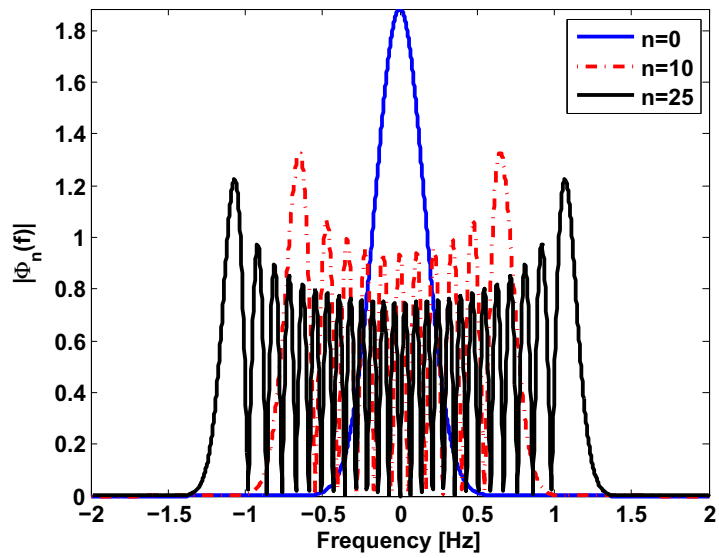
Hermite-Gauss functions are the solution for Schrodinger equation [26]. The n^{th} order Hermite-Gauss function $\phi_n(t)$, is given by,

$$\phi_n(t) = \frac{1}{\sqrt{\sigma n! 2^n \sqrt{\pi}}} e^{-\frac{(t/\sigma)^2}{2}} H_n\left(\frac{t}{\sigma}\right), \quad (4.1)$$

where, $H_n(t)$ is the n^{th} order Hermite polynomial [27], and σ is the scaling factor which shrinks and expands the waveform. Different orders of Hermite-Gauss functions are shown



(a)



(b)

Figure 4.1: Hermite-Gauss functions for different orders and $\sigma = 1$ in a) the time domain and, b) the frequency domain.

in Figs. 4.1a and 4.1b in the time and frequency domains, respectively.

Hermite-Gauss functions have many interesting properties including:

- Hermite-Gauss functions form a complete basis set for $L^2(\mathfrak{R})$ [28].
- Hermite-Gauss functions are eigenfunctions of the Fourier transform [23]. In other words, if $\Phi_n(j2\pi f)$ stands for the Fourier transform of the n^{th} Hermite-Gauss function, $\phi_n(t)$, then we can write:

$$\Phi_n(j2\pi f) = \frac{1}{2\pi\sigma} (-j)^n \phi_n(f\sigma). \quad (4.2)$$

- Hermite-Gauss functions form an orthonormal basis set for frequency domain functions with finite energies.

Proof:

If $x(t) \in L^2(\mathfrak{R})$ and $x(t) = \sum_{k=0}^{N-1} x_k \phi_k(t)$ then taking the Fourier transform of $x(t)$, yields,

$$X(f) = \sum_{k=0}^{N-1} \frac{(-j)^k}{2\pi\sigma} x_k \phi_k(f), \quad (4.3)$$

where, Fourier transform of the basis functions are replaced from (4.2). The arbitrary frequency-domain function $X(f)$, is a linear summation of mutually orthogonal ϕ_k s. Therefore Hermite-Gauss functions form an orthonormal basis set for frequency-domain functions as well.

- Signals N-tuple representations are related in the time and frequency domains.

When an arbitrary function such as $x(t)$ is expanded in terms of Hermite-Gauss functions, it is associated with an N-tuple vector representation $[x_1, x_2, \dots, x_N]^t$ as given in (3.6). The Fourier transform of the signal $X(f)$ is also associated with an N-tuple representation such as $[\hat{x}_1, \hat{x}_2, \dots, \hat{x}_N]^t$. The time and frequency domain vector representations are related as,

$$\hat{x}_k = \frac{(-j)^k}{2\pi\sigma} x_k \quad 1 \leq k \leq N. \quad (4.4)$$

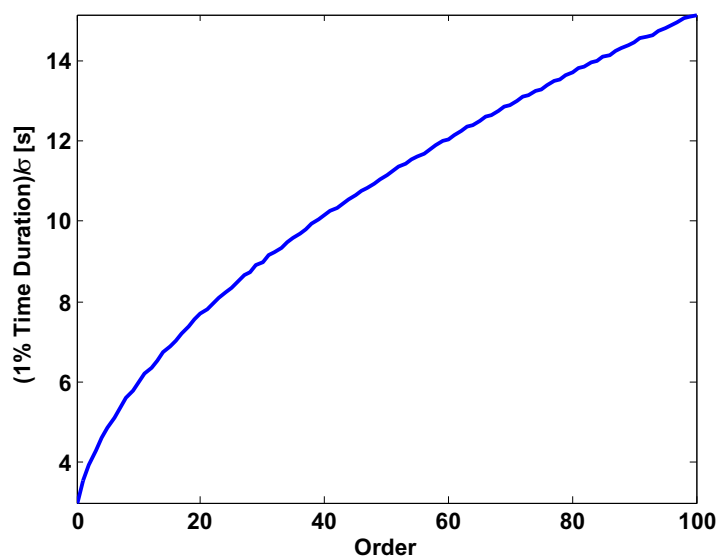
Applying the Fourier transform and its inverse on signals is then possible using this property. This is particularly used when calculating the transformation matrix using the measurement data.

- Hermite-Gauss signals have time durations which increases with the order.

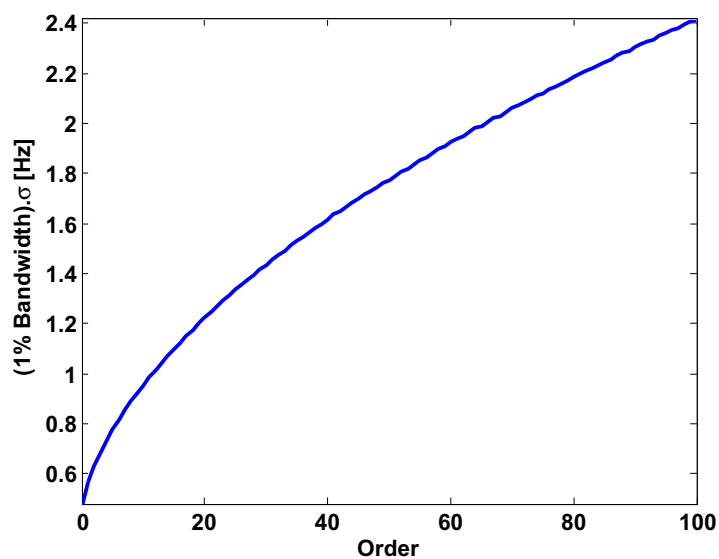
Fig. 4.2a shows the time duration where the amplitude of the pulses falls to one percent of the maximum value for different orders when a scaling factor of $\sigma = 1$ is selected. As it is seen the time duration increases when the order of Hermite-Gauss functions increases.

- Hermite-Gauss signals cover frequency ranges which increase with the order.

As Hermite-Gauss functions are eigenfunctions of the Fourier transform, they have a similar shape in the time and frequency domains. The frequency range where the



(a)



(b)

Figure 4.2: Variation of a) the time duration where time-domain Hermite-Gauss functions fall to 1% of their maximum and, b) the frequency range where the magnitude of the Fourier transform of Hermite-Gauss functions fall to 1% of their maximum, when $\sigma = 1$ is selected.

magnitude of Hermite-Gauss frequency domain functions falls to 1 percent of its maximum value is shown in Fig. 4.2b. Similar to the graph in Fig. 4.2a, this graph is calculated and plotted for a scaling factor of $\sigma = 1$. When N , or the number of Hermite-Gauss functions is selected, one can find the proper scaling factor such that the highest order covers the desired frequency range.

4.1.2 Selection of a Proper Scaling Factor

With an arbitrary scaling factor, Hermite-Gauss functions, form a complete basis set for $L^2(\mathfrak{R})$. However the choice of the scaling factor is important in order to be able to approximate a time-domain function with a limited time duration and bandwidth¹ with a reasonable number of basis functions. If the scaling factor is too big, then a very large number of basis functions will be needed to capture the variations. When the scaling factor is too small, the time duration of the basis functions will be too small comparing to the time duration of the signal. Therefore, a large number of basis functions will be needed in order in order to reconstruct the signal from the coefficients.

If the time-domain signal $x(t)$ has the time duration of τ and bandwidth BW , then the N^{th} basis function should cover the signal in both the time and frequency domains. Let's assume that $D_\tau(n)$ and $D_{BW}(n)$ are the functions plotted in Figs. 4.2a and b where n is the order. For a scaling factor of σ the time duration and frequency range covered by the

¹Precisely speaking, it is not possible to have a signal which covers limited ranges in the time and frequency domains. However, by limited bandwidth we mean the range of frequencies which the magnitude of the function Fourier transform falls to a percentage of its maximum value [29].

n^{th} basis function would be $D_\tau(n)\sigma$ and $D_{BW}(n)/\sigma$, respectively. If the expansion has N terms, then in order for the N^{th} Hermite-Gauss function to cover the signal in the time and frequency domains we should have,

$$\tau \leq D_\tau(N-1)\sigma, \quad (4.5)$$

$$BW \leq \frac{D_{BW}(N-1)}{\sigma}. \quad (4.6)$$

As Hermite-Gauss functions are related as (4.2) in the time and frequency domains, we have,

$$D_\tau(n) = \frac{1}{2\pi} D_{BW}(n). \quad (4.7)$$

Combining (4.5) to (4.7) yields,

$$\frac{1}{2\pi D_{BW}(N-1)} \leq \frac{\sigma}{\tau} \leq \frac{D_{BW}(N-1)}{BW\tau}. \quad (4.8)$$

The product τBW is called the time-bandwidth product of the signal, which is a different value for every time-domain signal. It also varies according to the definitions used for the time and frequency durations.

For a time-domain signal $x(t)$ with the Fourier transform $X(f)$, the time-domain variance around the mean value α is given as [30],

$$\sigma_t = \sqrt{\int_{-\infty}^{\infty} (t - \alpha) |x(t)|^2 dt}. \quad (4.9)$$

A similar quantity is defined in the frequency domain as the frequency domain variance around the mean value β as,

$$\sigma_f = \sqrt{\int_{-\infty}^{\infty} (f - \beta) |X(f)|^2 df}. \quad (4.10)$$

Heisenberg uncertainty principle states that [30],

$$\sigma_t \sigma_f \geq \frac{1}{4\pi}. \quad (4.11)$$

If the time duration and the frequency range is defined so that they are greater than the signal variances in the time and frequency domain or,

$$\tau \geq \sigma_t, \quad (4.12)$$

$$BW \geq \sigma_f, \quad (4.13)$$

then, one can use (4.11) to conclude

$$\frac{1}{2\pi D_{BW}(N-1)} \leq \frac{\sigma}{\tau} \leq 4\pi D_{BW}(N-1). \quad (4.14)$$

Although the upper limit in (4.14) is higher than the upper limit in (4.8), but (4.14) can be used as a rule of thumb to pick the proper value of the scaling factor σ .

4.1.3 Distortion Analysis in a Certain Frequency Range

Fig. 4.1b shows magnitude of the Fourier transform of Hermite-Gauss functions. From the figure it is observed that:

- 1- Hermite-Gauss functions are base-band signals.
- 2- Every order covers the frequency range which is shown in Fig. 4.1b.

For a distortion analysis in an N -dimensional subspace spanned by Hermite-Gauss functions V_N , one should first select a proper value for the scaling factor using Fig. 4.1b which gives the desired bandwidth for the maximum number of dimensions N . N should have been chosen beforehand for a reasonable resolution. The transformation matrix is calculated as given in (3.13) to (3.15). With a selected scaling factor σ , the i^{th} column of the transformation matrix means how the sensor performs when the incident electric field has the frequency contents of the i^{th} order Hermite-Gauss function. If the transformation matrix is $\mathbf{L} = [l_{ij}]_{1 \leq i, j \leq N}$, then $M \times M$ diagonal block sub-matrices of \mathbf{L} such as $\mathbf{L}_M = [m_{ij}]_{1 \leq i, j \leq M}$ and,

$$m_{11} = l_{kk} \quad 1 \leq k \leq N, \quad (4.15)$$

describe the sensor performance in an $M \times M$ subspaces of V_N when the incident field has the frequency content of BW_E , where,

$$BW_k \leq BW_E \leq BW_{k+M}. \quad (4.16)$$

BW_k and BW_{k+M} are frequency ranges covered by the k^{th} and $(k+M)^{th}$ Hermite-Gauss functions.² Recognizable diagonal block sub-matrices with the condition of (4.15), can be extracted from the transformation matrix. These sub-matrices should be compared to proper reference matrices. The following examples illustrate the method more clearly.

4.1.4 Examples

In this section, the transformation matrix for an ideal differentiator, a lowpass, a bandpass, and a highpass filter are calculated. The transformation matrices are illustrated as two-dimensional graphs. The norm of the distance matrices are also calculated as a measure of distortion.

An Ideal Differentiator

The associated transformation matrix of an ideal differentiator is given by,

$$T_D(x(t)) = \frac{dx(t)}{dt}, \quad (4.17)$$

where $x(t)$ is a real function in $L^2(\mathfrak{R})$ spanned by Hermite-Gauss functions as,

$$x(t) = \sum_{k=0}^{N-1} x_k \phi_k(t). \quad (4.18)$$

²It is assumed that $1 \leq k \leq N - M$.

In Appendix D it is proven that,

$$\frac{d\phi_n(t)}{dt} = \sqrt{\frac{n}{2\sigma^2}}\phi_{n-1}(t) - \sqrt{\frac{n+1}{2\sigma^2}}\phi_{n+1}(t) \quad n \geq 1. \quad (4.19)$$

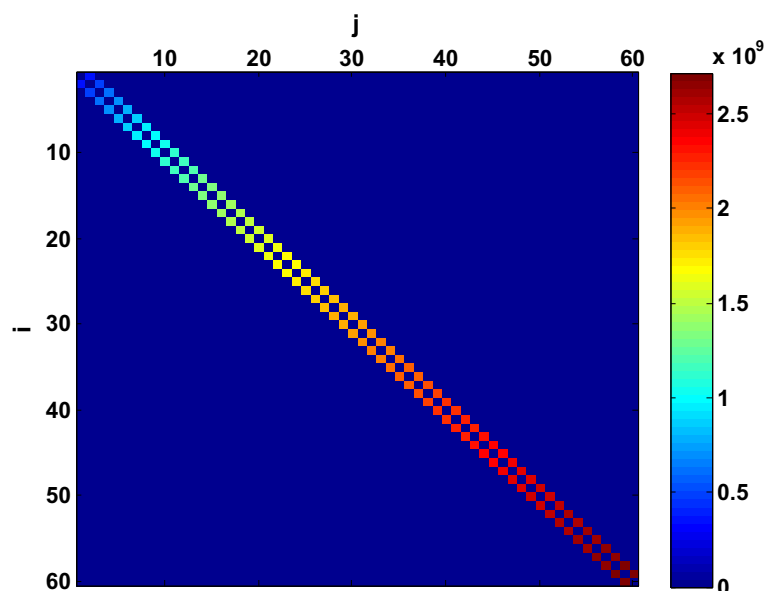
For $\phi_0(t)$ we have,

$$\frac{d\phi_0(t)}{dt} = -\sqrt{\frac{1}{2\sigma^2}}\phi_1(t). \quad (4.20)$$

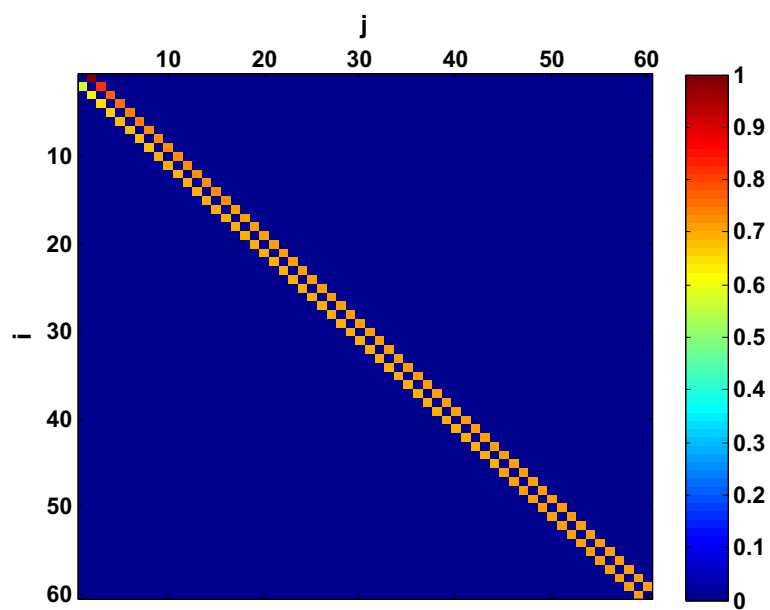
Therefore the transformation matrix for an ideal differentiator is a matrix with diagonal elements equal to zero. On the n^{th} column, the elements immediately above and below of the diagonal element will have values of $\sqrt{\frac{n}{2\sigma^2}}$ and $-\sqrt{\frac{n+1}{2\sigma^2}}$, respectively. The transformation matrix calculated for the ideal differentiator is shown in Fig. 4.3a. The transformation when every column is normalized, is shown in Fig. 4.3b. A scaling factor of $\sigma = 2$ ns is used for calculating the matrices.

Lowpass, Bandpass, and Highpass Filter

Transformation matrices are calculated for a lowpass filter and a highpass filter with cut-off frequencies of 500 MHz along with a bandpass filter with a passband of $400MHz \leq f \leq 600MHz$. The scaling factor is $\sigma = 2$ ns which corresponds to a 1-GHz bandwidth for the order of 60 in Hermite-Gauss functions as shown in Fig. 4.2b. The transformation matrices are shown in Figs. 4.4-4.6 for the lowpass, highpass, and bandpass filters, respectively. Lowpass filter transformation matrix is diagonal up to the 20^{th} row and column which is corresponding to 500 MHz bandwidth for Hermite-Gauss functions with



(a)



(b)

Figure 4.3: Transformation matrices calculated for an ideal differentiator with $\sigma = 2ns$ for a) normalized outputs, b) unnormalized outputs.

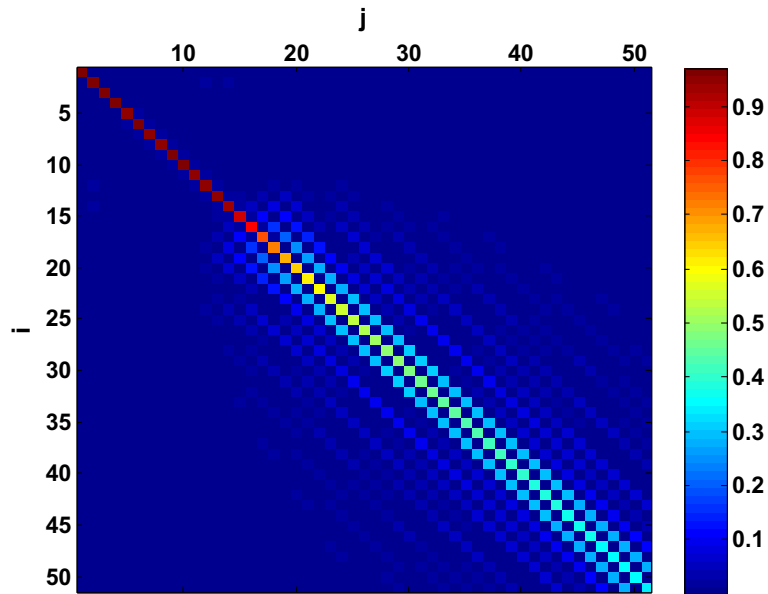


Figure 4.4: Transformation matrix calculated for a lowpass filter with a cut off frequency of 500 MHz using $\sigma = 2$ ns.

$\sigma = 2$ ns. The elements on the 30×30 sub-matrix starting at the 20^{th} diagonal element tend to vanish. An opposite behavior is recognized in the highpass filter transformation matrix in Fig. 4.5 as the upper 20×20 sub-matrix is nearly zero and the matrix tends to be more diagonal in the last rows and columns. Finally, the elements on the band-pass filter transformation matrix shown in Fig. 4.6 are negligible before the 20^{th} row and column and after the 30^{th} row and column which matches the filter pass band.

Comparing Lowpass filters with different cut-off frequencies

A lowpass filter with a nearly flat frequency response can be viewed as an identity system in its passband but distorts the signals which have frequencies higher than its cut-off frequency. Therefore a lowpass filter transformation matrix should be compared with an

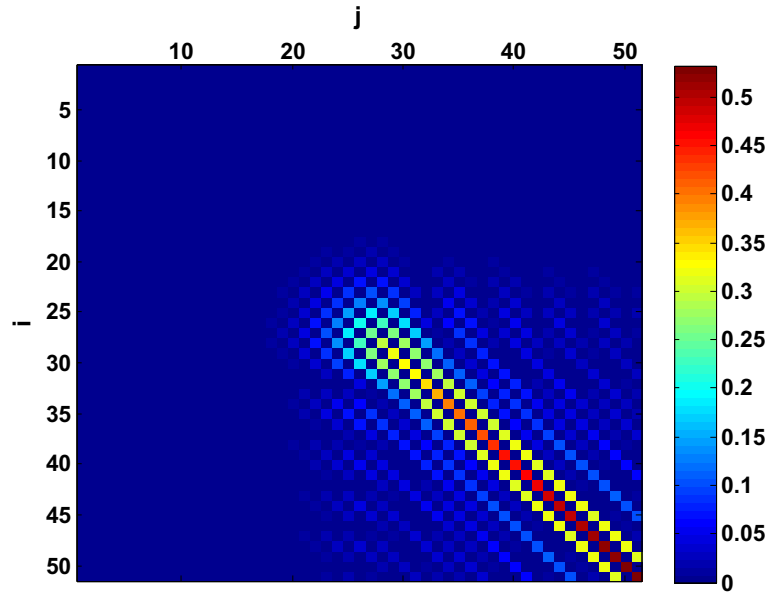


Figure 4.5: Transformation matrix calculated for a highpass filter with a cut off frequency of 500 MHz using $\sigma = 2$ ns.

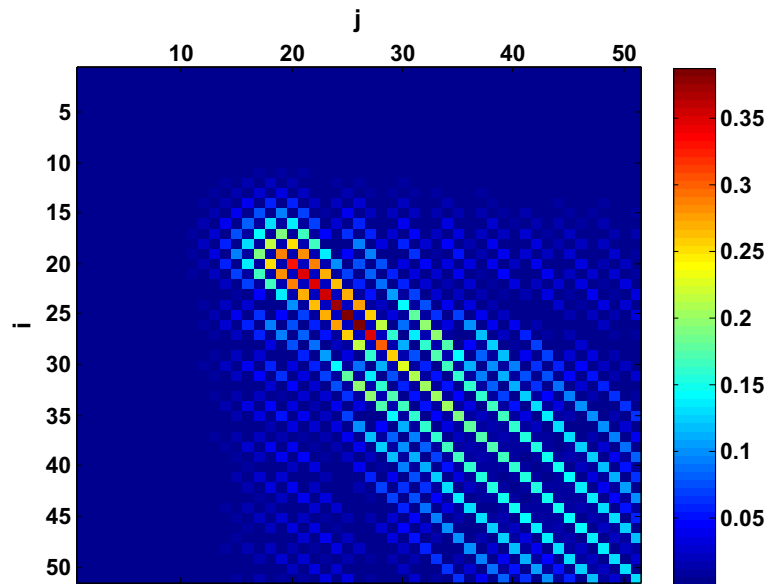


Figure 4.6: Transformation matrix calculated for a bandpass filter with a passband frequencies larger than 400 MHz and smaller than 600 MHz using $\sigma = 2$ ns.

identity matrix. Fig. 4.7 shows the norm of the distance matrix η_N , calculated for the different cutoff frequencies. The norm of the distance matrix is calculated using (3.18) using a scaling factor of $\sigma = 2 ns$ when a 51-dimensional subspace is selected. The filters all have 1 dB ripple in the pass band and the minimum loss in the stop band is set to be 80 dB. For a value of σ , depending on the number of dimensions, the calculated transformation matrix covers different frequency ranges, therefore the calculated η_N would be different. Calculated matrix norms are shown in Fig. 4.7 with respect to the filter cut-off frequency for three choice of $N = 10, 30, \text{ and } 51$, which cover frequency ranges up to 250, 600, and 1000 MHz, respectively. This figure shows how the distortion decreases as the cut-off frequency increases. It also demonstrates selecting a higher N increases the frequency scope of the analysis and yields larger values for η_N . A smaller number of N would mean that the distortion analysis is valid for a smaller subspace of input signals.

4.2 Infinite-dimensional Analysis

When the incident field subspace has infinite number of dimensions, infinite number of basis functions would be needed to approximate any waveform in the subspace. This means that vector representations have infinite number of elements. For the sensor under study, the transformation matrix is still calculated using (3.13) and (3.15) but is unbounded. Calculating the Frobenius norm of an unbounded matrix in the general case is not practical. However, if the matrix follows a certain pattern, it is possible to compare

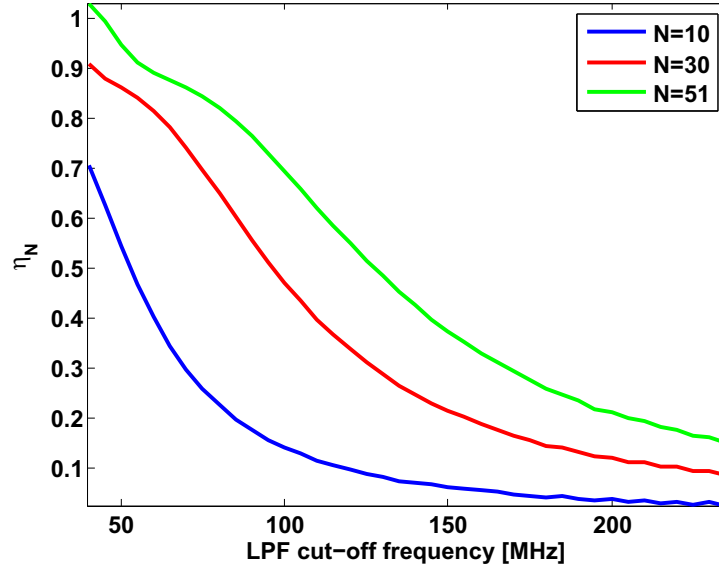


Figure 4.7: Variation of the calculated η_N for three different values of N using $\sigma = 2$ ns, for lowpass filters with respect to the lowpass filter cut-off frequency .

the transformation matrix with a reference transformation matrix. In this chapter, it is shown how Laguerre functions are used to form the transformation matrix. The unique property of Laguerre functions in preserving convolution is used to calculate the norm of an unbounded matrix. Using the approach that is described later, one can find a structural measure of distortion related to the sensor impulse response which is calculable in analytically. The link between the distortion measure obtained from this analysis and the frequency content or risetime of the incident field is presented as well. Finally, an example describes the method more clearly.

4.2.1 Laguerre Functions

Laguerre functions are defined as [31],

$$l_n^p(t) = (-1)^n \sqrt{2p} L_n(2pt) e^{-pt} \quad t \geq 0, \quad (4.21)$$

where, p is a parameter controlling the function duration in the time domain so that $1/p$ is the function scaling factor. $L_n(t)$ is the n^{th} order Laguerre polynomial given by [32],

$$L_n(x) = \sum_{k=0}^n \binom{n}{k} \frac{(-x)^k}{k!} \quad n = 0, 1, 2, \dots \quad (4.22)$$

Fig. 4.8 shows Laguerre functions for different orders assuming $p = 1$. Laguerre functions have many interesting properties including:

- The set of $B = \{l_n^p(t)\}_{n=0,1,2,\dots}$ forms a complete orthonormal set for $L^2([0, \infty))^3$ [33]. Orthonormality means,

$$\int_0^\infty l_n^p(t) l_m^p(t) dt = \delta_{n,m}, \quad (4.23)$$

where $\delta_{n,m}$ is the Kronecker delta function which has the value of 1 only if $n = m$, otherwise it is zero.

³ $L^2([0, \infty))$ is the set of all real causal quadratically integrable functions.

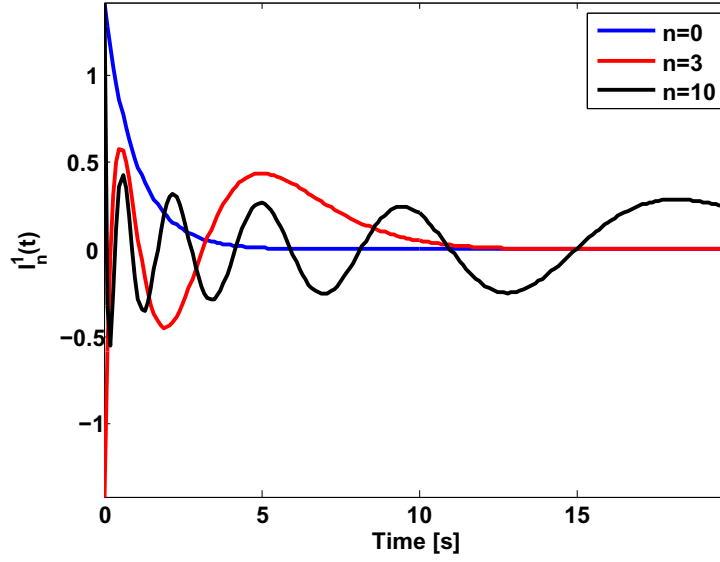


Figure 4.8: Different orders of Laguerre functions for $p=1$.

- The time duration in which Laguerre functions fall to one percent of their maximum approximately varies linearly with the order of functions. Fig. 4.9 shows the time duration calculated for $p = 1$.
- The Laplace transform of the n^{th} order Laguerre function is [24], [31],

$$\hat{l}_n^p(s) = \sqrt{2p} \frac{(p-s)^n}{(p+s)^{n+1}} \quad s \in \mathbb{C}, s \neq -p. \quad (4.24)$$

Therefore the Fourier transform of $l_n^p(t)$ shown as $L_n^p(j\omega)$ is given by,

$$L_n^p(j\omega) = \sqrt{2p} \frac{e^{-j(2n+1)\tan^{-1}(\frac{\omega}{p})}}{\sqrt{\omega^2 + p^2}}. \quad (4.25)$$

From (4.25) it is observed that the magnitude of the Fourier transform of Laguerre

functions is the same for any order of the function. This means that frequency contents of all the basis functions are the same. The frequency which the magnitude of $L_n^p(j\omega)$ falls to 10 percent of its maximum value is calculated using,

$$f_{10\%} = 1.59p. \quad (4.26)$$

Fig. 4.9b shows the magnitude of $L_n^p(j\omega)$ for $p = 1$. Laguerre functions can be assumed as baseband signals with a 10 dB frequency range of $f_{10\%}$.

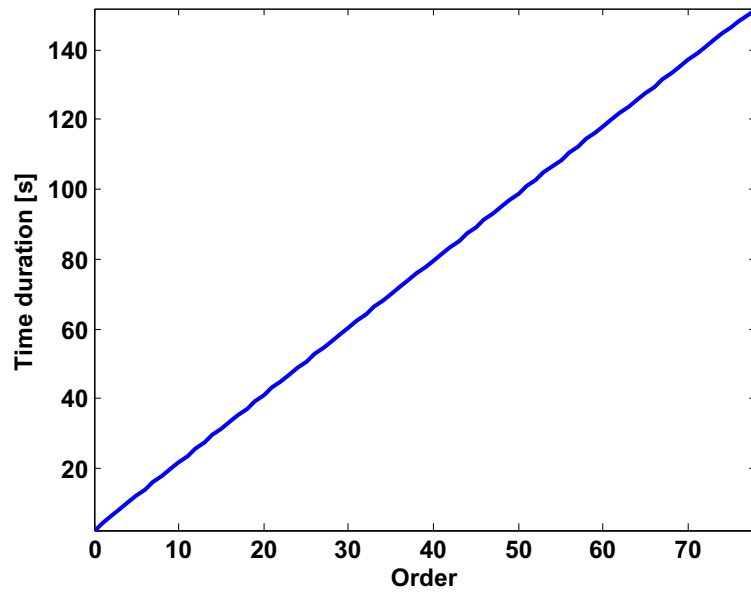
- Convolution of Laguerre functions is written as a summation of Laguerre functions [31],

$$l_n^p(t) * l_m^p(t) = \frac{1}{\sqrt{2p}} [l_{n+m}^p(t) + l_{n+m+1}^p(t)]. \quad (4.27)$$

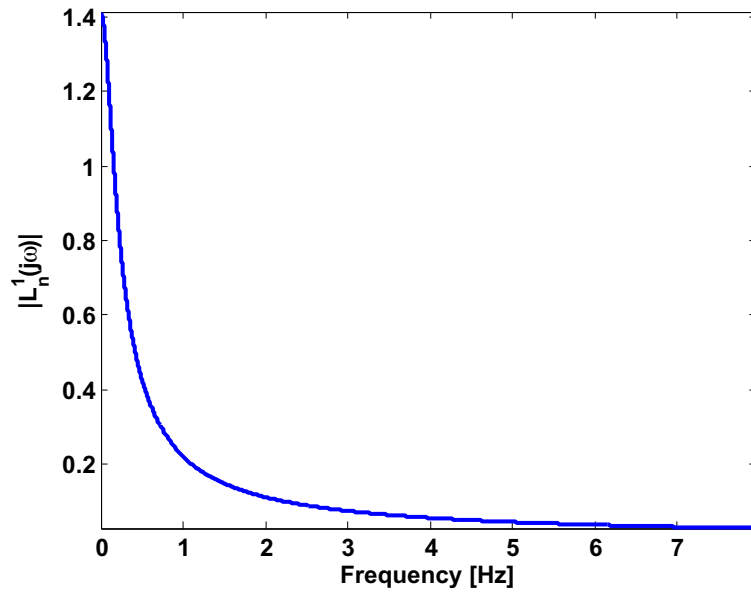
This is an extremely significant property which makes it possible to simplify the transformation matrix in terms of the sensor impulse response. The idea is described in more details in the next section.

4.2.2 Transformation Matrix Calculated in Laguerre Subspace

When the basis set is selected to be a set of Laguerre functions of different orders $\{l_n^p(t)\}_{n=0,1,2}$ as given in (4.21), the transformation matrix has a certain pattern. Similar to the finite-dimensional analysis (3.15), the unbounded transformation matrix $\mathbf{L} =$



(a)



(b)

Figure 4.9: Variation of a) time duration where Laguerre functions fall to 1% of the maximum with respect to the order and, b) magnitude of the Fourier transform of Laguerre functions with respect to the frequency.

$[l_{ij}]_{i,j=1,2,\dots}$, is calculated in a Laguerre subspace using,

$$l_{ij} = \left\langle h(t) * l_{(j-1)}^p(t), l_{(i-1)}^p(t) \right\rangle \quad i, j \geq 1, \quad (4.28)$$

where h is the system impulse response. In case of an electric field sensor, it is the component of sensor effective height as defined in (2.26) which is parallel to the incident field. Since the effective height $h(t)$ is a causal time-domain signal with finite energy it can be expressed in terms of the basis functions as,

$$h(t) = \sum_{k=0}^{\infty} h_k l_k^p(t). \quad (4.29)$$

Substituting (4.29) in (4.28) and exchanging the summation and the inner product results in,

$$l_{ij} = \sum_{k=0}^{\infty} h_k \left\langle l_k^p(t) * l_{(j-1)}^p(t), l_{(i-1)}^p(t) \right\rangle \quad i, j \geq 1, k \geq 0. \quad (4.30)$$

Using Laguerre convolution property given in (4.27), (4.30) can be written as,

$$l_{ij} = \frac{1}{\sqrt{2p}} \sum_{k=0}^{\infty} h_k \left\langle l_{k+j-1}^p(t), l_{(i-1)}^p(t) \right\rangle + \frac{1}{\sqrt{2p}} \sum_{k'=0}^{\infty} h_{k'} \left\langle l_{k'+j}^p(t), l_{(i-1)}^p(t) \right\rangle. \quad (4.31)$$

Due to orthogonality of Laguerre function (4.23), (4.31) is simplified to,

$$l_{ij} = \frac{1}{\sqrt{2p}} \sum_{k=0}^{\infty} h_k \delta_{k+j-1, i-1} + \frac{1}{\sqrt{2p}} \sum_{k'=0}^{\infty} h_{k'} \delta_{k'+j, i-1}. \quad (4.32)$$

To avoid zero values for delta function in (4.32),

$$k = i - j, \quad (4.33)$$

$$k' = i - j - 1. \quad (4.34)$$

Considering $k, k' \geq 0$, we can write (4.32) in a more compact form as,

$$l_{ij} = \frac{1}{\sqrt{2p}}(h_{i-j}u(i-j) + j_{i-j-1}u(i-j-1)), \quad (4.35)$$

where $u(\cdot)$ is a unit step function which is zero for negative arguments and is equal to one for arguments greater than or equal zero. The following properties result from (4.35):

- The diagonal elements are all equal to each other and have the value of $\frac{1}{\sqrt{2p}}h_0$.
- For $i < j$ both $u(i-j)$ and $u(i-j-1)$ vanish. In other words the elements above the matrix diagonal are all zero.
- The first column \mathbf{L}_1 has the form of,

$$\mathbf{L}_1 = [h_0, h_0 + h_1, h_1 + h_2, \dots, h_i + h_{i+1}, \dots]^t. \quad (4.36)$$

- Careful consideration of (4.35) reveals that different columns in the transformation matrix are shifted version of the first column. Precisely speaking, the j^{th} column

$$\mathbf{L} = \frac{1}{\sqrt{2^p}} \begin{pmatrix} h_0 & 0 & 0 & 0 & 0 & 0 & \dots \\ h_1 + h_0 & h_0 & 0 & 0 & 0 & 0 & \dots \\ h_2 + h_1 & h_1 + h_0 & h_0 & 0 & 0 & 0 & \dots \\ h_3 + h_2 & h_2 + h_1 & h_1 + h_0 & h_0 & 0 & 0 & \dots \\ h_4 + h_3 & h_3 + h_2 & h_2 + h_1 & h_1 + h_0 & h_0 & 0 & \dots \\ h_5 + h_4 & h_4 + h_3 & h_3 + h_2 & h_2 + h_1 & h_1 + h_0 & h_0 & \dots \\ \vdots & \vdots & \vdots & \vdots & \vdots & \vdots & \ddots \end{pmatrix}$$

Figure 4.10: Transformation matrix for a sensor associated with the impulse response $h(t)$ expanded as $h(t) = \sum_{k=0}^{\infty} h_k l_k^p(t)$, using Laguerre functions.

can be written as,

$$\mathbf{L}_j = \underbrace{[0, 0, \dots, 0]}_j, h_0, h_0 + h_1, h_1 + h_2, \dots, h_i + h_{i+1}, \dots]^t. \quad (4.37)$$

An illustration of the transformation matrix in a Laguerre subspace is shown in Fig. 4.10. As Fig. 4.10 shows, to determine the sensor transformation matrix, it is sufficient to calculate only the first column. The observed pattern also helps to derive a distortion measure for the unbounded matrix.

4.2.3 Distortion Analysis in Laguerre Subspace

Calculating Frobenius norm for an unbounded matrix is not practical in the general case.

However, if a pattern in the transformation matrix exists it is possible to compare it to a reference matrix. Suppose that the sensor is associated with the impulse response $h_{eff}(t)$ and the reference sensor impulse response is shown as $h_{ref}(t)$. Now if h_{ref}^{-1} is inverse of

the reference sensor impulse response, then instead of comparing h_{eff} to h_{ref} , one can compare $h = h_{ref}^{-1} * h_{eff}$ to the identity system. However for reference systems which have no zeros in the frequency domain it is not a place of question. Assume that $H_{ref}(f)$ is the Fourier transform of h_{ref} . If for all frequencies $H_{ref}(f) \neq 0$, then $\frac{1}{H_{ref}(f)}$ exists and the inverse of the reference system is given by,

$$h_{ref}^{-1} = \mathcal{F}^{-1}\left[\frac{1}{H_{ref}(f)}\right], \quad (4.38)$$

where $F^{-1}[\cdot]$ is the inverse of Fourier transform. The transformation matrix associated with $h = h_{ref}^{-1} * h_{eff}$ has the elements as calculated in (4.35) and shown in Fig. 4.10. As concluded before, only the first column of the transformation matrix would be enough to determine the rest of the matrix. As mentioned before the reference transformation matrix is the unbounded identity matrix shown as \mathbf{I}_∞ . \mathbf{I}_∞ has zero elements everywhere except on the diagonal where all the diagonal elements are equal to 1. Considering the pattern in the transformation matrix, the distance between a transformation matrix \mathbf{L} and the unbounded identity matrix $\mathbf{I}_\infty = [i_{kk'}]$ is given as,

$$\eta_\infty = \lim_{N \rightarrow \infty} \sqrt{\frac{\sum_{k=0}^{\infty} \sum_{k'=0}^{\infty} (l_{kk'} - i_{kk'})^2}{N}}, \quad (4.39)$$

where, $l_{kk'}$ is the element on the k^{th} row and k'^{th} column of \mathbf{L} . Now substituting $l_{kk'}$ from Fig. 4.10 results in,

$$\eta_{\infty} = \lim_{N \rightarrow \infty} \sqrt{\frac{N((h_0 - 1)^2 + \sum_{k=1}^{\infty} (h_k + h_{k-1})^2)}{N}} \quad (4.40)$$

$$= \sqrt{(h_0 - 1)^2 + \sum_{k=1}^{\infty} (h_k + h_{k-1})^2} \quad (4.41)$$

If each of the columns of \mathbf{L} is normalized to its norm, η_{∞} varies between 0 and $\sqrt{2}$.

4.2.4 Selection of a Proper Scaling Factor

In [24] a hybrid algorithm is provided to find the number of basis functions and the scaling factor simultaneously. Here, a similar procedure to what is presented in section 4.1.2 is perused to obtain a safe range for p . If $f_T(n)$ shows the time duration in which Laguerre function of order n falls to one percent of the maximum value shown in Fig. 4.9a, one-dimensional polynomial fitting results in,

$$f_T(n) = 1.92n + 2.64. \quad (4.42)$$

If τ and BW show the time and frequency content of the signal approximated with N basis functions we should have,

$$\tau \leq \frac{f_T(N)}{p} \quad (4.43)$$

$$BW \leq f_{10\%}, \quad (4.44)$$

where $f_{10\%}$ is given by (4.26). Comparing (4.43), (4.44), (4.42), and (4.26) results in,

$$\frac{BW}{1.59} \leq p \leq \frac{1.92N + 2.64}{\tau}. \quad (4.45)$$

Using (4.12) we have,

$$0.05 \leq p\tau \leq (1.92N + 2.64). \quad (4.46)$$

4.2.5 Distortion Analysis in a Certain Frequency Range

Fig. 4.9b shows that for a given p the frequency content of all of the basis functions would be the same. Using η_∞ calculated for a given p , one can compare the distortion level for different sensors. Using other values for p yields different values for η_∞ . As given in (4.26), larger values of p correspond to a higher 10 dB frequency range in Laguerre basis functions. Therefore, higher values of p , result in η_∞ s which describe the distortion characteristics in a higher frequency range. One way to relate calculated η_∞ to a frequency range, is to use the 10 dB frequency range of the used Laguerre functions. This is a result of inequality (4.44). Although this criteria is not exact, it gives an approximation of the frequency range which calculated distortion characteristics can be used in.

4.2.6 Example

As an example, η_∞ is calculated for low pass filters with different cut-off frequencies. In addition, different values of Laguerre 10 dB frequency ranges are used to calculate the

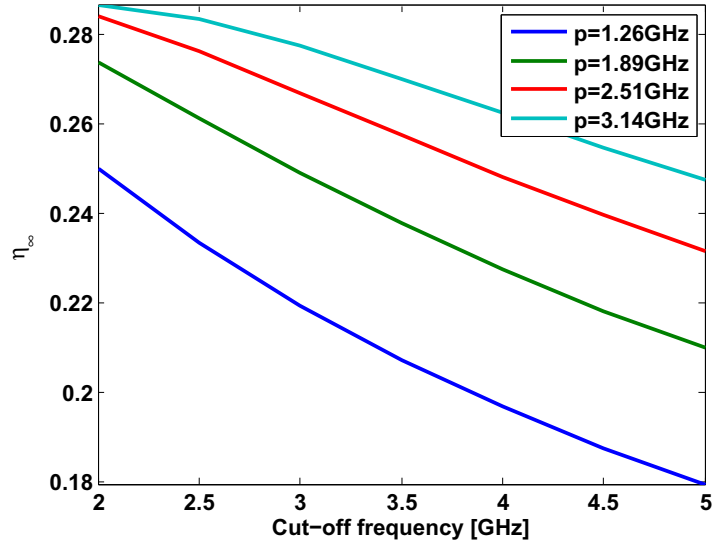


Figure 4.11: Different values obtained for η_∞ for lowpass filters with different cut-off frequencies when different values of p is used.

distortion measure η_∞ for the filters. The results are shown in Fig. 4.11. For a fixed value of p , as the cut-off frequency increases the value of η_∞ decreases. However, for a fixed cut-off frequency, η_∞ has a smaller value when smaller value of Laguerre 10 dB frequency range is used. This means that with increasing the value of p , the frequency range in which the distortion analysis is performed, is wider and therefore distortion level increases for a lowpass filter.

Chapter 5

Simulation and Measurement

Results

The electric field sensors studied in this thesis consist of wire monopoles of 5, 10, and 15 cm, a 3×3 cm parallel plate sensor with a 2 mm air dielectric, and a 5 cm high Asymptotic Conical Dipole (ACD) [34], [35]. Pictures of the parallel plate, the ACD, and the wire monopole are shown in Figs. 5.1-5.3. The parallel plate and monopole antennas were made at the University but the ACD is a commercial sensor made by Prodyn (Model AD-S30). Wire monopoles with different lengths are used in order to take sensor sensitivities into the account. Using a time-domain simulation, distortion characteristics described in Chapter 3 and 4 are calculated for the sensors. In addition, a method to derive the distortion characteristic from one set of measurement is described.

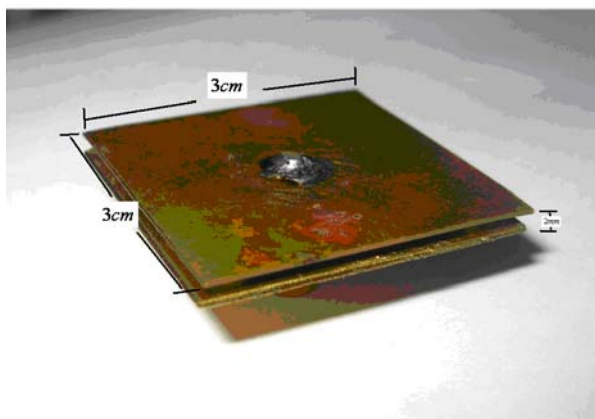


Figure 5.1: Photo of the 3×3 cm parallel plate sensor with 2 mm air dielectric, used in the experiments and modeled in the simulation.

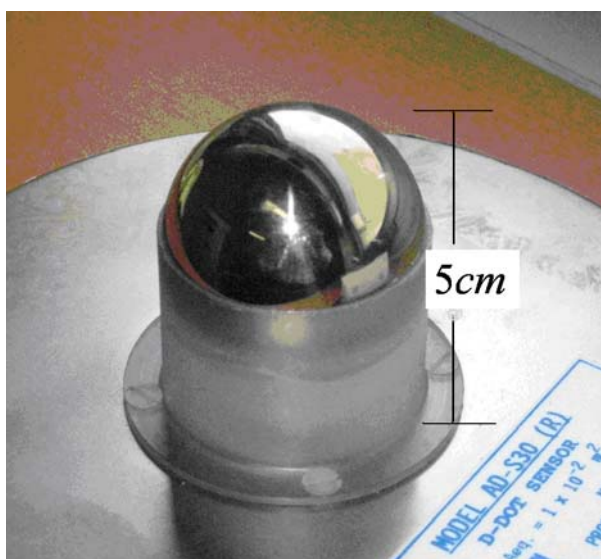


Figure 5.2: Photo of the 5 cm high AD-S30 ACD manufactured by Prodyn, uses in the experiments and modeled in the simulations.



Figure 5.3: Photo of the wire monopole used in the experiments and modeled in the simulations.

5.1 Simulation Method

The time-domain simulation is performed by modeling the sensors as wire structures. The wire monopoles modeling is straightforward. The ACD is modeled piece-wise linearly as shown in Fig. 5.4. The electric current of each wire segment is calculated by solving an Electric Field Integral Equation (EFIE) using the Method of Moments (MoM) [36]. For a selected time step of Δt , the length of each segment Δl should be selected so that,

$$\Delta l \leq c\Delta t, \quad (5.1)$$

where, c is the speed of light in the surrounding medium. All of the sensors are assumed to be terminated at 50Ω loads. As shown in Fig. 5.4, the sensor is oriented such that its polarization vector is in line with the incident electric field. Fig. 5.4 also shows the

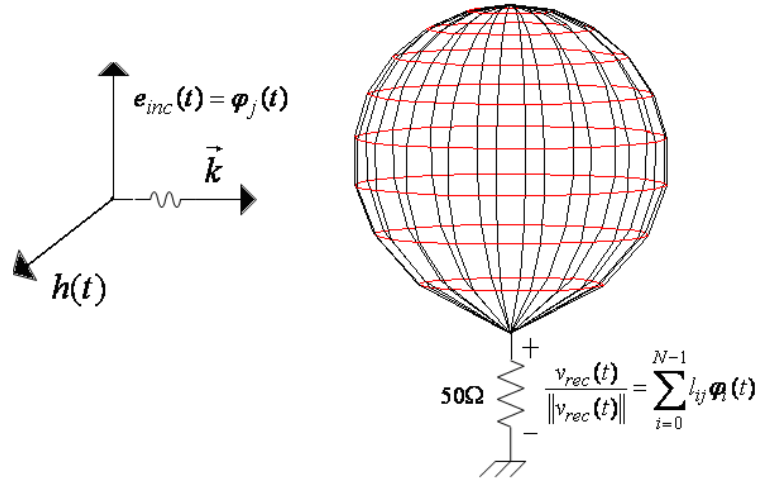


Figure 5.4: ACD wire model used in the time-domain simulations and the electromagnetic field. The sensor is terminated at a 50Ω load. An EFEI is solved using MOM to determine the voltage at the terminal of the sensor.

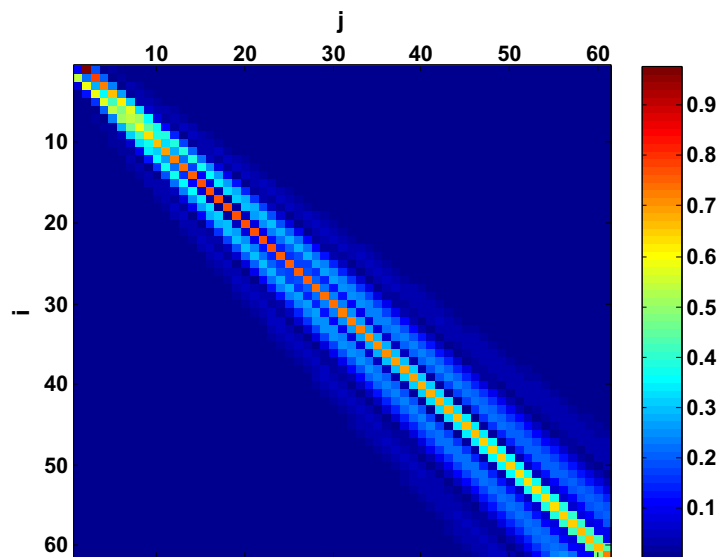
procedure to calculate the transformation matrix. To calculate the element on the i^{th} row and the j^{th} column of the transformation matrix, l_{ij} , the waveform of the incident electric field has to vary as the j^{th} basis function. The received voltage is then projected on the selected basis functions to yield the j^{th} column. The transformation matrices used in both finite and infinite dimensional techniques described in Chapter 4 are calculated as described. The only difference is that using Laguerre functions, one only has to simulate the received voltage for only one of the basis functions as every column of the transformation matrix is a shifted version of the first one. This property significantly reduced the computation time.

5.2 Finite-Dimensional Analysis

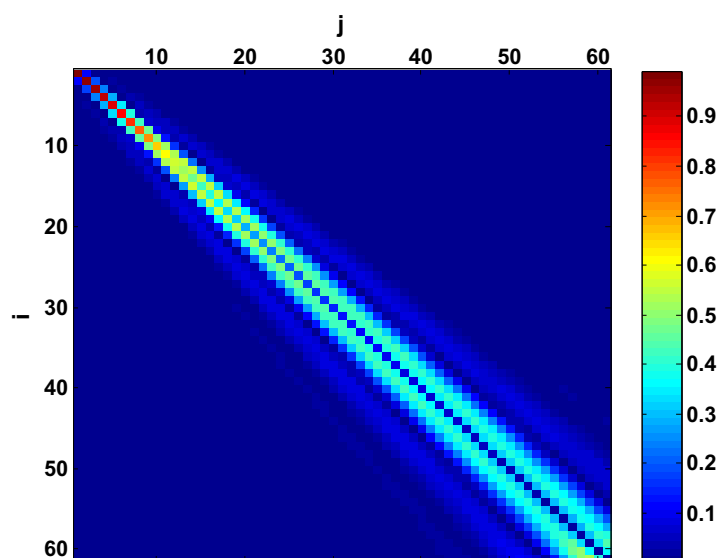
Hermite-Gauss functions are used to perform a finite-dimensional distortion analysis. As discussed earlier in Chapter 4, the value of the scaling factor σ in (4.1) determines the frequency range in which the distortion analysis is performed. Here, two scaling factors of 2 ns and 4 ns have been selected which are corresponding to one percent frequency ranges of 1 GHz and 500 MHz for the highest order of 60 in Hermite-Gauss functions. For every sensor, the simulation is repeated 61 times in order to obtain a 61×61 transformation matrix, for a maximum Hermite-Gauss function order of 60. These particular types of sensors are ideally expected to deliver the derivative of the incident electric field at their terminals. However, it is always worth investigating if the sensors perform as an identity systems. Therefore the transformation matrices are calculated for both the received voltages and their integrals. Figs. 5.5-5.9 show the transformation matrices for every sensor calculated for the voltages and their integrals for Hermite-Gauss functions with a scaling factor of $\sigma = 2$ ns. Fig. 5.10 to Fig. 5.14 illustrate the transformation matrices when $\sigma = 4$ ns is selected. To have a better graphical interpretation the absolute value of the transformation matrices are shown.

5.2.1 Interpretation of the Results

In all of the transformation matrices calculated for $\sigma = 2$ ns, shown in Figs. 5.5-5.9, two distinct regions are recognizable. This will be discussed for each of the sensors individually.

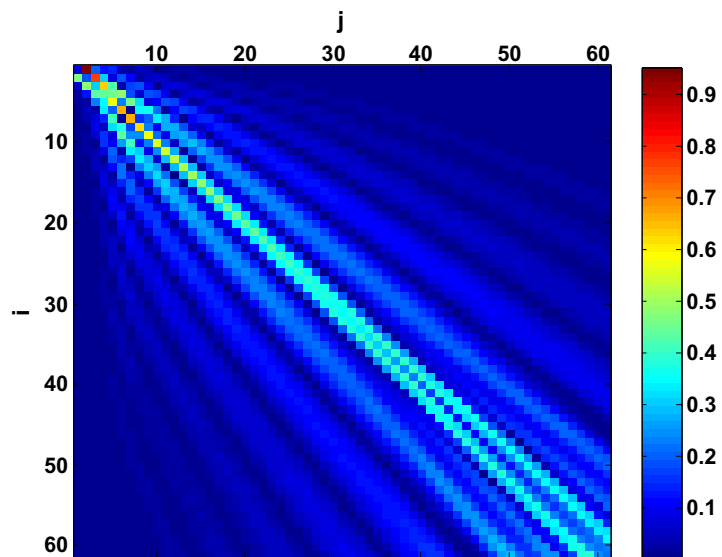


(a)

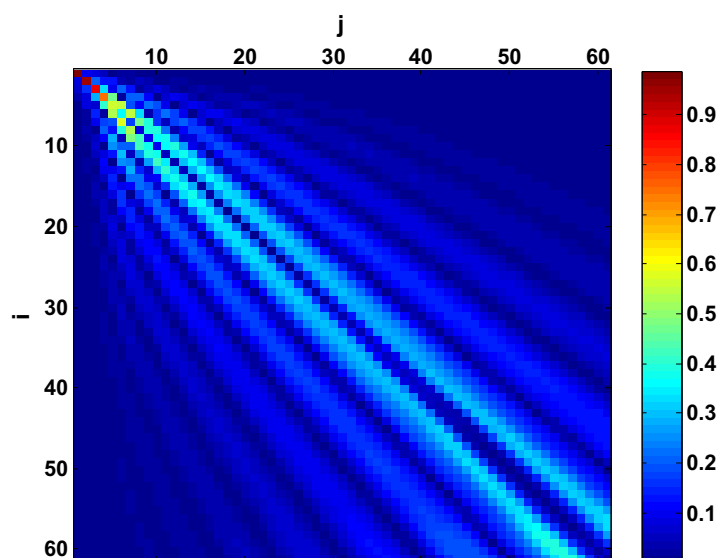


(b)

Figure 5.5: Transformation matrices calculated for the ACD using $\sigma = 2$ ns for a) the received voltage and, b) the integral of received voltage.

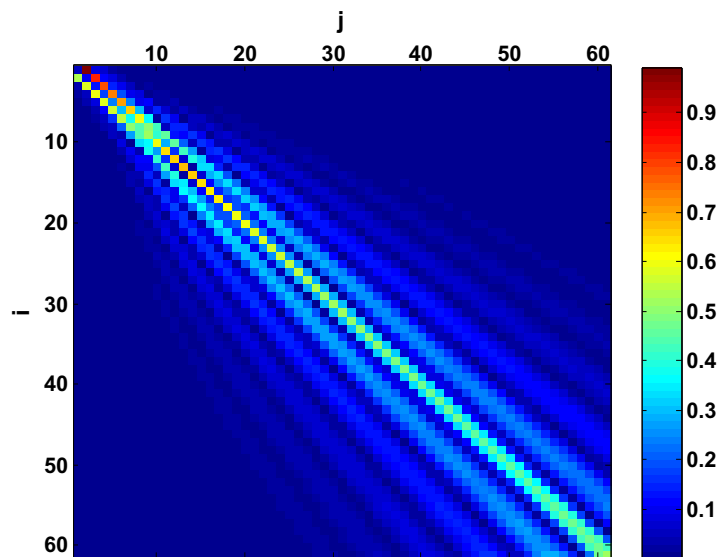


(a)

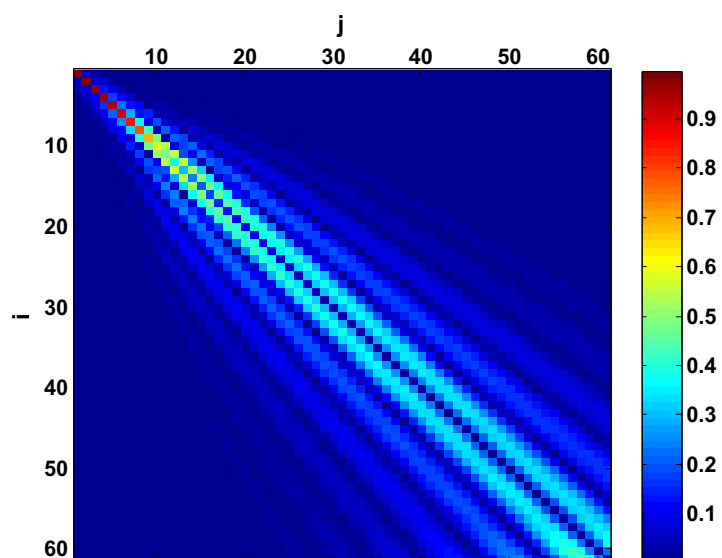


(b)

Figure 5.6: Transformation matrices calculated for the 15 cm monopole using $\sigma = 2$ ns for a) the received voltage and, b) the integral of received voltage.

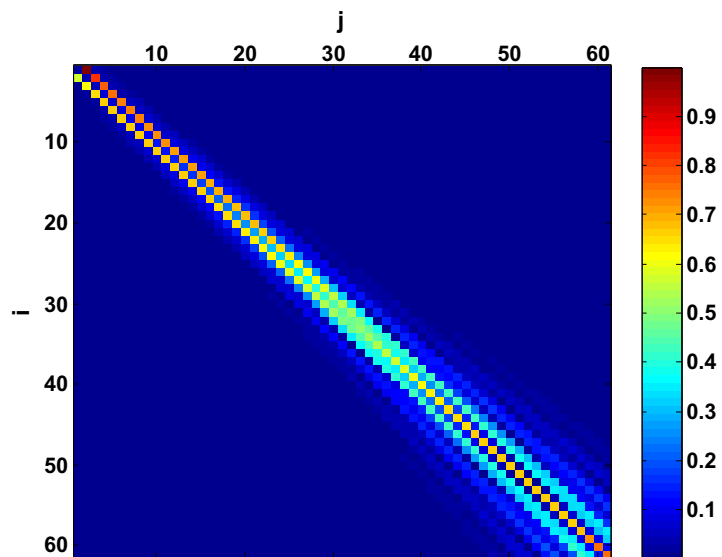


(a)

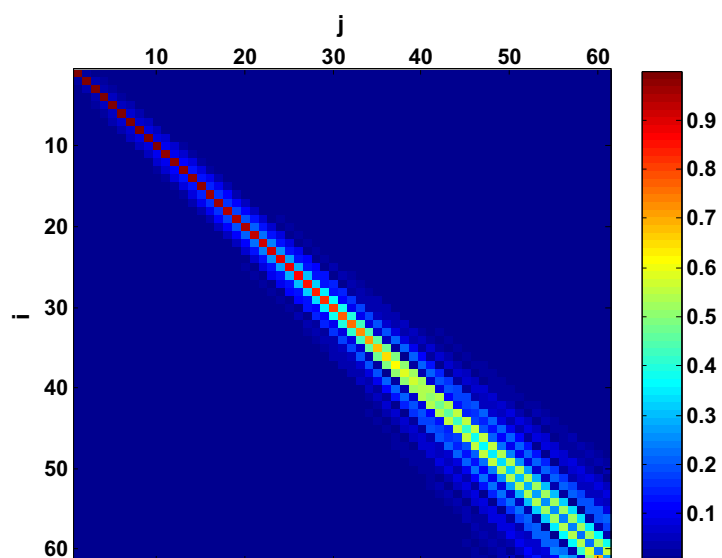


(b)

Figure 5.7: Transformation matrices calculated for the 10 cm monopole using $\sigma = 2$ ns for a) the received voltage and, b) the integral of received voltage.

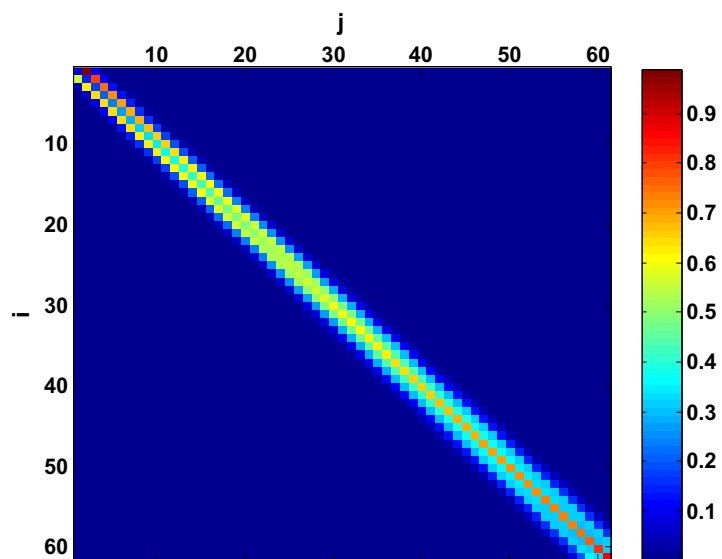


(a)

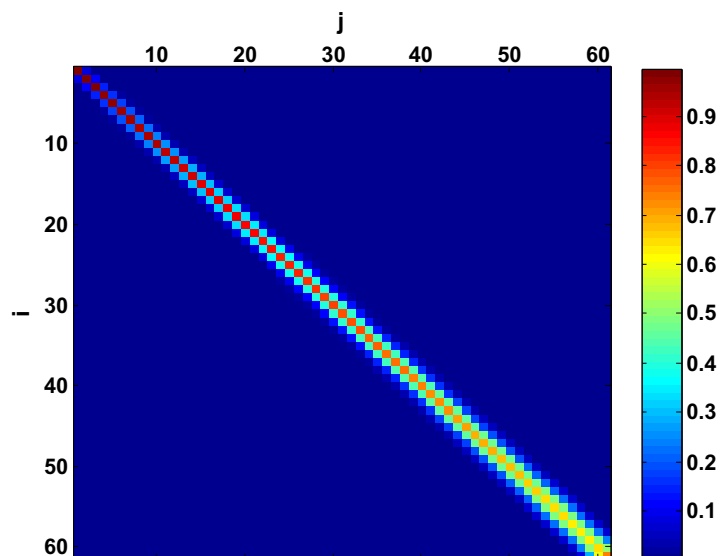


(b)

Figure 5.8: Transformation matrices calculated for the 5 cm monopole using $\sigma = 2$ ns for a) the received voltage and, b) the integral of received voltage.

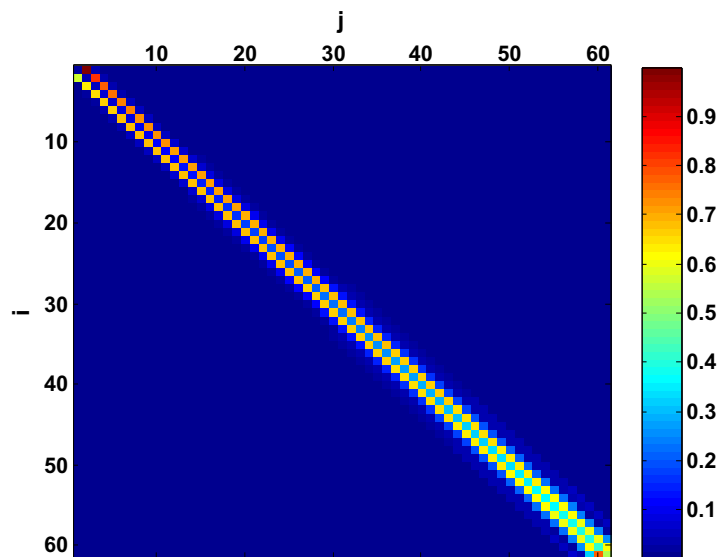


(a)

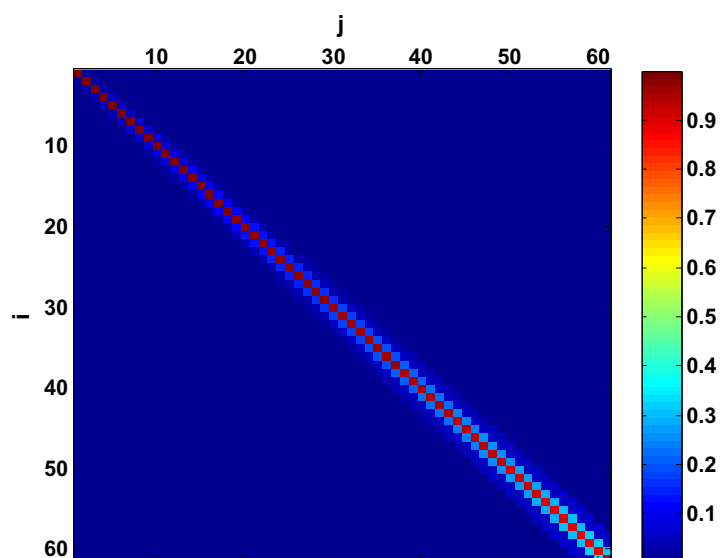


(b)

Figure 5.9: Transformation matrices calculated for the 3×3 cm parallel plate with 2 mm air dielectric, using $\sigma = 2$ ns for a) the received voltage and, b) the integral of received voltage.

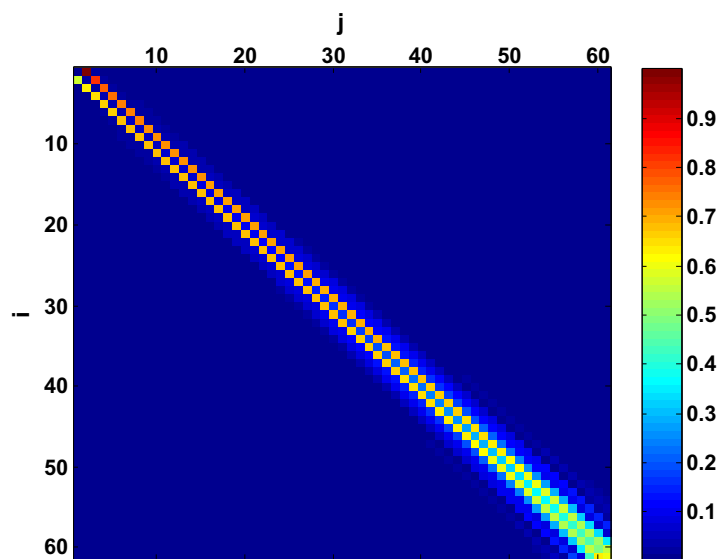


(a)

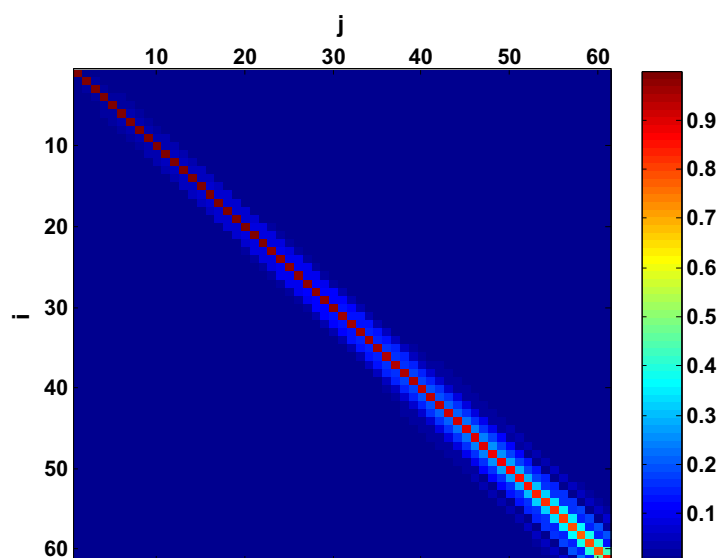


(b)

Figure 5.10: Transformation matrices calculated for the ACD using $\sigma = 4$ ns for a) the received voltage and, b) the integral of received voltage.

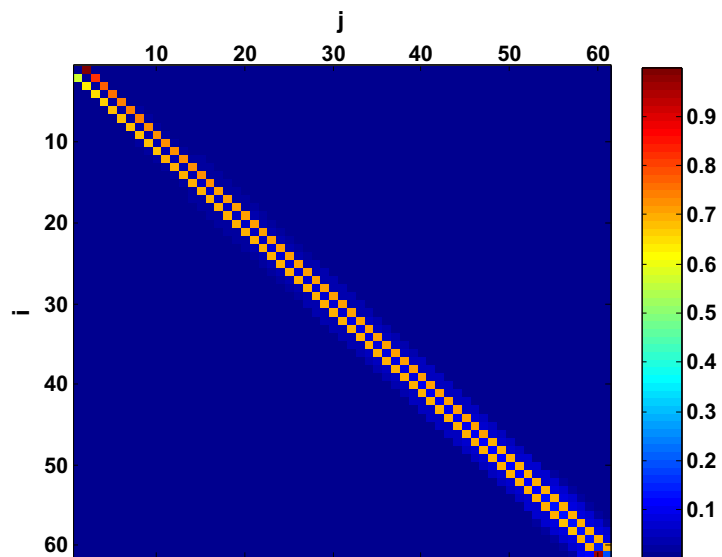


(a)

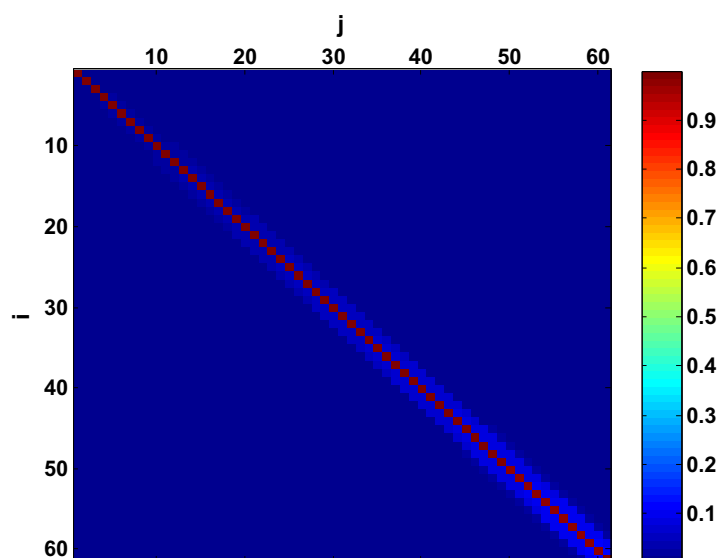


(b)

Figure 5.11: Transformation matrices calculated for the 15 cm monopole using $\sigma = 4$ ns for a) the received voltage and, b) the integral of received voltage.

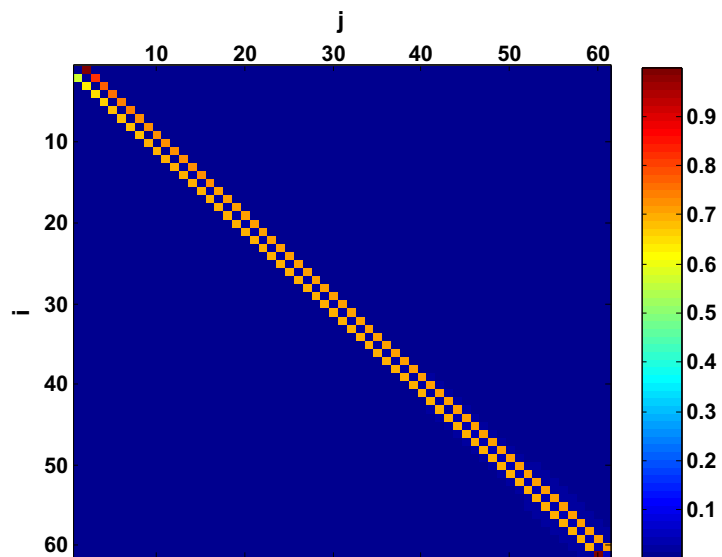


(a)

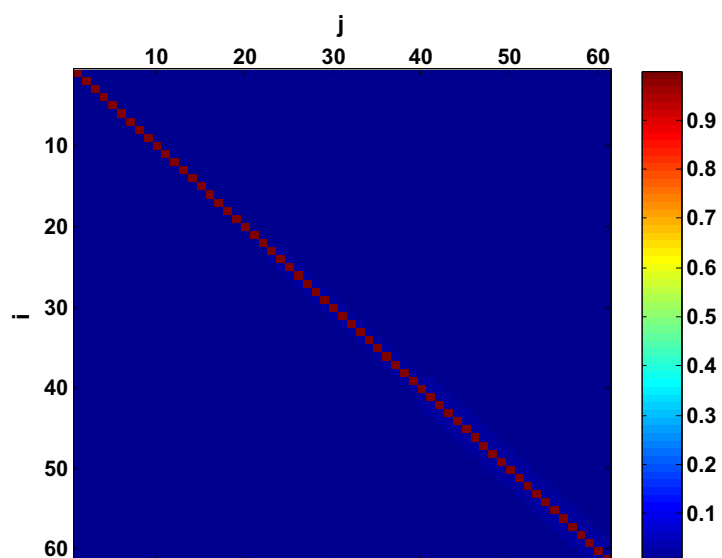


(b)

Figure 5.12: Transformation matrices calculated for the 10 cm monopole using $\sigma = 4$ ns for a) the received voltage and, b) the integral of received voltage.

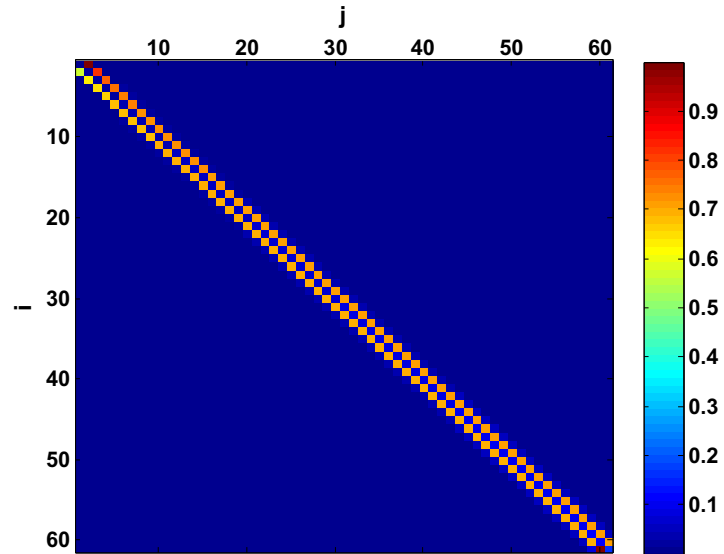


(a)

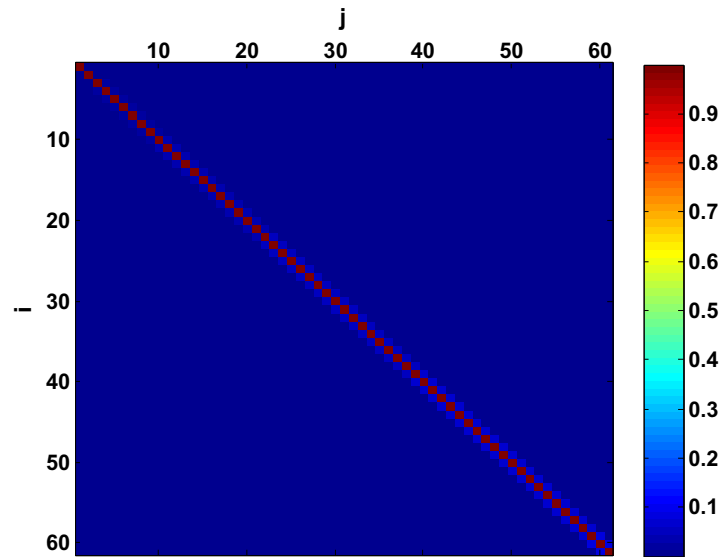


(b)

Figure 5.13: Transformation matrices calculated for the 5 cm monopole using $\sigma = 4$ ns for a) the received voltage and, b) the integral of received voltage.



(a)



(b)

Figure 5.14: Transformation matrices calculated for the 3×3 cm parallel plate with 2 mm air filling, using $\sigma = 4$ ns for a) the received voltage and, b) the integral of received voltage.

- The ACD

As shown in Fig. 5.5a, the transformation matrix shows a differentiator behavior similar to Fig. 4.3, up to the 11th row and column. This is confirmed by the transformation matrix calculated for the integrated voltages as a diagonal matrix is observed for the upper 11×11 sub-matrix in Fig. 5.5b. Therefore the ACD delivers a derivative version of the incident electric field at its terminals up to 500 MHz which is the corresponding bandwidth for the maximum order of 11 and $\sigma = 2$ ns, as shown in Fig. 4.2b. The ACD transformation matrix tends to be diagonal in 5.5a for the rows and columns greater than 11. This means that for higher frequencies up to 1 GHz, the ACD receives an electrical voltage which is more similar to the incident electric field itself.

- 15 cm monopole

The differentiative behavior is observed for the upper 4×4 sub-matrix in Fig. 5.6. For higher frequencies up to 1 GHz no diagonal pattern is observed in Fig. 5.6a. Therefore, the 15 cm monopole acts like a differentiator at low frequencies up to 365 MHz. At higher frequencies the monopole distorts the signal.

- 10 cm monopole

A similar behavior to the ACD's is observed in the 10 cm wire monopole. The differentiator behavior exists for frequencies lower than 500 MHz in Fig. 5.7. The only difference

with the ACD is that the monopole antenna transformation matrix does not show a diagonal behavior for higher frequencies. Therefore, it can be concluded that the ACD has a better distortion performance in the higher frequencies compared to the 10 cm monopole.

- 5 cm monopole

As Fig. 5.8a shows a differentiator behavior up to the 40th row and column which corresponds to a frequency range of 800 MHz. The 5 cm monopole delivers a derivative of the incident electric field at its terminal for frequencies up to 800 MHz.

- The parallel plate

The 3×3 cm parallel plate with 2 mm air dielectric acts as an differentiator up to 1 GHz. Fig. 5.9 has a similar pattern to what obtained in the case of an ideal differentiator transformation matrix in Fig. 4.3.

Table 5.1 summarizes calculated η_N defined in (3.18), for $N = 61$ when the reference matrix is selected to be the 61×61 identity matrix, \mathbf{I}_{61} . The numbers show that the ACD has the least distortion compared to an identity system. The distortion increases for the parallel plate, the 10 cm monopole, the 5 cm monopole and the 15 cm monopole. Table 5.2 summarizes the calculated η_N for $N = 61$ for the transformation matrices calculated for the integrated voltages and compared to \mathbf{I}_{61} . As differentiators, the least to the most distortive sensors are the parallel plate, the 5 cm monopole, the ACD, the 10 cm monopole,

and the 15 cm monopole. To see how the sensors perform in lower frequencies in more

Table 5.1: Calculated η_N for simulated voltages ($\sigma = 2ns$), for $N = 60$ which corresponds to a maximum frequency rang of 1 GHz. The ACD has the least distortion as an identity system.

Sensor Type	η_{61}
ACD	0.8254
10 cm monopole	1.0152
Parallel plate	1.0710
5 cm monopole	1.0760
15 cm monopole	1.1647

Table 5.2: Calculated η_N for the integral of simulated voltages ($\sigma = 2ns$), for $N = 61$ which is corresponding to a maximum frequency of 1 GHz. The parallel plate and 5 cm monopole have the least distortion introduced as a differentiator.

Sensor Type	η_{61}
Parallel plate	0.6316
5 cm monopole	0.7938
ACD	1.2039
10 cm monopole	1.2709
15 cm monopole	1.3612

details, the transformation matrices are calculated using $\sigma=4$ ns. The transformation matrices are shown in Figs. 5.10-5.14. $\sigma = 4ns$ corresponds to a one percent frequency range of 500 MHz for the highest order Hermite-Gauss functions is selected to be 60. A similar behavior is observed in the transformation matrices illustrated in Figs. 5.10-5.14. The transformation matrices calculated for the integrated voltages tend to be diagonal for the ACD, 5 and 10 cm monopole, and the parallel plate. The transformation matrix for the 15 cm monopole is diagonal up to the 37th row and column which corresponds to frequencies lower than 360 MHz. The calculated η_N are summarized in Table 5.3 when η_N shows the distance between the transformation matrices calculated for the integral of

voltages and \mathbf{I}_N for $N = 61$.

Table 5.3: Calculated η_N for the integral of simulated voltages ($\sigma = 4ns$).

Sensor Type	η_{61}
Parallel plate	0.0783
5 cm monopole	0.0328
ACD	0.2915
10 cm monopole	.1259
15 cm monopole	0.3539

5.2.2 Sensitivity Analysis

It is not practical to compare the distortion level without considering the sensitivities of the sensors. As the smaller antennas distortion levels are very small but so is their sensitivity. To give an idea of how the sensitivity should be involved, let's assume that an evaluation of distortion characterization of the ACD is desired. To find the proper sensor to compare with the ACD, the sensors received voltages are plotted in Fig. 5.15 when the incident electric field has a Gaussian waveform with a 10 dB frequency range of 1 GHz. Comparing the voltages show that the ACD and the 10 cm have close sensitivities as their maximum received voltages have a ratio of 1.2. Table 5.4 shows η_{11} calculated for both the the upper 11×11 sub-matrices of the transformation matrices shown in Fig. 5.5b and 5.7b when the reference matrix is selected as \mathbf{I}_{11} . Table 5.5 summarizes the η_N of the lower 50×50 sub-matrices shown in Fig. 5.5a and 5.7a when the reference matrix is selected to be \mathbf{I}_{50} . Table 5.4 shows that both sensors have similar distortion

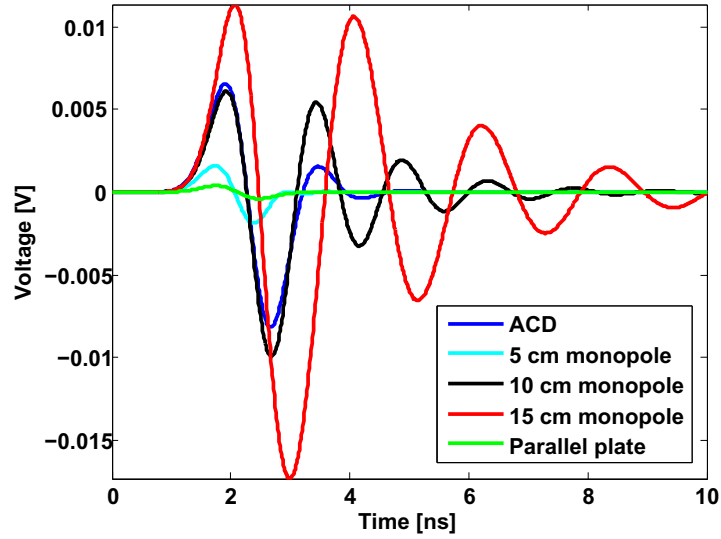


Figure 5.15: Received voltages when the incident electric field has a Gaussian waveform with 1 GHz bandwidth.

level for frequencies lower than 500 MHz while Table 5.5 shows that the ACD has a better distortion characteristic for frequencies higher than 500 MHz and up to 1 GHz.

Table 5.4: Calculated η_N for the integral of simulated voltages ($\sigma = 2$ ns).

Sensor Type	η_{11}
10 cm monopole	0.5330
ACD	0.5540

Table 5.5: Calculated η_N for the the simulated voltages ($\sigma = 2$ ns)

Sensor Type	η_{50}
10 cm monopole	.9733
ACD	.7646

5.2.3 Calculating the Transformation Matrix Using Measurement Data

The following challenges exist in calculating the transformation matrix using the measured voltages:

- Unlike the simulation, in measurement it is not feasible to generate electromagnetic waves which vary as Hermite-Gauss functions with time. This problem is accentuated particularly when it is needed to calculate the transformation matrix for various values of σ .
- To calculate an $N \times N$ transformation matrix, the simulation should be repeated N times. In both the simulation and the measurement this procedure is time consuming for large values of N .
- Unlike the simulation, the incident electric field is not known. A method of determining the electric field should be performed first.

In this section, we describe a methodology for obtaining the transformation matrix using only one set of time-domain measurement. Let's assume $v_{rec}(t)$ represents sensor measured voltage when the incident electric field is $e_{inc}(t)$. We can write,

$$v_{rec}(t) = \sum_{n=0}^{N-1} v_n \phi_n(t), \quad (5.2)$$

$$e_{inc}(t) = \sum_{n=0}^{N-1} e_n \phi_n(t), \quad (5.3)$$

where, $\phi_n(t)$ is the n^{th} order Hermite-Gauss function. Using the property of Hermite-Gauss functions given in (4.2), we can take the Fourier transform of (5.2) and (5.3) as,

$$V_{rec}(\omega) = \sum_{n=0}^{N-1} v_n(-j)^n \phi_n(\omega), \quad (5.4)$$

$$E_{inc}(\omega) = \sum_{n=0}^{N-1} e_n(-j)^n \phi_n(\omega). \quad (5.5)$$

If the sensor transfer function is denoted by $H(\omega)$, using (5.4) and (5.5) it can be expressed as,

$$H(\omega) = \frac{\sum_{n=0}^{N-1} v_n(-j)^n \phi_n(\omega)}{\sum_{n=0}^{N-1} e_n(-j)^n \phi_n(\omega)}. \quad (5.6)$$

As shown in (3.13)-(3.15), to calculate the ik element, l_{ik} , the received voltage v_{rec}^k should be known when the incident electric field is $\phi_k(t)$. The Fourier transform of $v_{rec}^k(t)$, $V_{rec}^k(\omega)$, is calculated as,

$$V_{rec}^k(\omega) = H(\omega) \cdot \mathcal{F}[\phi_k(t)]. \quad (5.7)$$

Using (4.4), $V_{rec}^k(\omega)$ also has the vector representation of \bar{V}_{rec}^k given by,

$$\bar{V}_{rec}^k = [v_0^k, (-j)v_1^k, \dots, (-j)^{N-1}v_{N-1}^k]^t. \quad (5.8)$$

The frequency-domain vector representation of the sensor received voltage \bar{V}_{rec}^k is related to its corresponding time-domain vector \bar{v}_{rec}^k as

$$\bar{v}_{rec}^k = [v_0^k, v_1^k, \dots, v_{N-1}^k]^t. \quad (5.9)$$

If the vector \bar{v}_{rec}^k is normalized to its energy norm, it forms the k^{th} column of the transformation matrix. In using this method, a proper σ should be selected so that (5.3) and (5.2) are reasonable approximations of the incident field and the received voltage, respectively. The inequality derived in (4.14) can be used to find a proper scaling factor.

Measurement Setup

A schematic of the measurement setup is shown in Fig. 5.16. The sensors are placed inside the GTEM cell.¹ A Picosecond Pulse Labs 1000A voltage generator² is used to generate the electromagnetic impulse. The impulse generator is connected to the GTEM cell apex. The received voltage at the terminal of the sensor is recorded using a Tektronix[®] TDS 8200 Digital Sampling Oscilloscope (DSO). The input impedance of the DSO is also 50 Ω . The DSO is triggered by the voltage generator. The voltage impulse directly measured by the DSO is shown in Fig. 5.17. The electric field sensors were tested separately and the voltages received at the terminal of the DSO are plotted in Fig. 5.18. To find the electric field waveform to be used in (5.3), a test sensor with a known effective height is used. Suppose that the test sensor is the parallel plate sensor. For a parallel plate sensor with an electrically small height, the effective height can be approximated using the fact

¹A GTEM cell is a suitable test environment for electrically small devices without interference from the ambient electromagnetic field. It has the shape of a triangular pyramid. The TEM field forms between the bottom edge and a middle plate. The middle plate distance from the bottom edge increases as shown in Fig. 5.16. The middle plate is terminated to a 50 Ω load. To prevent reflections from the edge in front of the apex, absorbers are installed on the frontier.

²The voltage generator is capable of generating a pulse with maximum amplitude of 45 V and a 370 ps risetime.

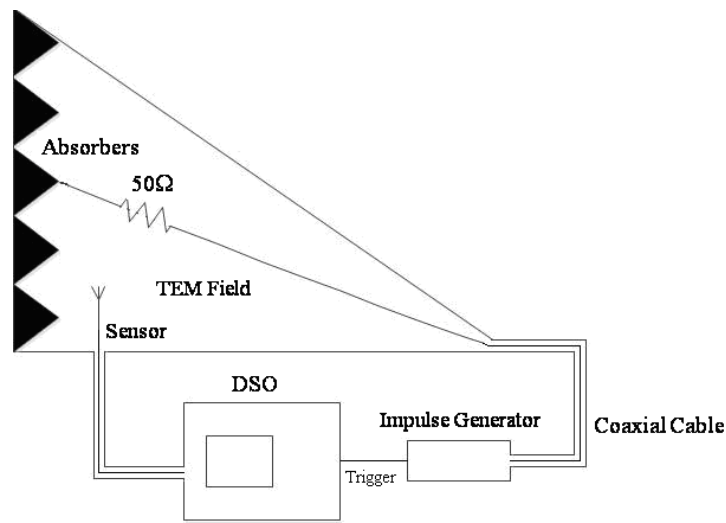


Figure 5.16: The measurement setup, including a GTEM cell as the test environment, the impulse generator and the DSO.

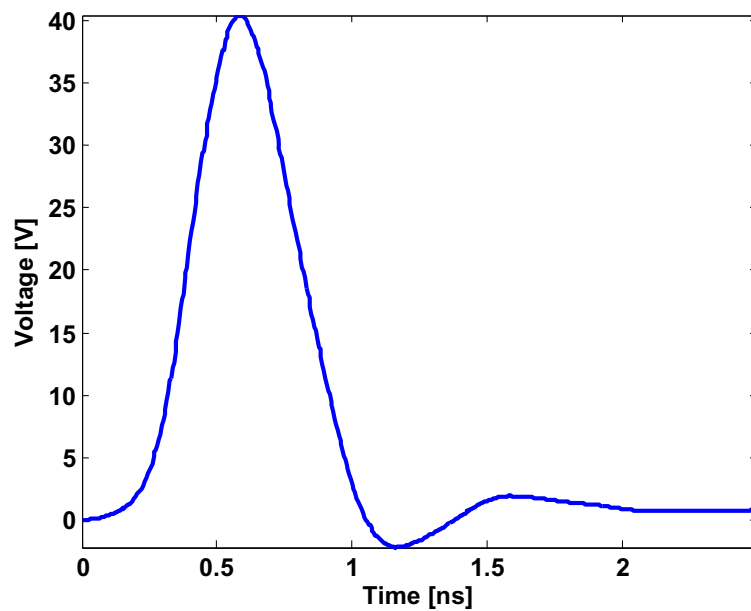


Figure 5.17: The voltage generator time-domain pulse directly measured by the DSO.

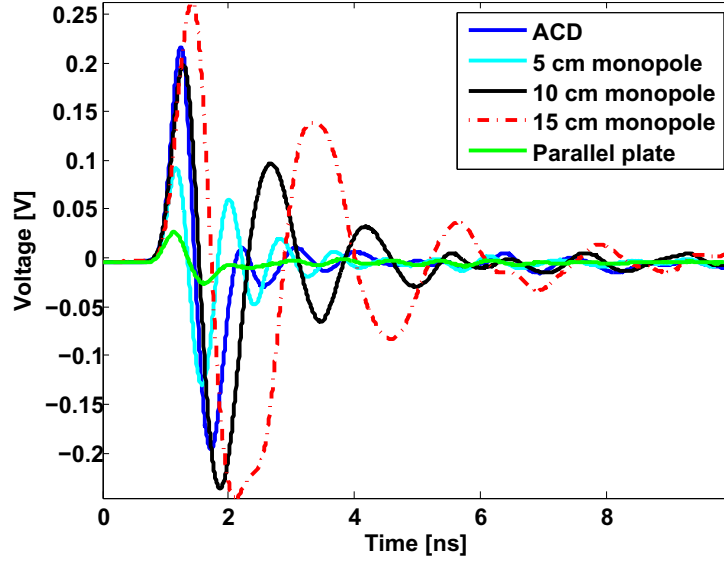


Figure 5.18: Time-domain measured voltages at the terminals of the sensors when located inside the GTEM cell.

that the electric field is distributed uniformly between the plates, so that,

$$v_{open}(t) = e_{inc}(t)h, \quad (5.10)$$

where h is the height of the parallel plate sensor and $v_{open}(t)$ is the received open circuit voltage when the incident electric field is e_{inc} . If the sensor is connected to a 50Ω load, the received voltage in (5.2) can be calculated using the circuit model shown in Fig. 5.19. For a parallel plate with a height of h and an area of the plates of A , the capacitance C is calculated using,

$$C = \epsilon \frac{A}{h}. \quad (5.11)$$

For the 3×3 cm parallel plate with a 2 mm air dielectric the capacitance is 4 pF. Using

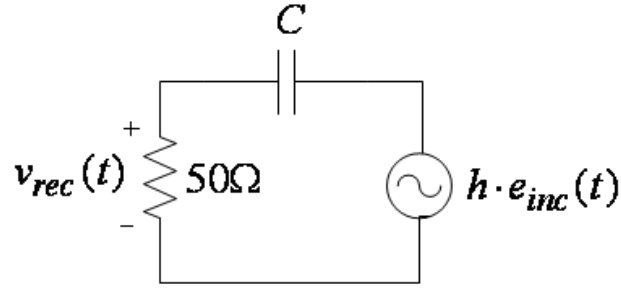


Figure 5.19: The circuit model for the parallel plate sensor with capacitance of C and height h .

the circuit model in Fig. 5.19, in the frequency domain we have,

$$V_{rec}(\omega) = \frac{50j\omega Ch}{50j\omega C + 1} E_{inc}(\omega). \quad (5.12)$$

Using (5.12), the Fourier transform of the incident field $E_{inc}(\omega)$ is determined. Taking the inverse Fourier transform of (5.12), we find the time-domain electric field. The incident electric field calculated using the parallel plate sensor is plotted in Fig. 5.20. It is noticeable that the GTEM cell has added reflections to the impulse generator voltage shown in Fig. 5.17. The transformation matrices calculated using the measured voltages shown in Fig. 5.18 and the electric field shown in Fig. 5.20 are shown in Figs. 5.21 to 5.24. The scaling factor is set to be 2 ns. This value satisfies the requirement given in (4.14) properly. Comparing Figs. 5.21 to 5.5a, 5.22 to 5.6a, 5.23 to 5.7a, and 5.24 to 5.8a, shows a close agreement between the simulation results and the measurement. Table 5.6

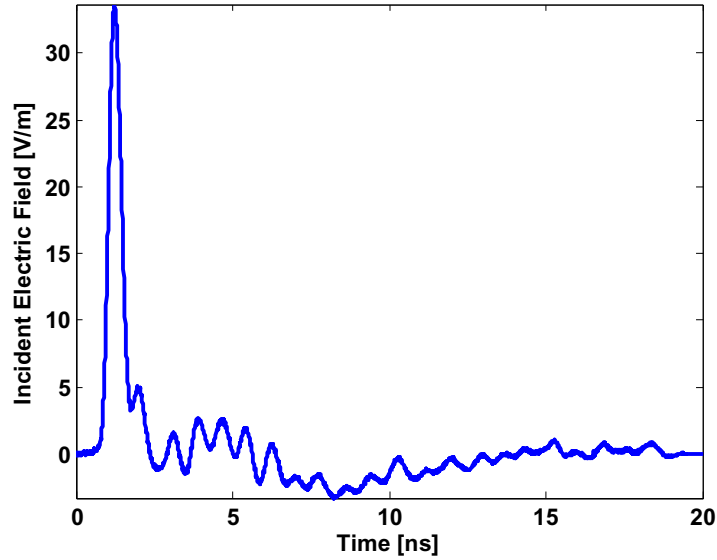


Figure 5.20: Measured time-domain electric field in the GTEM cell at the location of the sensors, using the parallel plate sensor.

summarizes η_{61} calculated for the mentioned transformation matrices. The values are close enough to confirm the visual inspection conclusion.

Table 5.6: Calculated η_N for the the simulated and measured voltages ($\sigma = 2ns$)

Sensor Type	η_{61} (Simulated)	η_{61} (Measured)
ACD	0.8254	0.8316
15 cm monopole	1.1647	1.1380
10 cm monopole	1.0152	0.9539
5 cm monopole	1.076	1.0881

5.3 Infinite-Dimensional Analysis

Laguerre functions are used to perform an infinite-dimensional distortion analysis. The transformation matrices for the 5, 10, and 15 cm monopole antennas and the ACD are shown in Figs. 5.25-5.28. The transformation matrices have been calculated using $p =$

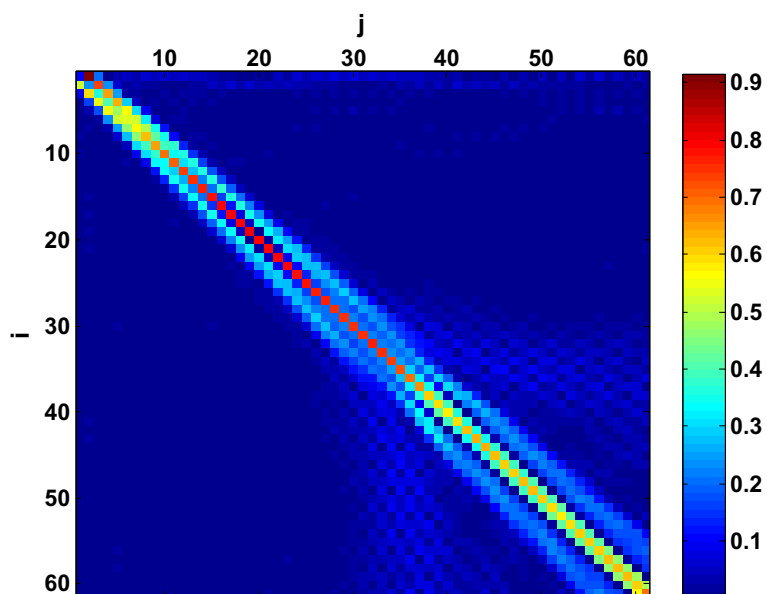


Figure 5.21: Calculated transformation matrix for the ACD using the time-domain measured voltage for $\sigma = 2$ ns, when the incident electric field varies as Fig. 5.20.

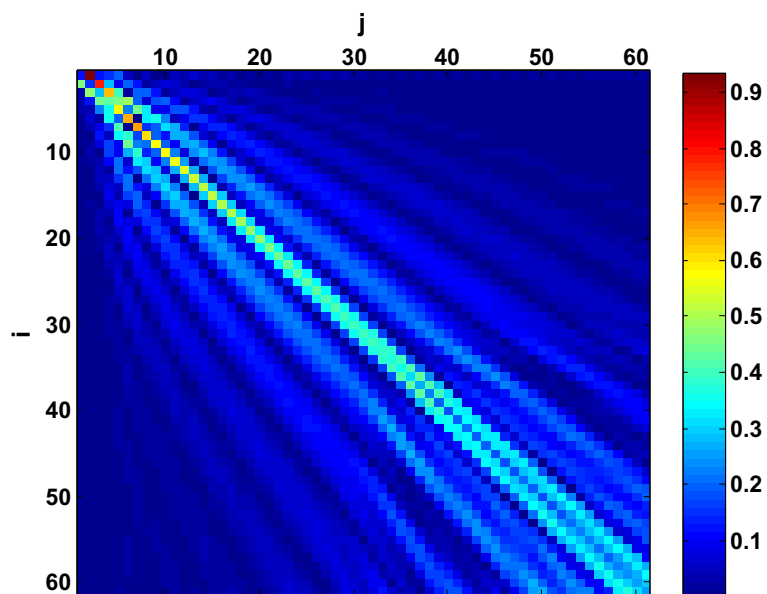


Figure 5.22: Calculated transformation matrix for the 15 cm monopole antenna using the time-domain measured voltage for $\sigma = 2$ ns, when the incident electric field varies as Fig. 5.20.

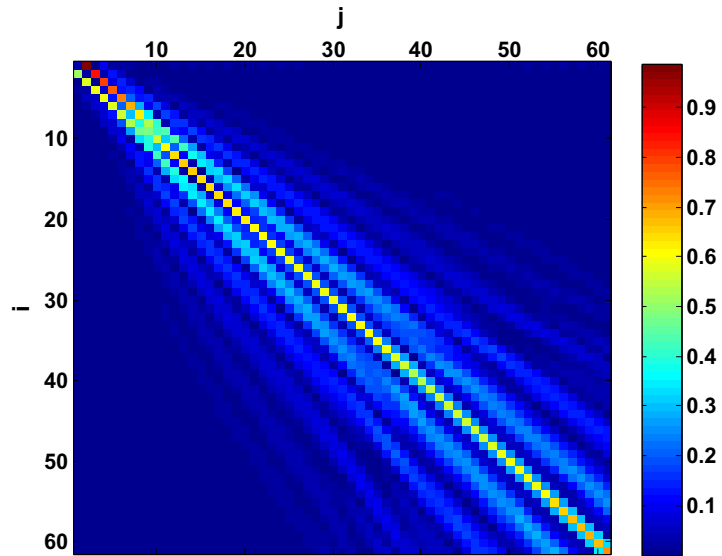


Figure 5.23: Calculated transformation matrix for the 10 cm monopole antenna using the time-domain measured voltage for $\sigma = 2$ ns, when the incident electric field varies as Fig. 5.20.

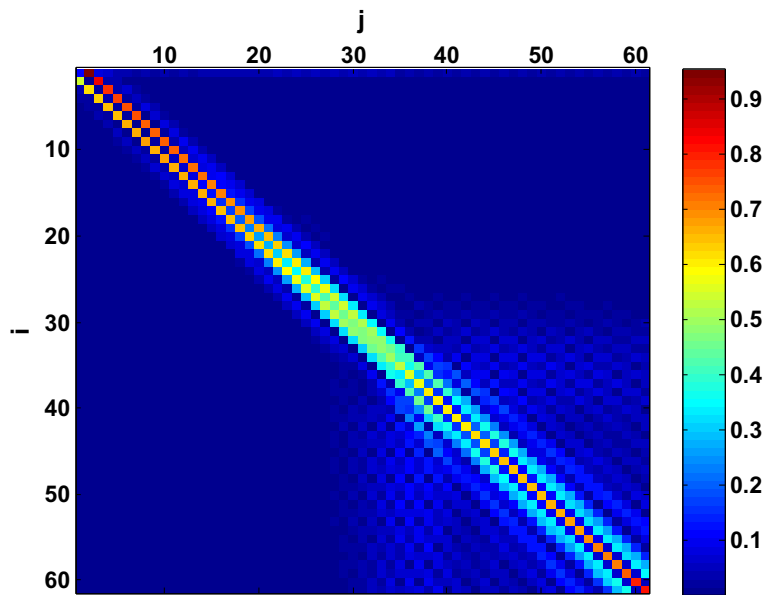


Figure 5.24: Calculated transformation matrix for the 5 cm monopole antenna using the time-domain measured voltage for $\sigma = 2$ ns, when the incident electric field varies as Fig. 5.20.

10^{10} in (4.21). It is observed that the transformation matrices have the same shape of Fig. 4.10. To calculate the distortion characteristic η_∞ as given in (4.40), one should first calculate the effective height of the sensors under study. The time domain impulse responses have been calculated simply by simulating the received voltage of the sensors when illuminated with a Gaussian pulse with 10 GHz bandwidth. The frequency-domain transfer functions are calculated as the ratio of the frequency-domain received voltage to the frequency-domain incident field. Taking the Fourier transforms yields the effective heights. The effective heights calculated for the 4 sensors are plotted in Fig. 5.29.

Time-domain effective heights are used to calculate η_∞ as a measure of the distortion introduced by the sensor comparing to the identity system. Calculated η_∞ for the sensors is shown in Fig. 5.30 as a function of the frequency range which Laguerre functions cover. The values shown in the figure confirm the relative values for η_{61} listed in Table 5.1. In other words, the sensors performance can be compared in a similar way using both methods. Alternatively, one can calculate η_∞ for the integral of the effective heights to obtain a measure of distortion when the sensors are compared to the ideal differentiators. The values for η_∞ obtained using the integrated effective heights are shown in Fig. 5.31 and are in agreement with values summarized in Table 5.2 and 5.1.

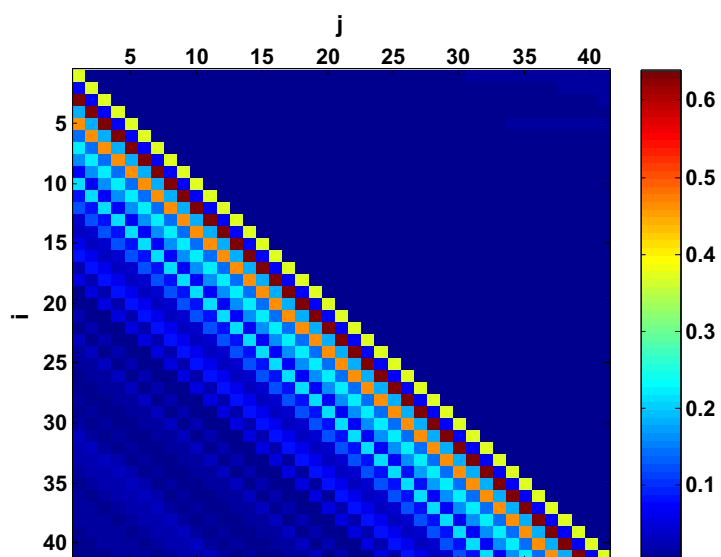


Figure 5.25: Calculated transformation matrix using Laguerre functions with $p = 10^{10}$ for a 5 cm monopole antenna.

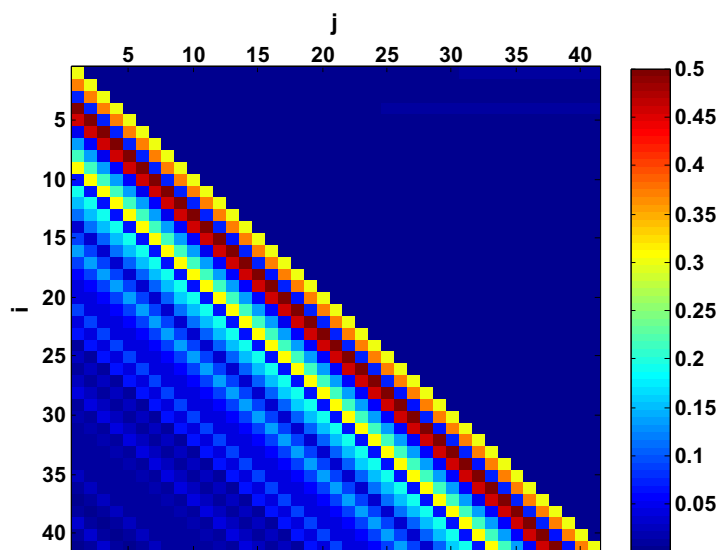


Figure 5.26: Calculated transformation matrix using Laguerre functions with $p = 10^{10}$ for a 10 cm monopole antenna.

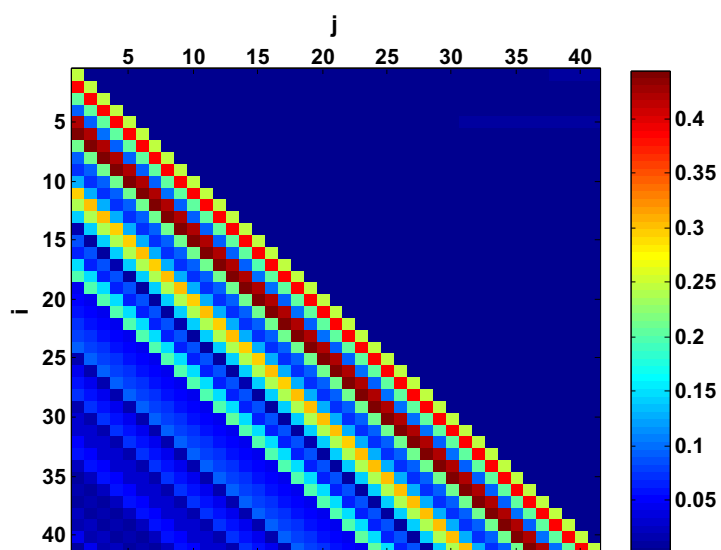


Figure 5.27: Calculated transformation matrix using Laguerre functions with $p = 10^{10}$ for a 15 cm monopole antenna.

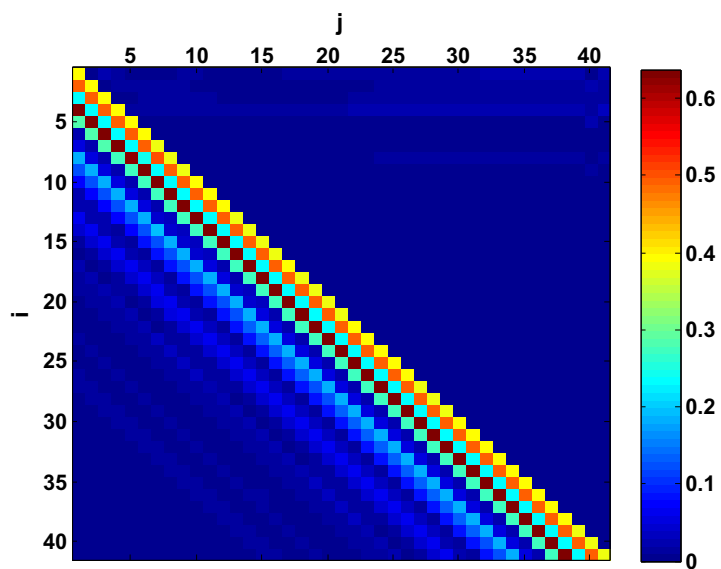


Figure 5.28: Calculated transformation matrix using Laguerre functions with $p = 10^{10}$ for a 5 cm ACD.

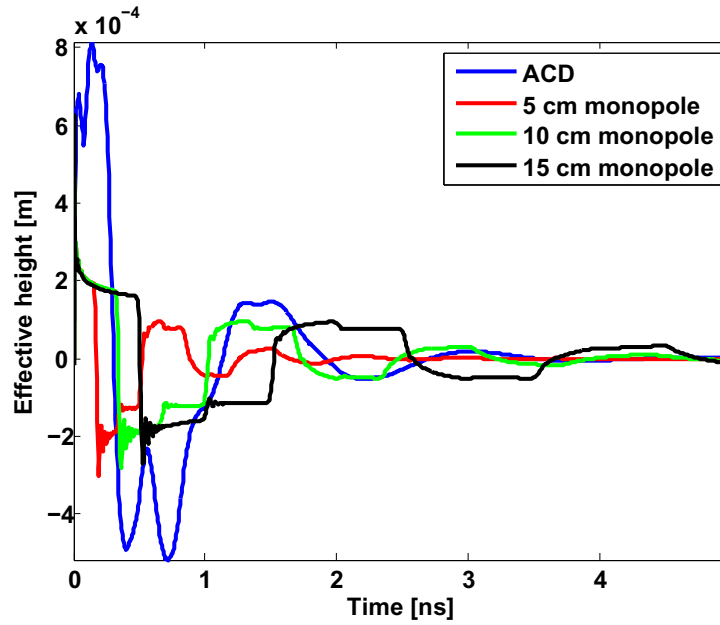


Figure 5.29: Effective heights calculated for the electric field sensors, when the sensors received voltages are simulated when illuminated by an incident electric field which has a Gaussian waveform with a 10 GHz bandwidth.

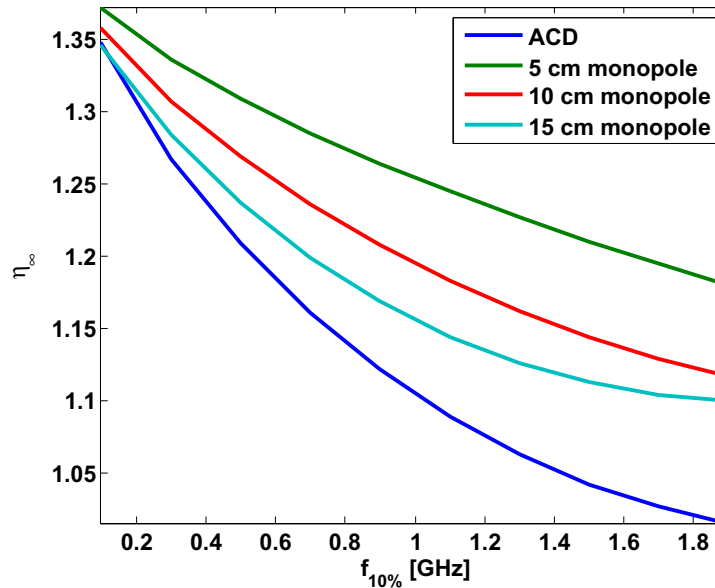


Figure 5.30: Calculated η_{∞} for the sensors effective heights.

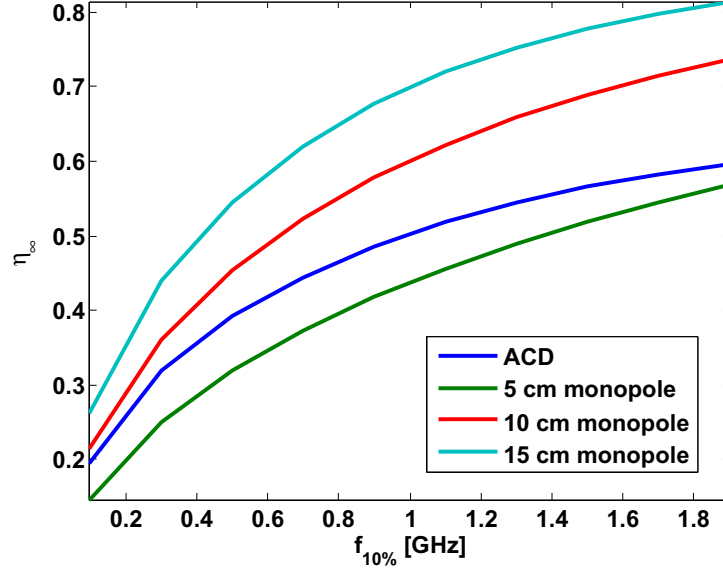


Figure 5.31: Calculated η_∞ for the integral of sensors effective heights.

5.3.1 Calculating the Effective Height Using one Set of Measurement

It is possible to calculate the effective height Laguerre expansion coefficients using one set of time-domain measurement. Assume that the effective height is $h_{eff}(t) = \sum_{k=0}^{\infty} h_k l_k^p(t)$. If the incident electric field is $e_{inc}(t) = \sum_{k=0}^{\infty} e_k l_k^p(t)$ and the received voltage is $v_{rec}(t) = \sum_{k=0}^{\infty} v_k l_k^p(t)$, then we can write,

$$v_{rec}(t) = h(t) * e_{inc}(t). \quad (5.13)$$

Substituting Laguerre expansions of $h(t)$ and $e_{inc}(t)$ in (5.13) results in,

$$v_{rec}(t) = \sum_{k=0}^{\infty} \sum_{k'=0}^{\infty} e_k h_{k'} l_k^p(t) * l_{k'}^p(t), \quad (5.14)$$

which using (4.27) yields to,

$$\sqrt{2p}v_{rec}(t) = \sum_{k=0}^{\infty} \sum_{k'=0}^{\infty} e_k h_{k'} [l_{k+k'}^p(t) + l_{k+k'+1}^p(t)]. \quad (5.15)$$

The j^{th} coefficient in $v_{rec}(t)$ Laguerre expansion, v_j is given by,

$$v_j = \langle v_{rec}(t), l_j^p(t) \rangle. \quad (5.16)$$

Substituting (5.15) in (5.16) gives,

$$\sqrt{2p}v_j = \sum_{k=0}^{\infty} \sum_{k'=0}^{\infty} e_k h_{k'} \langle l_{k+k'}^p(t), l_j^p(t) \rangle + \sum_{k=0}^{\infty} \sum_{k'=0}^{\infty} e_k h_{k'} \langle l_{k+k'+1}^p(t), l_j^p(t) \rangle. \quad (5.17)$$

Recalling orthogonality in (4.23) simplifies (5.17) to,

$$\sqrt{2p}v_j = \sum_{k=0}^{\infty} \sum_{k'=0}^{\infty} e_k h_{k'} \delta_{k+k',j} + \sum_{k=0}^{\infty} \sum_{k'=0}^{\infty} e_k h_{k'} \delta_{k+k'+1,j}. \quad (5.18)$$

(5.18) can be solved for different values of j , to find the unknown $h_{k'}$ coefficients. The unknown coefficients can be solved recursively as,

$$h_0 = \frac{\sqrt{2p}v_0}{e_0}, \quad (5.19)$$

$$h_1 = \frac{\sqrt{2p}v_1 - h_0(e_1 + e_0)}{e_0}, \quad (5.20)$$

$$h_2 = \frac{\sqrt{2p}v_2 - [h_0(e_2 + e_1) + h_1(e_1 + e_0)]}{e_0},$$

$$h_N = \frac{\sqrt{2p}v_N - [h_0(e_N + e_{N-1}) + h_1(e_{N-1} + e_{N-2}) + \dots + h_{N-1}(e_1 + e_0)]}{e_0}. \quad (5.22)$$

The above solution has been used to calculate the impulse response of various systems.

The choice of p in Laguerre functions is incredibly critical in order to reach convergence

[24]. Proposed as the future work, the convergence was not achieved to calculate the

effective heights in the electric field sensors studied in this thesis.

Chapter 6

Concluding Remarks and Future Work

6.1 Concluding Remarks

In this thesis, a distortion analysis of electromagnetic field sensors was performed using orthogonal polynomials. Hermite and Laguerre orthogonal polynomials were used to form basis sets which in turn span subspaces of $L^2(\mathfrak{R})$. A transformation matrix has been calculated for every electric field sensor. This transformation matrix was compared to a reference transformation matrix as a measure of distortion. Distortion characteristic of a 5 cm ACD, a 5, 10, and 15 cm monopoles were compared to each other using two method of distortion characterization. In the first method, the transformation matrices are calculated in a finite-dimensional subspace which gives a valid distortion characteristic for frequencies up to 1 GHz using the selected parameters. The results summarized in

Tables 5.1 , 5.2, and 5.3 show that when the sensors electric sizes decrease, the sensors tend to perform as differentiators up to a higher frequency range. In the case of the monopoles the signal is distorted after that certain frequency. Whereas, The ACD performs as a differentiator in lower frequencies while being more like an identity system in the higher frequencies.

Using an infinite-dimensional vector space, one can calculate the transformation matrices using Laguerre functions as described in Chapter 4. In the infinite-dimensional analysis, one has to calculate the sensors effective heights in order to calculate η_∞ . The results shown in Figs. 5.30 and 5.31 confirms the distortion characteristic calculated in Tables 5.1 and 5.2. The followings are the highlights of this thesis:

- Unlike the classical distortion characteristic, fidelity, transformation matrices describe the sensor performance for a subspace of waveforms.
- The relation of the studied subspace and the polynomials parameters is discussed.
- A discussion on selecting proper scaling factors is presented.
- In Laguerre subspace, it has been proved that only one column of the transformation matrix is sufficient for a complete distortion analysis.
- Methods have been presented to calculate the transformation matrix from only one set of time-domain measurement.

6.2 Future Work

There are many aspects of the work which need further investigation. Some of those are:

- This analysis is not able to recognize delay in the signals. In other words, a delay system is considered as a ditortive system. There still is a need to work out methods which are able to distinguish delay.
- The frequency-dependency of the subspaces still needs to be worked on. In this thesis, it is assumed that the frequency range of interest is the frequency range which is covered by the basis functions. However, no mathematical proof is given.
- Other sensors, including magnetic field sensors should be tested using this method.
- The sensitivity should be included in a quantitative manner in the distortion characteristic in order to obtain a realistic measure.
- Fabrication of a variety of 2-D and 2.5-D ACDs allows us to investigate the distortion characteristic of these sensors in more details.

Bibliography

- [1] *IEEE Standard for Calibration of Electromagnetic Field Sensors and Probes, Excluding Antennas, From 9 kHz to 40 GHz*, Std., 2005.
- [2] M. Kanda, “Time domain sensors for radiated impulsive measurements,” *Antennas and Propagation, IEEE Transactions on*, vol. 31, no. 3, pp. 438 – 444, may. 1983.
- [3] C. Baum, E. Breen, J. Giles, J. O’Neill, and G. Sower, “Sensors for electromagnetic pulse measurements both inside and away from nuclear source regions,” *Electromagnetic Compatibility, IEEE Transactions on*, vol. EMC-20, no. 1, pp. 22 –35, feb. 1978.
- [4] “IEEE standard definitions of terms for antennas,” *IEEE Std 145-1983*, 1983.
- [5] Q. Wu, B. shi Jin, L. Bian, Y. ming Wu, and L.-W. Li, “An approach to the determination of the phase center of vivaldi-based uwb antenna,” in *Antennas and Propagation Society International Symposium 2006, IEEE*, 2006, pp. 563 –566.
- [6] D. Lamensdorf and L. Susman, “Baseband-pulse-antenna techniques,” *Antennas and Propagation Magazine, IEEE*, vol. 36, no. 1, pp. 20–30, Feb 1994.
- [7] P. Carro and J. De Mingo, “Ultrawide-band antenna distortion characterization using hermite-gauss signal subspaces,” *Antennas and Wireless Propagation Letters, IEEE*, vol. 7, pp. 267–270, 2008.
- [8] C. A. Balanis, *Antenna theory, analysis and design*, 3rd ed. Hoboken, New Jerse: John Wiley and Sons INC, 2005.
- [9] J. McLean, H. Foltz, and R. Sutton, “Pattern descriptors for UWB antennas,” *Antennas and Propagation, IEEE Transactions on*, vol. 53, no. 1, pp. 553 – 559, 2005.
- [10] C. E. Baum and E. G. Farr, “Extending the definitions of antenna gain and radiation pattern into the time domain,” *Sensor and Simulation Notes*, no. 350, Nov 1992.
- [11] C. Baum, “General properties of antennas,” *Electromagnetic Compatibility, IEEE Transactions on*, vol. 44, no. 1, pp. 18 –24, Feb. 2002.

- [12] A. Shlivinski, E. Heyman, and R. Kastner, "Antenna characterization in the time domain," *Antennas and Propagation, IEEE Transactions on*, vol. 45, no. 7, pp. 1140–1149, Jul 1997.
- [13] S. Licul and W. Davis, "Unified frequency and time-domain antenna modeling and characterization," *Antennas and Propagation, IEEE Transactions on*, vol. 53, no. 9, pp. 2882–2888, Sept. 2005.
- [14] W. Van Cappellen, R. de Jongh, and L. Ligthart, "Potentials of ultra-short-pulse time-domain scattering measurements," *Antennas and Propagation Magazine, IEEE*, vol. 42, no. 4, pp. 35–45, Aug 2000.
- [15] O. Allen, D. Hill, and A. Ondrejka, "Time-domain antenna characterizations," *Electromagnetic Compatibility, IEEE Transactions on*, vol. 35, no. 3, pp. 339–346, Aug. 1993.
- [16] J. B. Conway, *A course in functional analysis*, 2nd ed. Springer-Verlag, New York: Springer, 1990.
- [17] A. M. Mood, F. A. Graybill, and D. C. Boes, *Introduction to the theory of statistics*, 3rd ed. McGraw-Hill, Inc., 1950.
- [18] D.-H. Kwon, "Effect of antenna gain and group delay variations on pulse-preserving capabilities of ultrawideband antennas," *Antennas and Propagation, IEEE Transactions on*, vol. 54, no. 8, pp. 2208–2215, 2006.
- [19] G. Strang, *Linear algebra and its applications*, 3rd ed. Orlando, FL: Harcourt Brace Jovanovich College Publishers, 1986.
- [20] S. Roman, *Advanced linear algebra*, 3rd ed. New York, NY: Springer, 2008.
- [21] C. Abou-Rjeily, N. Daniele, and J.-C. Belfiore, "Mimo uwb communications using modified hermite pulses," in *Personal, Indoor and Mobile Radio Communications, 2006 IEEE 17th International Symposium on*, 2006, pp. 1–5.
- [22] R. P. Boas and B. R. Creighton, *Polynomial expansions of analytic functions*, 2nd ed. Berlin, Gottingen, Heidelberg: Springer-Verlag, 1964.
- [23] N. Wiener, *The Fourier integral and certain of its applications*. Cambridge University Press, 1933.
- [24] M. Yuan, J. Koh, T. Sarkar, W. Lee, and M. Salazar-Palma, "A comparison of performance of three orthogonal polynomials in extraction of wide-band response using early time and low frequency data," *Antennas and Propagation, IEEE Transactions on*, vol. 53, no. 2, pp. 785–792, 2005.

- [25] H. T. Davis and K. T. Thomson, *Linear algebra and linear operators in engineering*. San Diego, CA: Academic Press, 2000.
- [26] S. S. Bayin, *Mathematical methods in science and engineering*. John Wiley and Sons, 2006.
- [27] J. P. Keener, *Principles of applied mathematics (Transformation and approximation)*. Addison-Wesley Publishing Company, 1988.
- [28] N. I. Nagnibida, “Completeness of subsequences of hermite polynomials,” *Siberian Mathematical Journal*, vol. 8, p. 1118, 1967.
- [29] D. Slepian, “On bandwidth,” *Proceedings of the IEEE*, vol. 64, no. 3, pp. 292 – 300, 1976.
- [30] A. Sitaram. Springerlink (encyclopedia of mathematics). [Online]. Available: <http://eom.springer.de/U/u130020.htm>
- [31] G. Budke, “On a convolution property characterizing the laguerre functions,” *Monatshefte fr Mathematik*, vol. 107, pp. 281–285, 1989, 10.1007/BF01517355. [Online]. Available: <http://dx.doi.org/10.1007/BF01517355>
- [32] G. Szego, *Orthogonal polynomials*, 4th ed. American Mathematical Society Providence, 1939.
- [33] L. H. Loomis, “A short proof of the completeness of the laguerre functions,” *Bulletin of the American Mathematical Society*, vol. 50, no. 6, pp. 386–387, 1944.
- [34] C. Baum, “An equivalent-charge method for defining geometries of dipole antennas,” *Sensor and Simulation notes*, no. 72, Jan 1969.
- [35] N. De, T. Ghosh, D. Poddar, and S. Chowdhury, “Design and experimental investigation of the asymptotic conical dipole antenna,” *Electromagnetic Compatibility, IEEE Transactions on*, vol. 37, no. 2, pp. 282 –285, May 1995.
- [36] E. Miller, A. Poggio, and G. Burke, “An integro-differential equation technique for the time-domain analysis of thin wire structures,” *Computational Physics, journal of*, vol. 12, pp. 24–48, 1973.
- [37] M. L. Saunders and B. Garrett, *Algebra*, 3rd ed. AMS Celsea Publishing, 1991.

Appendices

Appendix A

Proposition:

If $x(t), y(t) \in L^2(\mathfrak{R})$ then $\mathbf{R}_{x*y} = \mathbf{R}_x * \mathbf{R}_y$

- Lemma: $\mathbf{R}_x(\tau) = \mathbf{R}_x(-\tau)$

Proof:

$$\mathbf{R}_x(\tau) = \int_{-\infty}^{\infty} x(t)x(t-\tau)dt = \int_{-\infty}^{\infty} x(\alpha+\tau)x(\alpha)d\alpha = \mathbf{R}_x(-\tau)$$

Proof:

$$\mathbf{R}_{x*y} = \int_{-\infty}^{\infty} (x*y)(t)(x*y)(t-\tau)dt = \int_{-\infty}^{\infty} \int_{-\infty}^{\infty} x(\alpha)y(t-\alpha)d\alpha \int_{-\infty}^{\infty} x(\lambda)y(t-\tau-\lambda)d\lambda dt$$

If $u = t - \alpha$

$$\int_{-\infty}^{\infty} \int_{-\infty}^{\infty} x(\alpha)x(\lambda)d\alpha \int_{-\infty}^{\infty} y(u)y(u+\alpha-\tau-\lambda)dud\lambda = \int_{-\infty}^{\infty} \int_{-\infty}^{\infty} x(\alpha)x(\lambda)d\alpha \mathbf{R}_y(\tau+\lambda-\alpha)d\lambda$$

If $u' = \lambda - \alpha$

$$\int_{-\infty}^{\infty} \int_{-\infty}^{\infty} x(\alpha)x(u'+\alpha)d\alpha \mathbf{R}_y(\tau+u')du'$$

$$= \int_{-\infty}^{\infty} \mathbf{R}_x(u')\mathbf{R}_y(u'+\tau)du'$$

Using the above lemma we have $\mathbf{R}_x(u') = \mathbf{R}_x(-u')$ then

$$\begin{aligned}\mathbf{R}_x(\tau) &= \int_{-\infty}^{\infty} x(t)x(t-\tau)dt = \int_{-\infty}^{\infty} \mathbf{R}_x(-u')\mathbf{R}_y(u'+\tau)du' \\ &= \int_{-\infty}^{\infty} \mathbf{R}_x(\theta)\mathbf{R}_y(\tau-\theta)d\theta = \mathbf{R}_x * \mathbf{R}_y. \quad \triangle\end{aligned}$$

Appendix B

The following is a summary of the mathematical terms used in this thesis.

- Field

Consider a non-empty set F , which has two elements 1 and 0, and two binary operations, addition and multiplication. For two arbitrary elements of F such as a and b , addition is shown as $(a, b) \mapsto a + b$, while multiplication is shown by $(a, b) \mapsto a \cdot b$. F is a field if:

$$\forall a, b, c \in F \quad (a + b) + c = a + (b + c),$$

$$\forall a, b, c \in F \quad (a \cdot b) \cdot c = a \cdot (b \cdot c),$$

$$\forall a, b \in F \quad a + b = b + a,$$

$$\forall a, b \in F \quad a \cdot b = b \cdot a,$$

$$\forall a \in F \quad a + 0 = a,$$

$$\forall a \in F \quad a \cdot 1 = a,$$

$$\forall a \in F \quad \exists -a \in F \text{ so that, } a + (-a) = 0,$$

$$\forall a \in F \quad \exists a^{-1} \in F \text{ so that, } a \cdot a^{-1} = 1,$$

$$\forall a, b, c \in F \quad a \cdot (b + c) = a \cdot b + a \cdot c \text{ [37].}$$

- Vector space

Consider V as a collection of elements, $V = \{x, y, \dots\}$. If addition operation is defined as, $(x, y) \mapsto x + y$, V is a vector space over the field F , if [25],

1- If $x, y \in V$ then, $x + y \in V$,

2- $\forall x, y \in V, x + y = y + x$,

3- $\exists \mathbf{0} \in V$ so that $\forall x \in V, \quad x + \mathbf{0} = x$,

4- $\forall x \in V, \quad \exists -x \in V$ so that $x + (-x) = \mathbf{0}$,

5- $\forall \alpha, \beta \in F$

$$\alpha(\beta x) = (\alpha \cdot \beta)x,$$

$$(\alpha + \beta)x = \alpha x + \beta x,$$

$$\alpha(x + y) = \alpha x + \alpha y.$$

- Linear transformation

A linear transformation, T , is a function which maps vectors from the vector space V_D into the vector space V_R ,

$T : x \mapsto y$, where, $x \in V_D, y \in V_R$, and is additive and homogeneous, or [37],

$$\forall x, \acute{x} \in V_D, \quad T(x + \acute{x}) = T(x) + T(\acute{x}) \text{ (additivity),}$$

$$\forall \alpha \in F, \forall x \in V_D, \quad T(\alpha x) = \alpha T(x) \text{ (being homogeneous).}$$

- Subspace

A subspace V of the vector space U is a non-empty subset of U which is a vector space itself.

- Domain subspace, Range subspace

A linear transformation maps vectors from a vector space V_D to a vector space V_R . As V_D and V_R can be considered subspaces of a larger vector space, V_D and V_R are denoted as the domain and the range subspaces, respectively.

- Inner product

The inner product is an operation defined in the vector space V which maps every two arbitrary vectors $x, y \in V$ to a scalar in the field F , which V is defined over.

As,

$$(x, y) \longmapsto \langle x, y \rangle.$$

- Orthogonality

Two vectors x, y in the vector space V are orthogonal if and only if,

$$\langle x, y \rangle = 0.$$

- Norm of a vector

Norm of an arbitrary vector x in the vector space V with a certain inner production is defined as [25],

$$\|x\| \triangleq \sqrt{\langle x, x \rangle}.$$

- $L^2(\mathfrak{R})$

Is a vector space including functions which are quadratically integrable, or ,

$$\forall f(t) \in L^2(\mathfrak{R}) \quad \exists M \in \mathfrak{R} \text{ so that } \int_{-\infty}^{\infty} |f(t)|^2 dt < M.$$

- Span

Consider the set $S = \{s_1, s_2, \dots, s_N\}$ in the vector space V . S spans V if and only if,

$$\forall x \in V, \exists \alpha_i \in F, \text{ so that, } x = \sum_{i=1}^N \alpha_i s_i.$$

- Basis vector, Basis set

The set $B = b_1, b_2, \dots, b_N$ in the vector space V is said to be a basis set for V if and only if,

1- B spans V ,

2- b_1, b_2, \dots, b_N are mutually orthogonal.

The vectors, b_1, b_2, \dots, b_N are called the basis vectors. N determines the dimension of the vector space. Every arbitrary vector x in V is written uniquely as a linear summation of the basis vectors as,

$$x = \sum_{i=1}^N x_i b_i.$$

- n-tuple representation

For every arbitrary vector x in the vector space V with the basis set $B = b_1, b_2, \dots, b_N$,

the $1 \times n$ matrix, $\mathbf{x} = [x_1, x_2, \dots, x_N]^t$ is the n-tuple representation. The superscript

t stands for the transposition while x_i s are the coefficients in the expansion,

$$x = \sum_{i=0}^N x_i b_i.$$

- Linear operator

A linear operator is the matrix representation for a linear transformation. An $M \times N$ matrix \mathbf{L} , can be viewed as a linear operator which maps a $1 \times N$ matrix, \mathbf{x} , to a $1 \times M$ matrix using,

$$\mathbf{y} = \mathbf{L}\mathbf{x} \text{ [25].}$$

- Frobenius norm

For an $M \times N$ matrix $\mathbf{A} = [a_{ij}]$, the Frobenius norm is defined as [25],

$$\|\mathbf{A}\|_F = \sqrt{\sum_{j=1}^N \sum_{i=1}^M a_{ij}^2}.$$

- Infinite-dimensional vector space

An infinite-dimensional vector space is a vector space which has a denumerable basis set. $L^2(\mathfrak{R})$ is an example [25].

Appendix C

Proposition:

$\eta_N = \sqrt{1 + \frac{\text{tr}(LL^H - 2\text{tr}(L))}{N}}$ if the reference matrix is $\mathbf{I}_N = [a_{ij}]_{1 \leq i, j \leq N}$

Proof:

When the reference matrix is the identity matrix, η_N can be written as,

$$\eta_N = \frac{\|\mathbf{L} - \mathbf{I}_N\|}{\sqrt{N}}. \quad (\text{C.1})$$

Using (3.17), (C.1) is written as,

$$\eta_N = \sqrt{\frac{\sum_{i=1}^N \sum_{j=1}^N (l_{ij} - a_{ij})^2}{N}}. \quad (\text{C.2})$$

Using this, we have,

$$\eta_N = \sqrt{\frac{\sum_{i=1}^N \sum_{j=1}^N |l_{ij}|^2 + \sum_{i=1}^N \sum_{j=1}^N a_{ij}^2 - 2 \sum_{i=1}^N \sum_{j=1}^N l_{ij} a_{ij}}{N}}. \quad (\text{C.3})$$

As a_{ij} are the elements of the identity matrix, they are equal to one when $i = j$ and are equal to zero otherwise. Therefore, (C.3) is simplified to,

$$\eta_N = \sqrt{\frac{\sum_{i=1}^N \sum_{j=1}^N |l_{ij}|^2 + N - 2 \sum_{i=1}^N l_{ii}}{N}}. \quad (\text{C.4})$$

In (C.4),

$$\sum_{i=1}^N \sum_{j=1}^N |l_{ij}|^2 = \text{tr}(\mathbf{L}\mathbf{L}^H), \quad (\text{C.5})$$

$$\sum_{i=1}^N l_{ii} = \text{tr}(\mathbf{L}). \quad (\text{C.6})$$

So we have:

$$\eta_N = \sqrt{1 + \frac{\text{tr}(\mathbf{L}\mathbf{L}^H) - 2\text{tr}(\mathbf{L})}{N}}. \quad \triangle \quad (\text{C.7})$$

Appendix D

D.1 Hermite Polynomials

Schrodinger equation is stated as [26],

$$\frac{d^2\Psi(\zeta)}{d\zeta^2} + \frac{2}{\zeta} \frac{\Psi(\zeta)}{d\zeta} + \frac{1}{\zeta^4} \left(\epsilon - \frac{1}{\zeta^4} \right) \Psi(\zeta) = 0. \quad (\text{D.1})$$

When it is assumed that $\epsilon - 1 = 2n, n = 0, 1, 2, \dots$ and $x = \frac{1}{\zeta}$, the solution to (D.1) is given by,

$$\Psi(x) = H_n(x) e^{-x^2/2}. \quad (\text{D.2})$$

$H_n(x)$ in (D.2) is the n^{th} order Hermite polynomial and is given in the closed form as [26],

$$H_n(x) = \sum_{j=0}^{\lfloor \frac{n}{2} \rfloor} \frac{(-1)^j 2^{n-2j} n!}{(n-2j)! j!} x^{n-2j}. \quad (\text{D.3})$$

D.2 Hermite Polynomials Properties

- Recursion relations [26]:

$$H_{n+1}(x) = 2xH_n(x) - 2nH_{n-1}(x) \quad n \geq 1, \quad (\text{D.4})$$

$$H_1(x) = 2xH_0(x), \quad (\text{D.5})$$

$$\frac{dH_n(x)}{dx} = 2nH_{n-1}(x) \quad n \geq 1, \quad (\text{D.6})$$

$$\frac{dH_0(x)}{dx} = 0. \quad (\text{D.7})$$

- Orthogonality

Hermite polynomials are orthogonal to each other with respect a weight function of e^{-x^2} , as we have [26],

$$\int_{-\infty}^{\infty} e^{-x^2} H_n(x) H_m(x) dx = \begin{cases} 0 & \text{if } n \neq m; \\ 2^n n! \sqrt{\pi} & \text{if } n = m. \end{cases}$$

(D.8)

- The n^{th} derivative of the n^{th} order polynomial is given by [26],

$$\frac{d^n H_n(x)}{dx^n} = 2^n n!. \quad (\text{D.9})$$

- Rodriguez formula

$$H_n(x) = (-1)^n e^{x^2} \frac{d^n}{dx^n} [e^{-x^2}]. \quad (\text{D.10})$$

D.3 Hermite-Gauss Functions and Their Properties

Hermite-Gauss functions are the solution to (D.1). The n^{th} order Hermite-Gauss function is defined as [26],

$$\phi_n(x) = \frac{1}{\sqrt{2^n n! \sqrt{\pi}}} H_n(x) e^{-\frac{x^2}{2}}. \quad (\text{D.11})$$

Hermite-Gauss functions have many interesting properties including:

- Hermite-Gauss functions form a complete basis set for $L^2(\mathfrak{R})$ [28].
- Hermite-Gauss functions are the eigenfunctions of the Fourier transform [23]. Fourier transform of the n^{th} order Hermite-Gauss function is given by,

$$\mathcal{F}[\phi_n(x)] = \frac{1}{2\pi} (-j)^n \phi_n(f). \quad (\text{D.12})$$

- The first derivative of the Hermite-Gauss functions can be written in terms of other Hermite-Gauss functions, or,

$$\frac{d\phi_n(x)}{dx} = \sqrt{\frac{n}{2}} \phi_{n-1}(x) - \sqrt{\frac{n+1}{2}} \phi_{n+1}(x).$$

Proof:

Taking the first derivative of (D.11), results in,

$$\frac{d\phi_n(x)}{dx} = \frac{e^{-\frac{x^2}{2}}}{\sqrt{2^n n!} \sqrt{\pi}} \left[-xH_n(x) + \frac{dH_n(x)}{dx} \right]. \quad (\text{D.14})$$

Assuming $n \geq 1$, we can substitute $xH_n(x)$ and $dH_n(x)/dx$ from (D.7) and (D.6), respectively, to have,

$$\frac{d\phi_n(x)}{dx} = \frac{e^{-\frac{x^2}{2}}}{\sqrt{2^n n!} \sqrt{\pi}} \left[nH_{n-1} - \frac{1}{2}H_{n+1} \right], \quad (\text{D.15})$$

Which recalling (D.11) results in (D.13).

Appendix E

E.1 Laguerre Polynomials

The solution to the time-independent Schrodinger differential equation can be separated to two functions, one only dependent on the radius and one dependent on the azimuth and inclination angles. The solution to the radius dependent function leads to the Laguerre equation, given by [26],

$$x \frac{d^2 L_n(x)}{dx^2} + (1-x) \frac{dL_n(x)}{dx} + ny = 0. \quad (\text{E.1})$$

The solution to (E.1) is given by the n^{th} order polynomial, $L_n(x)$, as [26],

$$L_n(x) = \sum_{r=0}^n (-1)^r \frac{n! x^r}{(n-r)!(r!)^2}. \quad (\text{E.2})$$

E.2 Laguerre Polynomials Properties

Some of the properties can be summarized as [26],

– Rodriguez formula

$$L_n(x) = \frac{e^x}{n!} \frac{d^n}{dx^n} (x^n e^{-x}). \quad (\text{E.3})$$

– Orthogonality

Hermite polynomials are orthogonal to each other with respect to the weight function e^{-x} , in the positive real numbers [26],

$$\int_0^\infty e^{-x} L_n(x) L_m(x) dx = \delta_{n,m} \quad (\text{E.4})$$

– Recursion relation

$$L_{n+1}(x) = \frac{(2n+1-x)L_n(x) - nL_{n-1}(x)}{n+1}. \quad (\text{E.5})$$

$$\frac{dL_n(x)}{dx} = \frac{nL_n(x) - nL_{n-1}(x)}{x}. \quad (\text{E.6})$$

E.3 Associated Laguerre Polynomials and Properties

The associated Laguerre polynomials are the solution to the differential equation

MathMeth,

$$x \frac{d^2 L_n^k(x)}{dx^2} + (k + 1 - x) \frac{dL_n^k(x)}{dx} + nL_n^k(x). \quad (\text{E.7})$$

The associated Laguerre polynomials are given by [26],

$$L_n(x) = \sum_{s=0}^n \frac{(-1)^s (n+k)! x^s}{(n-s)! (k+s)! s!}. \quad (\text{E.8})$$

Some of the associated Laguerre polynomials properties can be summarized as [26],

– Orthogonality

Associated Laguerre polynomials are orthogonal to each other with respect to the weight function $x^k e^{-x}$ as,

$$\int_0^\infty e^{-x} x^k L_n^k(x) L_m^k(x) dx = \frac{(n+k)!}{n!} \delta_{n,m}. \quad (\text{E.9})$$

– Recursion relation

$$L_{n+1}^k(x) = \frac{(2n+k+1-x)L_n^k(x) - (n+k)L_{n-1}^k(x)}{n+1}. \quad (\text{E.10})$$

$$\frac{dL_n^k(x)}{dx} = \frac{nL_n^k(x) - (n+k)L_{n-1}^k(x)}{x}. \quad (\text{E.11})$$

– Rodriguez formula

$$L_n^k(x) = \frac{e^x x^{-k}}{n!} \frac{d^n}{dx^n} (x^{n+k} e^{-x}). \quad (\text{E.12})$$

Laguerre polynomials given in (E.2) are in fact the associated Laguerre polynomials for $k = 0$.

E.4 Laguerre Functions

Laguerre functions are defined in relation to the Laguerre polynomials as [31],

$$l_n(x) = (-1)^n L_n(x) e^{-\frac{x}{2}}. \quad (\text{E.13})$$

Laguerre functions have many interesting properties, including:

– Completeness of the spanned subspace

Laguerre functions form a complete orthogonal basis set for $L^2(\mathfrak{R}^+)$ [33].

– Recursive relations

Using (E.5) and (E.13), we can write,

$$l_{n+1}(x) = -\frac{(2n+1-x)l_n(x) - nl_{n-1}(x)}{n+1}. \quad (\text{E.14})$$

- Convolution of Laguerre functions [31]

$$l_n(x) * l_m(x) = l_{n+m}(x) + l_{n+m+1}(x). \quad (\text{E.15})$$

- Frequency domain relation

The Fourier transform of Laguerre functions is given as [31],

$$\mathcal{F}[l_n(x)] = \frac{e^{-j(2n+1)\tan^{-1}(2\omega)}}{\sqrt{\omega^2 + (\frac{1}{2})^2}}. \quad (\text{E.16})$$

Therefore, different orders of Laguerre functions have frequency-domain counterparts which are all the same in the magnitude and are only different in the phase.